Paleoenvironment reconstruction in extreme climates using organic geochemical investigations

by

Ross H. Williams

B.S., Rensselaer Polytechnic Institute, 2011

Submitted to the Department of Earth, Atmospheric, and Planetary Sciences

in partial fulfillment of the requirements for the degree of

Doctor of Philosophy

at the

MASSACHUSETTS INSTITUTE OF TECHNOLOGY

September 2016

Author: Signature redacted

Department of Earth, Atmospheric, and Planetary Sciences

July 25th, 2016

Certified by: Signature redacted

Roger E. Summons

Professor of Geobiology, MIT

Thesis Supervisor

Accepted by: Signature redacted

Robert van der Hilst

Schlumberger Professor of Earth and Planetary Sciences

Head, Department of Earth, Atmospheric, and Planetary Sciences

Paleoenvironment reconstruction in extreme climates using organic geochemical investigations

by

Ross H. Williams

Thesis Abstract

Organic geochemistry provides researchers with an extensive suite of tools for reconstructing past environments. Using these tools, a set of unique locations situated in climatic extremes have been investigated. During the Early Cenozoic the planet was much warmer than today. In addition to this higher background temperature a series of rapid warming events occurred termed hyperthermals. The largest of these, the Paleocene-Eocene Thermal Maximum is perhaps the best analog to modern day anthropogenic climate change. It is paramount to understand the global effects of this event to elucidate potential changes in our near future. To further this area of research two very different regions were chosen to seek out potential deposits that record the hyperthermals. First, in the Cambay Basin of Western India an extensive core was taken during exploration for lignite deposits. This site would have been near the equator during the time of deposition, a region that is important yet not well established in the current literature pertaining to the hyperthermals. Biostratigraphy and palynology combined with bulk organic carbon isotope records reveals that the lowermost portion of the core likely contains the hyperthermal events. Compound-specific isotopic investigation across multiple realms reveals potential variability of carbon in the ocean-atmosphere system that was then complemented by examination of the corresponding kerogens through application of pyrolysis gas chromatography-mass spectrometry. Expanding upon this study the Canadian High Arctic was assessed in the form of paleosols from Banks Island and shales from Strathcona Fiord. Biomarker distributions revealed a shift in environmental conditions from marine to coastal environments from the Paleocene into the Eocene. Hydrogen isotopic investigation reveals that the *n*-alkanes from paleosols can preserve the same signals as rocks from the same time and that the paleohydrology was far different from present day. Finally, a study was conducted of the recent history of Lagunas Miscanti and Miñiques due to their location at high elevations in the dry Chilean Altiplano. Examination of biomarker distribution as well as associated proxies shows that the lakes have undergone significant changes on centennial time scales along with varying biotic communities, water chemistry and lake level.

Thesis Supervisor: Roger E. Summons, Professor of Geobiology, MIT

Acknowledgements

Over the course of my Ph.D. there has been an ever growing list of people I find myself thankful to. The following is my humble attempt at addressing them all.

First and foremost I would like to thank Roger Summons for serving as my advisor throughout this process. His excitement for his work and his desire to ask the big questions is what first brought me in to this field. Together we have pursued projects with uncertain outcomes and though perhaps we didn't always find what we hoped to, I learned that there is a story in every outcome. I have been fortunate to be Roger's student in that he always encouraged developing a sound foundational understanding of analytics that I feel will serve me throughout my career.

I cannot speak about analytics without expressing my sincere gratitude towards Carolyn Colonero. Not only did she work to keep everything running in the lab she was always generous with her time when I wanted to learn how. For years it seemed like every possible malfunction would occur right when I needed a machine and I learned many things I did not expect to with her help.

I would also like to thank my committee for their advice and guidance this past year. Mick Follows always brought a positive energy to our meetings and his excitement about the work always provided a bright outlook. I'd like to thank Kate Freeman for inviting me to her lab on several occasions and for always providing critical feedback in a way that I always left our meetings feeling better about my work.

I especially would like to thank David McGee for his help over the years. David served as my second general examination advisor before joining my thesis committee. He has always been generous with his time even when my questions weren't at all related to our work together. Finally, I would like to thank him for including me on his MISTI-Chile grant that allowed me to conduct the field work that led to one of the chapters of this thesis.

I have had a number of collaborators over the year I would like to thank. First, Suryendu Dutta who has provided samples and hosted several exciting trips to India. I would further like to thank his students and postdocs, especially Anindya Nandi and Jyoti Sharma who conducted biostratigraphy and palynology of samples used in this thesis. I would also like the acknowledge Blas Valero-Garcés and his crew at IPE-CSIC who I got to work with in Chile and welcomed me to their labs in Spain.

I would like to acknowledge the wonderful people of E25 who I had the pleasure of interacting with on a daily basis. I cannot list all the people in the other labs on the

floor but they all deserve thanks for building such a supportive community. I need to single out Sara Lincoln for supervising me my first summer when I knew little about organic chemistry and being a mentor in my early years. I'd like to thank my officemate Sharon Newman who has been my sounding board much to my benefit. Further I would like to thank Christopher Kinsley and Christine Chen for making sure my days were never dull. I'd also like to thank all the administrators working behind the scenes to keep everything going but especially Melody Abedinejad who has been a great office neighbor who greeted me with a smile each morning.

I would also like to thank all the fellow students I have worked alongside over the years including Emily Matys, Katherine French, Christian Illing, Aimee Gillespie, Marie Giron, and Jon Grabenstatter. A number of postdocs have influenced my work and provided guidance such as Shane O'Reilly, Xiaolei Liu, Genming Luo, David Gold, Julio Sepulveda, Florence Schubotz, Ben Kotrc, Kristen Slawter, Paula Welander and Christian Hallman. I've also had the privilege of supervising a number of students and lab techs that have contributed to my success as a student and my development as a mentor. These brave souls were Jane Gracie Van Adzin, Kelden Pehr, Madonna Yoder, Jaynar Bolati, and Kerstin McAndrews.

I would like to express my gratitude to my friends and family members that have supported me for all these years. I'd like to thank my mother, Karen Williams and father, Kevin Williams for always encouraging me to pursue my interests no matter where they take me. I'd also like to thank the Plummer and Barber families for being a loving, positive influence in my life for many years now. I'd like to make special note of my grandfathers Donald Williams and Warren "Bud" Fisher. Donald for instilling in me a deep love for the outdoors at a young age that shaped my eventual interests in the geoscience. Bud I would like to thank for supporting my education and career. I would not be here without him.

Lastly I would like to thank my loving wife Christina. She has been with me every step of the way since before I even knew I would be a scientist. She has been a constant source of support and understanding whose presence can allow me to weather any storm. I am immensely pleased that as I end this chapter of my life we are starting a new chapter in ours together and I cannot wait to share every lesson I have learned with our new family.

Funding for this work was provided by the NASA Astrobiology Institute (NNA13AA90A) and the NASA Exobiology Program. Travel support was provided by the MISTI-Chile, the MISTI-India Innovation Seed Fund and the MIT-USTC summer intern program.

Table of Contents

List of Figures

List of Tables

Chapter 1

1. Introduction

1.1 Organic Geochemistry as a tool for paleoenvironmental reconstructions

The application of molecular techniques to the study of paleoenvironmental conditions often has the potential to reveal a wealth of information not available through other means. Examination of macroscale fossils can uncover information about a particular flora or fauna, and fossil assemblage analysis can elucidate larger group scale effects, but neither of these capture the amount of information organic geochemical methods can provide. A single extract of organic matter can contain the molecular fossils of a multitude of organisms across a variety of realms, providing a snapshot of time and a glimpse at what the environment as a whole actually was like.

With varying degrees of specificity, biomarkers are diagnostic for a particular source organism or group. Through careful study of modern analogs, many modern biomolecules have been shown to be the likely precursors to common fossil molecular structures. After deposition these biomolecules undergo alterations into more chemically stable compounds that remain in the rock record for long stretches of geologic time. By uncovering these fossil molecules, organisms from all domains of life can be shown to have existed at the time of deposition. This is very significant specifically to the study of those organisms that do not form the hard body parts

that typically leave macrofossil remains such as the bacteria and archaea. These groups, while small in size are incredibly important on a far larger scale as their metabolisms have altered the very composition of the atmosphere.

The eventual endosymbiosis of cyanobacteria led to the rise of another very important group, the plants. The radiation of vascular plants during the Devonian is established to have enhanced chemical weathering and drawn down atmospheric carbon dioxide levels (Berner, 1997). Later, during the Carboniferous, the seed forming gymnosperms grew to prominence followed by the angiosperms, or flower bearing plants in the Cretaceous. These angiosperms would rapidly diversify and soon overtake gymnosperms as the prominent form of seed bearing plants.

Higher plants can be located in the molecular record by the distinct compounds they form. Higher plant detection is one of the earliest forms of molecular paleoenvironmental reconstruction, dating to the discovery that higher plant leaf waxes have a distinct pattern of odd chain length preference and maxima usually in the C_{25}-C_{31} range for *n*-alkanes, and an even preference in the related fatty acids, alkanols, and aldehydes (Eglinton and Hamilton, 1967; Eglinton et al., 1962). It has been further demonstrated that n-alkane production varies significantly among the higher plants, in particular between angiosperms and gymnosperms (Diefendorf et al. 2011). Beyond being a source indicator, the odd chain length preference was found to be anti-correlated to thermal maturity. Early on this process was noted and exploited as the carbon preference index (CPI) (Bray and Evans, 1961) and later refined as the odd-even preference (OEP) (Scalan and Smith, 1970). More

recently, the discovery that aquatic vegetation often produces distributions of *n*-alkanes with a C_{23} predominance led to the creation of the percent aqueous (P_{aq}) proxy (Ficken et al., 2000). By assessing the relative amounts of *n*-alkanes an increase in this proxy reflects the presence of emergent then submerged macrophytes. Further, in certain environments this can be used to determine the presence of sphagnum due to its *n*-C_{23} preference as well (Inglis et al., 2015).

The presence of higher plants can also be determined by the presence of more complex molecules. For instance, plants are known to produce C_{29} sterols (Huang and Meinschein, 1979) resulting in C_{29} sterane geolipids. There are many groups of compounds that can be more diagnostic for certain types of higher plants. For example, polycadinene is a polymer prominent in the dammar resins formed by the angiosperm dipterocarps common to Southeast Asia (Van Aarssen et al., 1994). Compounds such as bicadinane and tricadinane are products of the breakdown of such resins. Other common markers for angiosperms are the pentacyclic triterpenoids known as oleananes and lupanes (Moldowan et al., 1994). For gymnosperms, there are a great variety of terpenoids thought to originate from conifers. These include the bicyclic labdanes, tricyclic pimaranes and abietanes, and tetracyclic karuanes and phyllocladanes (Fig. 1.1).

Beyond simply providing information about the source of organic matter, biomarkers also have the potential to be indicators of the physical condition of the paleoenvironment. For instance, microbes have been shown to adjust the structure of their lipid membranes in response to environmental factors such as pH and

temperature. Both archaea and bacteria form tetraether membrane lipids known as glycerol dialkyl glycerol tetraethers. The archaea form these compounds with isoprenoidal alkyl chains while the bacteria's are non-isoprenoidal (aka branched). The non-isoprenoidal set of GDGTs is formed more specifically by soil bacteria and thus represents input of terrestrial organic matter. To quantify the relative contributions of these two groups, which affects the application of further proxies, the BIT index was created (Hopmans et al., 2004; Weijers et al., 2006). These groups modify their alkyl chains with changing conditions through the establishment of cyclic moieties and, in the case of branched GDGTs, the addition of methylations. Bases upon this behavior, as well as the production of specific types of GDGTs by certain groups, a number of proxies have developed for paleoenvironmental reconstructions.

The addition of cyclic moieties to isoprenoidal GDGTs was discovered to be related to the sea surface temperature of the waters in which they were formed (Schouten et al., 2002). This proxy, known as TEX_{86}, has been widely applied to a great number of climatic studies since it was established. Given the widespread attention it has garnered it has undergone careful examination and recalibrations. For instance, based upon trends noted in Arctic Oceans two new measures were recommended, TEX_{86}^{L} for low temperature and TEX_{86}^{H} for high (Kim et al., 2010).

Within the non-isoprenoidal GDGTs it was shown that the number of cyclizations is correlated to the environmental pH while the number of methylations is to both the pH and the mean annual temperature (MAT) (Weijers et al., 2007).

From this relationship the cyclization of branched tetraethers (CBT) and methylation of branched tetraethers (MBT) indices were established. Through the combination of both indices it is then possible to determine both the pH and temperature of the paleoenvironment.

It can be difficult however to extend these established proxies to different depositional settings such as lakes. With varying degrees of success calibrations have been proposed such as that for TEX_{86} by Powers et al., 2010. For the MBT/CBT proxy several different approaches have been taken. First, several adjustments were proposed to correct apparent significant offsets in lake environments (Pearson et al., 2011; Tierney et al., 2010) and recently a regional calibration (Foster et al., 2016). Such regional calibrations, while hampered by lack of data in many areas, are important for improving measurement accuracy, but they also raise the issues of why such compounds behave differently in these areas.

The amounts of different types of GDGTs have also been recently applied in a number of other ways. The fact that halophile archaea apparently only produce archaeol type compounds and not GDGTs led to the relative amounts of these compounds being used as a paleosalinity proxy, the archaeol and caldarchaeol ecometric was created (ACE index) (Birgel et al., 2014; Turich and Freeman, 2011). This correlation was confirmed in subsequent studies (Wang et al., 2013) but does not seem applicable in all cases (Huguet et al., 2015).

Another recently proposed proxy is the %thaum proxy for lake level changes (Wang et al., 2014). This proxy is based upon the idea that thaumarchaeota prefer

to live at deeper depths. As such, the relative amount of their produced thaumarchaeol would be seen to increase with the size of the water column. This proxy is relatively young and untested so it should be used with significant caution. Recent examinations have demonstrated significant diversity in the groups forming different GDGTs so care must be taken when applying such proxies (Pearson et al., 2016).

1.2 Early Cenozoic hyperthermal events

The Early Cenozoic was the warmest time period of the past 65 million years (Zachos et al., 2008). During the Early Eocene Climatic Optimum (EECO) global temperatures are thought to have been ~14°C than preindustrial levels (Caballero and Huber, 2013). This elevated temperature was likely due to higher atmospheric CO_2 levels. Estimates of CO_2 levels range from 500 parts per million to over 4,000 parts per million (Beerling and Royer, 2011; Loptson et al., 2014; Lowenstein and Demicco, 2006) with recent estimates based upon boron isotopes at 1,400 parts per million (Anagnostou et al., 2016).

On top of the already elevated CO_2 levels there was a rapid increase that resulted in a warming known as the Paleocene-Eocene Thermal Maximum (PETM). This event was discovered by the concurrent shifting of carbon and oxygen isotopic compositions in benthic foraminifera indicating a synchronous change in the carbon cycle and temperature (Kennett and Stott, 1991). This was rapidly confirmed to have been a large scale event as it was extended into the terrestrial realm through studies of mammalian teeth and paleosol carbonates (Koch et al., 1992). The

warming from this event, which occurred on the order of thousands of years, was ~5°C (Dunkley Jones et al., 2013; Fricke and Wing, 2004; Tripati and Elderfield, 2005).

While the PETM is the most prominent and well-studied event there were a number of other hyperthermals in the Early Cenozoic. Following the PETM was the Eocene Thermal Maxima 2 (ETM2) (Lourens et al., 2005). While similar in characteristics to the PETM, the ETM2 was found to have a smaller CIE and climatic impact. Subsequently a third event ETM3 (Or 'X') was discovered (Röhl et al., 2005). Less well established are events that preceded the PETM such as Latest Danian Event (LDE), Dan-C2 event and Early Late Paleocene Event (ELPE) (Quillévéré et al., 2008; Röhl et al., 2004; Westerhold et al., 2011).

One of the best methods of locating the hyperthermal events is by locating the associated carbon isotope excursion (CIE). As this excursion occurred within the ocean-atmosphere system it has been located in a great variety of reservoirs from the marine and terrestrial realms (McInerney and Wing, 2011). While the evidence of an input of isotopically depleted carbon is undeniable, the actual source of the carbon is still debated.

The most popular candidate by far for the source of carbon are seafloor methane clathrates (Dickens et al., 1995). Methane clathrates are a clear choice for carbon isotopic excursion due to their highly depleted nature. By starting with a much depleted source, less carbon is needed to cause an excursion of a set magnitude. However, it has been argued that this is the hypothesis's own downfall as it may not

release enough carbon to cause the observed shoaling of the calcite compensation depth (Panchuk et al., 2008). It has further been suggested that the already warm background conditions of the Early Cenozoic would not enable significant enough stores of methane clathrates to exist to account for the whole event (Pagani et al., 2006).

Alternatively, it has been argued that the hyperthermal events were triggered by orbital forcing and carbon release through positive climate feedbacks (Cramer et al., 2003; Littler et al., 2014; Lourens et al., 2005). This explanation is attractive in that it offers an explanation for the lesser hyperthermal events given their correspondence to orbital cyclicity (Galeotti et al., 2010). However, the observation that the PETM and ETM2 do not coincide with the dominant 405kyr eccentricity cycles has been used to argue against this (Westerhold et al., 2007).

There also exists a magmatic explanation for the PETM. If magma comes into contact with organic rich sediments there can be a substantial release of carbon in the form of carbon dioxide and methane (Cooper et al., 2007). For the PETM, the North Atlantic or offshore Norway have been proposed to be potential candidate areas for such an event to have occurred (Aarnes et al., 2015; Svensen et al., 2004). This mechanism however would require extreme amounts of carbon to be released to cause the CIE since the carbon released would not be as isotopically depleted as other mechanisms.

In addition to these three potential triggers there have also been a number of other suggestions that haven't gained the same traction. This is usually due to the

lack of physical evidence supporting their theories. Two examples of this are the impact of a carbon rich comet (Cramer and Kent, 2005) or drying of epicontental seaways exposing organic rich sediment to air (Higgins and Schrag, 2006). More often now a multiple step scheme is invoked, usually involving one process leading to the dissociation of methane clathrates. This framework has gained traction lately with the description of a "pre-excursion" before the main event (Bowen et al., 2014).

1.3 Thesis Structure

This goal of this thesis is to apply the principles of paleoenvironmental reconstruction to several distinct cases. Each of these cases is unique in some way and represent times of environmental variability of differing scales. The sites described below span from multimillion year examination of tropical equatorial conditions during hyperthermal events to centennial scale study of lakes in a cold and dry climate. Throughout the question of how biota responds to such a variety of environmental changes will be addressed.

Beginning at the upper extreme, Chapter 2 will study the conditions at the equator during the warmest period of the past 65 million years. During the Early Cenozoic the coastal environments of Western India led to the deposition of economically important lignite seams. Here we will present a detailed examination of core material from this region that will explore aspects of depositional environment, post depositional alteration of organic matter, and establish multiple carbon isotopic profiles that when integrated with biostratigraphic records reveal

the potential of this area to furnish invaluable records of hyperthermal events that address current poorly constrained paleoequatorial conditions.

Chapter 3 shifts this examination northward to the Canadian High Arctic. Here, a comparison of records preserved in paleosols and shales is presented. Further, changing environmental conditions from marine to coastal deposition reflected by changing lithologies and biomarker distributions are shown across the Paleocene-Eocene boundary, as revealed by lithostratigraphy. Also, the hydrogen isotopic composition of *n*-alkanes is examined to elucidate paleohydrological conditions at the time of deposition.

Finally, in Chapter 4 a very different type of paleoenvironmental reconstruction is conducted. There, centennial scale changes within two neighboring high altitude lakes are described over the past 4 millenia. These lakes of the Chilean Altiplano provide a detailed history of recent climatic variations that are poorly established compared to their northern hemisphere counterparts. Examination of biomarker distributions and proxies establishes several times in the past four millennia that lake conditions changed significantly in terms of euxinia, salinity, and lake level as well as biotic community structure.

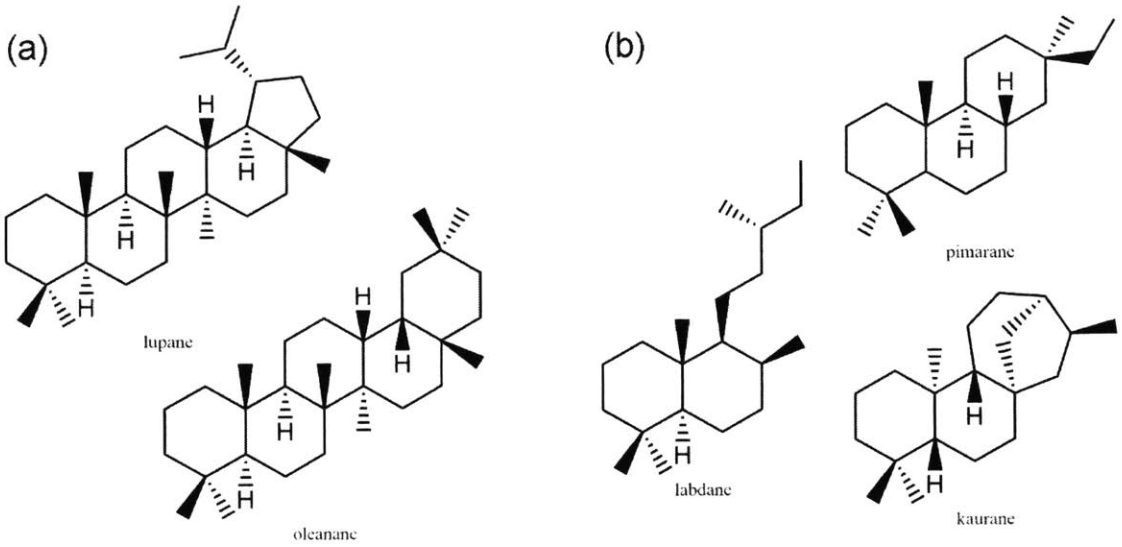

Figure 1.1: Examples of common higher plant molecules commonly used as indicators of (a) angiosperm and (b) gymnosperm content.

References

Aarnes, I., Planke, S., Trulsvik, M., Svensen, H., 2015. Contact metamorphism and thermogenic gas generation in the Vøring and Møre basins, offshore Norway, during the Paleocene–Eocene thermal maximum. J. Geol. Soc. London. 172, 588–598. doi:10.1144/jgs2014-098

Anagnostou, E., John, E.H., Edgar, K.M., Foster, G.L., Ridgwell, A., Inglis, G.N., Pancost, R.D., Lunt, D.J., Pearson, P.N., 2016. Changing atmospheric CO2 concentration was the primary driver of early Cenozoic climate. Nature 533, 380–384. doi:10.1038/nature17423

Beerling, D.J., Royer, D.L., 2011. Convergent Cenozoic CO2 history. Nat. Geosci. 4, 418–420. doi:10.1038/ngeo1186

Berner, R.A., 1997. Geochemistry and Geophysics: The Rise of Plants and Their Effect on Weathering and Atmospheric CO2. Science (80-.). 276, 544–546. doi:10.1126/science.276.5312.544

Birgel, D., Guido, A., Liu, X., Hinrichs, K.-U., Gier, S., Peckmann, J., 2014. Hypersaline conditions during deposition of the Calcare di Base revealed from archaeal di- and tetraether inventories. Org. Geochem. 77, 11–21. doi:10.1016/j.orggeochem.2014.09.002

Bowen, G.J., Maibauer, B.J., Kraus, M.J., Röhl, U., Westerhold, T., Steimke, A., Gingerich, P.D., Wing, S.L., Clyde, W.C., 2014. Two massive, rapid releases of carbon during the onset of the Palaeocene–Eocene thermal maximum. Nat.

Geosci. 8, 44–47. doi:10.1038/ngeo2316

Bray, E.., Evans, E.., 1961. Distribution of n-paraffins as a clue to recognition of source beds. Geochim. Cosmochim. Acta 22, 2–15. doi:10.1016/0016-7037(61)90069-2

Caballero, R., Huber, M., 2013. State-dependent climate sensitivity in past warm climates and its implications for future climate projections. Proc. Natl. Acad. Sci. U. S. A. 110, 14162–7. doi:10.1073/pnas.1303365110

Cooper, J.R., Crelling, J.C., Rimmer, S.M., Whittington, A.G., 2007. Coal metamorphism by igneous intrusion in the Raton Basin, CO and NM: Implications for generation of volatiles. Int. J. Coal Geol. 71, 15–27. doi:10.1016/j.coal.2006.05.007

Cramer, B.S., Kent, D. V., 2005. Bolide summer: The Paleocene/Eocene thermal maximum as a response to an extraterrestrial trigger. Palaeogeogr. Palaeoclimatol. Palaeoecol. 224, 144–166. doi:10.1016/j.palaeo.2005.03.040

Cramer, B.S., Wright, J.D., Kent, D. V., Aubry, M.-P., 2003. Orbital climate forcing of δ 13 C excursions in the late Paleocene-early Eocene (chrons C24n-C25n). Paleoceanography 18, n/a–n/a. doi:10.1029/2003PA000909

Dickens, G.R., O'Neil, J.R., Rea, D.K., Owen, R.M., 1995. Dissociation of oceanic methane hydrate as a cause of the carbon isotope excursion at the end of the Paleocene. Paleoceanography 10, 965–971. doi:10.1029/95PA02087

Diefendorf, A.F., Freeman, K.H., Wing, S.L., Graham, H. V., 2011. Production of n-

alkyl lipids in living plants and implications for the geologic past. Geochim. Cosmochim. Acta 75, 7472–7485. doi:10.1016/j.gca.2011.09.028

Dunkley Jones, T., Lunt, D.J., Schmidt, D.N., Ridgwell, A., Sluijs, A., Valdes, P.J., Maslin, M., 2013. Climate model and proxy data constraints on ocean warming across the Paleocene–Eocene Thermal Maximum. Earth-Science Rev. 125, 123–145. doi:10.1016/j.earscirev.2013.07.004

Eglinton, G., Hamilton, R.J., 1967. Leaf Epicuticular Waxes. Science (80-.). 156, 1322–1335. doi:10.1126/science.156.3780.1322

Eglinton, G., Hamilton, R.J., Martin-Smith, M., 1962. The alkane constituents of some New Zealand plants and their possible taxonomic implications. Phytochemistry 1, 137–145. doi:10.1016/S0031-9422(00)82815-0

Ficken, K.., Li, B., Swain, D.., Eglinton, G., 2000. An n-alkane proxy for the sedimentary input of submerged/floating freshwater aquatic macrophytes. Org. Geochem. 31, 745–749. doi:10.1016/S0146-6380(00)00081-4

Foster, L.C., Pearson, E.J., Juggins, S., Hodgson, D.A., Saunders, K.M., Verleyen, E., Roberts, S.J., 2016. Development of a regional glycerol dialkyl glycerol tetraether (GDGT)–temperature calibration for Antarctic and sub-Antarctic lakes. Earth Planet. Sci. Lett. 433, 370–379. doi:10.1016/j.epsl.2015.11.018

Fricke, H.C., Wing, S.L., 2004. Oxygen isotope and paleobotanical estimates of temperature and 18O-latitude gradients over North America during the early Eocene. Am. J. Sci. 304, 612–635. doi:10.2475/ajs.304.7.612

Galeotti, S., Krishnan, S., Pagani, M., Lanci, L., Gaudio, A., Zachos, J.C., Monechi, S., Morelli, G., Lourens, L., 2010. Orbital chronology of Early Eocene hyperthermals from the Contessa Road section, central Italy. Earth Planet. Sci. Lett. 290, 192–200. doi:10.1016/j.epsl.2009.12.021

Higgins, J.A., Schrag, D.P., 2006. Beyond methane: Towards a theory for the Paleocene–Eocene Thermal Maximum. Earth Planet. Sci. Lett. 245, 523–537. doi:10.1016/j.epsl.2006.03.009

Hopmans, E.C., Weijers, J.W.., Schefuß, E., Herfort, L., Sinninghe Damsté, J.S., Schouten, S., 2004. A novel proxy for terrestrial organic matter in sediments based on branched and isoprenoid tetraether lipids. Earth Planet. Sci. Lett. 224, 107–116. doi:10.1016/j.epsl.2004.05.012

Huang, W.-Y., Meinschein, W.G., 1979. Sterols as ecological indicators. Geochim. Cosmochim. Acta 43, 739–745. doi:10.1016/0016-7037(79)90257-6

Huguet, A., Grossi, V., Belmahdi, I., Fosse, C., Derenne, S., 2015. Archaeal and bacterial tetraether lipids in tropical ponds with contrasting salinity (Guadeloupe, French West Indies): Implications for tetraether-based environmental proxies. Org. Geochem. 83-84, 158–169. doi:10.1016/j.orggeochem.2015.02.010

Inglis, G.N., Collinson, M.E., Riegel, W., Wilde, V., Robson, B.E., Lenz, O.K., Pancost, R.D., 2015. Ecological and biogeochemical change in an early Paleogene peat-forming environment: Linking biomarkers and palynology.

Palaeogeogr. Palaeoclimatol. Palaeoecol. 438, 245–255. doi:10.1016/j.palaeo.2015.08.001

Kennett, J.P., Stott, L.D., 1991. Abrupt deep-sea warming, palaeoceanographic changes and benthic extinctions at the end of the Palaeocene. Nature 353, 225–229. doi:10.1038/353225a0

Kim, J.-H., van der Meer, J., Schouten, S., Helmke, P., Willmott, V., Sangiorgi, F., Koç, N., Hopmans, E.C., Damsté, J.S.S., 2010. New indices and calibrations derived from the distribution of crenarchaeal isoprenoid tetraether lipids: Implications for past sea surface temperature reconstructions. Geochim. Cosmochim. Acta 74, 4639–4654. doi:10.1016/j.gca.2010.05.027

Koch, P.L., Zachos, J.C., Gingerich, P.D., 1992. Correlation between isotope records in marine and continental carbon reservoirs near the Palaeocene/Eocene boundary. Nature 358, 319–322. doi:10.1038/358319a0

Littler, K., Röhl, U., Westerhold, T., Zachos, J.C., 2014. A high-resolution benthic stable-isotope record for the South Atlantic: Implications for orbital-scale changes in Late Paleocene–Early Eocene climate and carbon cycling. Earth Planet. Sci. Lett. 401, 18–30. doi:10.1016/j.epsl.2014.05.054

Loptson, C.A., Lunt, D.J., Francis, J.E., 2014. Investigating vegetation–climate feedbacks during the early Eocene. Clim. Past 10, 419–436. doi:10.5194/cp-10-419-2014

Lourens, L.J., Sluijs, A., Kroon, D., Zachos, J.C., Thomas, E., Röhl, U., Bowles, J.,

Raffi, I., 2005. Astronomical pacing of late Palaeocene to early Eocene global warming events. Nature 435, 1083–7. doi:10.1038/nature03814

Lowenstein, T.K., Demicco, R. V, 2006. Elevated Eocene atmospheric CO2 and its subsequent decline. Science 313, 1928. doi:10.1126/science.1129555

McInerney, F.A., Wing, S.L., 2011. The Paleocene-Eocene Thermal Maximum: A Perturbation of Carbon Cycle, Climate, and Biosphere with Implications for the Future. Annu. Rev. Earth Planet. Sci. 39, 489–516. doi:10.1146/annurev-earth-040610-133431

Moldowan, J.M., Dahl, J., Huizinga, B.J., Fago, F.J., Hickey, L.J., Peakman, T.M., Taylor, D.W., 1994. The molecular fossil record of oleanane and its relation to angiosperms. Science 265, 768–71. doi:10.1126/science.265.5173.768

Pagani, M., Caldeira, K., Archer, D., Zachos, J.C., 2006. An ancient carbon mystery. Science 314, 1556–7. doi:10.1126/science.1136110

Panchuk, K., Ridgwell, A., Kump, L.R., 2008. Sedimentary response to Paleocene-Eocene Thermal Maximum carbon release: A model-data comparison. Geology 36, 315. doi:10.1130/G24474A.1

Pearson, A., Hurley, S.J., Shah Walter, S.R., Kusch, S., Lichtin, S., Zhang, Y.G., 2016. Stable carbon isotope ratios of intact GDGTs indicate heterogeneous sources to marine sediments. Geochim. Cosmochim. Acta 181, 18–35. doi:10.1016/j.gca.2016.02.034

Pearson, E.J., Juggins, S., Talbot, H.M., Weckström, J., Rosén, P., Ryves, D.B.,

Roberts, S.J., Schmidt, R., 2011. A lacustrine GDGT-temperature calibration from the Scandinavian Arctic to Antarctic: Renewed potential for the application of GDGT-paleothermometry in lakes. Geochim. Cosmochim. Acta 75, 6225–6238. doi:10.1016/j.gca.2011.07.042

Powers, L., Werne, J.P., Vanderwoude, A.J., Sinninghe Damsté, J.S., Hopmans, E.C., Schouten, S., 2010. Applicability and calibration of the TEX86 paleothermometer in lakes. Org. Geochem. 41, 404–413. doi:10.1016/j.orggeochem.2009.11.009

Quillévéré, F., Norris, R.D., Kroon, D., Wilson, P.A., 2008. Transient ocean warming and shifts in carbon reservoirs during the early Danian. Earth Planet. Sci. Lett. 265, 600–615. doi:10.1016/j.epsl.2007.10.040

Röhl, U., Westerhold, T., Bralower, T.J., Petrizzo, M.R., Zachos, J.C., 2004. An early Late Paleocene global dissolution event and new constraints for an astronomically tuned Early Paleogene time scale, paper presented at 8th International Conference on Paleoceanography., in: Environ. et Paleonenviron. Oceanique, Biarritz, France. pp. 5–10.

Röhl, U., Westerhold, T., Monechi, S., Thomas, E., Zachos, J.C., Donner, B., 2005. The third and final early Eocene thermal maximum: Characteristics, timing, and mechanisms of the "X" event, in: Geological Society of America.

Scalan, E.., Smith, J.., 1970. An improved measure of the odd-even predominance in the normal alkanes of sediment extracts and petroleum. Geochim. Cosmochim.

Acta 34, 611–620. doi:10.1016/0016-7037(70)90019-0

Schouten, S., Hopmans, E.C., Schefuß, E., Sinninghe Damsté, J.S., 2002. Distributional variations in marine crenarchaeotal membrane lipids: a new tool for reconstructing ancient sea water temperatures? Earth Planet. Sci. Lett. 204, 265–274. doi:10.1016/S0012-821X(02)00979-2

Svensen, H., Planke, S., Malthe-Sørenssen, A., Jamtveit, B., Myklebust, R., Rasmussen Eidem, T., Rey, S.S., 2004. Release of methane from a volcanic basin as a mechanism for initial Eocene global warming. Nature 429, 542–5. doi:10.1038/nature02566

Tierney, J.E., Russell, J.M., Eggermont, H., Hopmans, E.C., Verschuren, D., Sinninghe Damsté, J.S., 2010. Environmental controls on branched tetraether lipid distributions in tropical East African lake sediments. Geochim. Cosmochim. Acta 74, 4902–4918. doi:10.1016/j.gca.2010.06.002

Tripati, A., Elderfield, H., 2005. Deep-sea temperature and circulation changes at the Paleocene-Eocene Thermal Maximum. Science 308, 1894–8. doi:10.1126/science.1109202

Turich, C., Freeman, K.H., 2011. Archaeal lipids record paleosalinity in hypersaline systems. Org. Geochem. 42, 1147–1157. doi:10.1016/j.orggeochem.2011.06.002

Van Aarssen, B.G.K., de Leeuw, J.W., Collinson, M., Boon, J.J., Goth, K., 1994. Occurrence of polycadinene in fossil and recent resins. Geochim. Cosmochim. Acta 58, 223–229. doi:10.1016/0016-7037(94)90459-6

Wang, H., Dong, H., Zhang, C.L., Jiang, H., Zhao, M., Liu, Z., Lai, Z., Liu, W., 2014. Water depth affecting thaumarchaeol production in Lake Qinghai, northeastern Qinghai–Tibetan plateau: Implications for paleo lake levels and paleoclimate. Chem. Geol. 368, 76–84. doi:10.1016/j.chemgeo.2014.01.009

Wang, H., Liu, W., Zhang, C.L., Jiang, H., Dong, H., Lu, H., Wang, J., 2013. Assessing the ratio of archaeol to caldarchaeol as a salinity proxy in highland lakes on the northeastern Qinghai–Tibetan Plateau. Org. Geochem. 54, 69–77. doi:10.1016/j.orggeochem.2012.09.011

Weijers, J.W.H., Schouten, S., Spaargaren, O.C., Sinninghe Damsté, J.S., 2006. Occurrence and distribution of tetraether membrane lipids in soils: Implications for the use of the TEX86 proxy and the BIT index. Org. Geochem. 37, 1680–1693. doi:10.1016/j.orggeochem.2006.07.018

Weijers, J.W.H., Schouten, S., van den Donker, J.C., Hopmans, E.C., Sinninghe Damsté, J.S., 2007. Environmental controls on bacterial tetraether membrane lipid distribution in soils. Geochim. Cosmochim. Acta 71, 703–713. doi:10.1016/j.gca.2006.10.003

Westerhold, T., Röhl, U., Donner, B., McCarren, H.K., Zachos, J.C., 2011. A complete high-resolution Paleocene benthic stable isotope record for the central Pacific (ODP Site 1209). Paleoceanography 26. doi:10.1029/2010PA002092

Westerhold, T., Röhl, U., Laskar, J., Raffi, I., Bowles, J., Lourens, L.J., Zachos, J.C., 2007. On the duration of magnetochrons C24r and C25n and the timing of early

Eocene global warming events: Implications from the Ocean Drilling Program Leg 208 Walvis Ridge depth transect. Paleoceanography 22. doi:10.1029/2006PA001322

Zachos, J.C., Dickens, G.R., Zeebe, R.E., 2008. An early Cenozoic perspective on greenhouse warming and carbon-cycle dynamics. Nature 451, 279–283. doi:10.1038/nature06588

Chapter 2

Biogeochemistry of Early Cenozoic deposits of the Cambay Basin, Western India

Biogeochemistry of Early Cenozoic deposits of the Cambay Basin, Western India

Ross H. WILLIAMS[a]*, Anindya NANDI[b], Jyoti SHARMA[b], Suryendu DUTTA[b], and Roger E. SUMMONS[a]

[a] Department of Earth, Atmospheric and Planetary Sciences, Massachusetts Institute of Technology, 77 Massachusetts Avenue, Cambridge, MA 02139-4307, USA

[b] Department of Earth Sciences, Indian Institute of Technology Bombay, Mumbai-400076, India

*rosshw@mit.edu

Abstract

An extensive analysis has been conducted on a 500 meter drill core taken from the Cambay Basin of Western India near the Valia Lignite mine with the goal of examining evidence of hyperthermal events in this region. The Early Cenozoic hyperthermal events have been of particular importance in light of modern day climate projections, yet extensive study of paleoequatorial conditions at this time remains sparse.

Biomarker distributions, palynology and kerogen typing show that the organic content of the sampled materials is primarily of a terrestrial plant origin. This organic matter has further undergone bacterial degradation, especially in the oldest portion of the core as evidenced by the abundances of degraded *des*-a-triterpenoids, aromatic triterpenoids, pristane/*n*-C17 and phytane/*n*-C18 ratios.

Benthic foraminiferal based biostratigraphy has indicated that the lowermost reaches of the core likely fall in the late Paleocene. Further, palynology corroborates this finding and reveals the presence of an *Apectodinium* acme such as those known for marking the most prominent hyperthermal event, the Paleocene-Eocene Thermal Maximum (PETM). Bulk and compound-specific isotope records illustrate the need for high resolution sampling but also indicate several potential stratigraphic locations of hyperthermal events. Additionally, pyrolysis-GC-IRMS has been used to compare conventional compound-specific isotope analyses of extractable lipids with components of the remaining kerogens and revealed that

such compounds do reliably reflect the same environmental isotopic changes over time as the free hydrocarbons.

2.1. Introduction

The Early Cenozoic has proven to be a valuable asset as a record of what recent Earth was like under increased temperature conditions. While already significantly warmer than present day, it also experienced a series of transient rapid warming events termed the Eocene Thermal Maxima (ETM). The first and most pronounced of these is known as the Paleocene-Eocene Thermal Maximum (PETM, 55.8Ma). During the PETM there was an increase in global temperature of around 5°C (Bralower et al., 1995; Zachos et al., 2003). Due to the magnitude and pace of the PETM, it is often cited as the best recent analogue for future climate projections (Zachos et al., 2008), though it was still a much more gradual process than the contemporary temperature rise (Zeebe et al., 2016). This event was subsequently followed by a less intense anomaly known as ETM2 as well as several others diminishing in magnitude (Cramer et al., 2003; Lourens et al., 2005).

Despite the current interest, the majority of sites known to exhibit the Paleocene-Eocene transition are located at middle to high latitudes (McInerney and Wing, 2011). Furthermore, of the known sites located in the tropics and subtropics, even fewer record significant terrestrial influence (Jaramillo et al., 2010). It is important to expand upon this assemblage of sections to better understand how the biosphere reacted in these types of environments if we want to use this time period to better understand future conditions. Alteration of latitudinal temperature gradients can greatly affect climate models. By providing constraints on the

equatorial conditions models can be better defined and produce results with greater confidence.

During the Early Cenozoic the Indian Plate was moving northward after its separation from Gondwana in the Jurassic on a trajectory leading to subsequent collision with the Asia Plate (Ali and Aitchison, 2005; Reeves and de Wit, 2000). When the hyperthermal events were occurring, Western India was positioned very near to the equator (Acton, 1999). Extensive deposition is known to have occurred in this region in marine marsh-bay complexes that resulted in the formation of economically important lignite bearing formations (Singh et al., 2012, 2010; Thakur et al., 2010). However, only a few prior attempts have been made to locate sedimentary successions that could potentially preserve the events in enough detail to warrant detailed biomarker study of the Early Cenozoic hyperthermals (Samanta et al., 2013a, 2013b).

One method to locate the Paleocene-Eocene transition is through the use of carbon isotopic records. The hyperthermal events themselves were first noted due to concurrent isotopic excursions in carbon and oxygen (Kennett and Stott, 1991). Subsequently it has been demonstrated that the warmings were caused by massive inputs of isotopically light carbon to the ocean-atmosphere system. As such, the formal boundary between these two times is officially assigned to the onset of the carbon isotope excursion. The source of the carbon remains under debate with several possible candidates (Cramer and Kent, 2005; Cramer et al., 2003; DeConto

et al., 2012; Dickens et al.; Higgins and Schrag, 2006; Katz, 1999; Svensen et al., 2004).

While this excursion is often notable in bulk carbon isotope records, it is far more diagnostic when found at a compound-specific level (Handley et al., 2008; Pagani et al., 2006; Tipple et al., 2011). For terrestrial sites it is common practice to analyze paleosol carbonates to establish carbon isotope records (Smith et al., 2007). However, it has been noted that other factors such as temperature and soil moisture can amplify isotopic excursions in these settings (Bowen et al., 2004; McInerney and Wing, 2011) or be subject to alterations due to contributions of allochthonous carbon or changes in microbial degradation (Baczynski et al., 2016). On a molecular level, long chain n-alkanes from higher plants have been commonly utilized due to their recalcitrant nature and common presence (Handley et al., 2008; Pagani et al., 2006; Smith et al., 2007), but other biomarkers should not be precluded. In the present study attempts are made to circumvent the lack of prevalent n-alkanes amenable to isotopic examination by seeking out other compounds that should reflect the same information.

While compound-specific isotope analyses are conventionally applied to the free extractable hydrocarbons there is additional information contained within the dominant macromolecular organic component, namely the kerogen. An alternative method to reveal the nature of this kerogen is through the use of pyrolysis-gas chromatography-mass spectrometry (Py-GC-MS) (Giraud, 1970; Larter and Senftle, 1985). By applying the same pyrolysis conditions to isotopic measurements via

pyrolysis-gas chromatography-isotope ratio mass spectrometry (Py-GC-IRMS) it is possible to examine individual components of kerogen and how they relate to the extractable fraction. This methodology has commonly been applied to meteorites (Okumura and Mimura, 2011; Sephton and Gilmour, 2001) and other molecules such as carbohydrates (González-Pérez et al., 2015) but has yet to be extensively applied to kerogens or in a paleorecord framework.

2.2. Geologic Context

The Cambay Basin lies on the western edge of the Indian subcontinent along the Gulf of Cambay. The region is a peri-cratonic basin that began rifting soon after the Cretaceous Deccan Traps eruptions (Biswas, 1982; Tewari et al., 1995). While the neighboring Kutch basin was first to begin rifting, Tertiary sedimentation is more extensive in the Cambay Basin due to a higher degree of subsidence at that time (Biswas, 1987). The rifting continued into the Miocene and resulted in a horst-graben terrain divided into five main blocks. From North-South these are the Sanchor-Patan, Mehsana-Ahmedabad, Tarapur-Cambay, Jambusar-Broach, and Narmada-Tapti blocks.

Overlying the Deccan Trap floor are extensive Tertiary deposits of sedimentary rocks comprising conglomerates, shales, lignites, greywackes, clays and sandstones (Mishra et al., 2015). Depositional thicknesses in the basin can vary significantly over short distances. Further, lignite seams are often laterally discontinuous and faulting is evident in many exposures which can complicate regional correlations. The Cambay Shale Formation, with its interbedded grey and

carbonaceous shales and lignite beds is a major component of these basins and has been extensively examined in terms of its hydrocarbon source potential (A. Banerjee, 1993, 2002; Mishra et al., 2015), paleoenvironmental (Dutta et al., 2011; Mathews et al., 2015; Paul et al., 2015) and paleontological studies (Clementz et al., 2010; Rose et al., 2009, 2006).

Coring for this study was conducted near Ankleshwar, Gujarat by the Gujarat Mineral Research & Development Society (GMRDS) (Latitude 21° 25' 47" N; Longitude 73° 07' 30" E) (Fig. 2.1). This location is within the southernmost Narmada-Tapti block of the basin. While coring did not reach the Deccan Trap floor, the 501m core contains a very extensive shale interval with lignite beds present towards the base as illustrated by the litholog prepared during coring (Fig. 2.2). The base of the core is clay which likely is derived from the weathering of the underlying trap rock and as such is part of the lowermost sedimentary unit known as the Olpad/Vagadkol formation.

2.3. Methods

Samples were acquired courtesy of the GMRDS and were taken directly after drilling and packaged in clean foil. Approximately 300 samples were taken from the drillhole which is designated borehole U2. Drilling reached a depth of 501 meters and was sampled from 77.5m-501m. Samples were alternatingly designated for micropaleontology, palynology, and biomarker study.

For examination of foraminifera samples were heated and stirred at 80°C with presence of Na_2CO_3 as a dispersing agent. Next, they were cleaned using a 300-mesh sieve and dried. Examination of the distribution of genera was accomplished via microscopy.

Palynology was conducted on six samples (~20g each) from the bottom portion of core. These samples were treated with mild HCl followed by HF and HNO_3. Staining of samples was accomplished using safranin. For microscopy slides were prepared in polyvinyl alcohol and mounted in Canada balsam.

For biomarker examination the outer portion was first removed using a solvent cleaned rock saw. Samples were then powdered using a clean ceramic puck mill and shatterbox. Subsamples were decalcified with 6N HCl for bulk organic carbon isotope analysis. Lipid extraction was accomplished using a Dionex ASE-200 with a solvent mixture of dichloromethane:methanol (DCM:MeOH 9:1). Each sample was extracted until the resulting eluent was clear a minimum of 3 times and maximum of 12. Combusted sand was utilized as a procedural blank every six samples and revealed no significant systemic contamination.

Asphaltenes were removed from the total lipid extract (TLE) by the introduction of excess n-hexane and subsequent cooling overnight at 4°C. The resulting maltene was then desulfurized by the addition of activated copper shot. Subsequently, the maltene was separated into 5 fractions by column chromatography using silica gel 60 (aliphatics: hexane (3/8 DV), aromatics: hexane:DCM 4:1 (2 DV), ketones: DCM (2 DV), acids: DCM:MeOH 1:1 (2 DV) and

alcohols: MeOH (2 DV)). The acid and alcohol fractions were then recombined prior to further analysis.

Kerogen isolation was performed on six samples form the lower core with the goal of concentrating organic matter with minimal alteration. Extracted residues were initially treated with 6N HCl for removal of carbonates. Then a small amount of HCl was added again and HF (32%) for the removal of silicates. Fresh HF was introduced to the sample until the remaining residue appeared free of grit. Samples were then neutralized with ultrapure water and dried.

Bulk rock properties (T_{max}, HI, OI and S2) were determined using a Rock Eval 6. Bulk organic carbon isotopes were measured using a Fisons Elemental Analyzer coupled to a Finnigan DELTA^{plus} XP. Isotopic abundances were assigned relative to reference gas calibrated to VPDB scale with Mix A (n-C_{16} to n-C_{30} alkanes; Arndt Schimmelmann; Indiana University). Measured values were corrected using a suite of standard compounds (CH-6 n=24, Urea n=32, Acetanalide n=60 and NBS-22 n=14). Average standard deviation of replicate analyses was ±0.3‰.

Compound distributions were assessed on an Agilent 6890N gas chromatograph interfaced with a Micromass Autospec Ultima operated in full scan mode with a DB-1MS column (Agilent J&W 60m length, 0.25mm diameter, 0.25µm film). For aliphatics, the oven was programmed to operate at an initial temperature of 60°C for 2 minutes before ramping at 10°C/min to 150C followed by 3°C/min to 330°C where it was held for 19 minutes. For aromatics, the oven the initial

conditions were the same but the ramp rates were altered to a single ramp at 3°C to 330°C where it was held for 30 minutes. Compound-specific isotope analyses were performed using a Thermo Scientific Trace 1310 gas chromatograph coupled to a Thermo MAT 253 via a GC-Isolink II. The GC temperature programs were the same as those used for determining compound distribution above. Isotopic abundances were assigned relative to reference gas calibrated to VPDB scale with Mix A (n=135, n-C_{16} to n-C_{30} alkanes; Arndt Schimmelmann; Indiana University).

Pyrolysis was accomplished with a CDS Analytical 5250-T pyroprobe. Samples were pyrolyzed at 750°C with a ramp of 10°C/mS and held for 60 seconds. For compound identification the pyroprobe was attached to the same Agilent 6890N gas chromatograph interfaced with a Micromass Autospec Ultima. The oven settings were adjusted to an initial temperature of 40°C for 2 minutes followed by a ramp of 4°C/min to 310°C where it was held for 20.5 minutes. For isotopic measurements the pyroprobe was interfaced with a ThermoFinnigan TraceGC coupled to a Finnigan DELTAplus XP via a combustion furnace and water removal interface. To monitor performance, Mix A was now pyrolyzed and checked for isotopic abundance and reproducibility. Isotopic abundances were assigned relative to the same reference gas as above.

2.4. Results

2.4.1. Bulk Rock Properties

Rock-Eval data was obtained for 117 samples throughout the entire core (Table 2.1). Total organic carbon (TOC %) has a minimum value of 0.16% and averages 3.3% but this is skewed by the presence of lignite samples as seen by the maximum value of 45.7% and a median value 1.1%. The average value excluding lignite samples is lower at 1.5%. Samples are predominantly immature with average T_{max} values of 431°C. Excluding one anomalous sample (Depth 449m, T_{max}= 545°C) the next highest T_{max} is 445°C. The hydrogen and oxygen indices (HI & OI) show significant variability with ranges of 21-310 (average 60) for the HI and 25-800 (average 133) for the OI. S2 has an average value of 1 and range of 0.05-34 (excluding lignite samples). The record of $\delta^{13}C_{org}$ displays a clear trend toward less depleted values from the base of the core to the top (Fig. 2.3d). A possible excursion is clear at the bottom of the core (minima at 478m) but it is relatively small (1.5‰) and below what would be expected for this hyperthermal event (2-5‰) (McInerney and Wing, 2011).

2.4.2. Shallow Benthic Zonations and Palynology

Examination of benthic foraminifera has allowed several sections of the core to be assigned to specific shallow benthic zones (SBZ) (Nandi, 2014). The establishment of SBZs is based upon changes in the benthic foraminifera over time. Key marker taxa are assigned to certain zones based upon long term changes in

diversity or morphology. Correlations between these zones and other forms of biostratigraphy or events, such as the onset of the CIE, allow the zones to then be calibrated to certain time intervals (Scheibner and Speijer, 2009; Serra-Kiel et al., 1998).

Towards the base of the core there is a small window in which benthic foraminifera are present from 425.5-443.5m. From 434-443.5m the presence of *N. solitarius* and *N. gamardensis* indicate SBZ 5/6 while 425.5-434m contains *N. burdigalensis keupperi* and *N. burdigalensis burdigalensis* of SBZ 10. Outside of this small window the core is largely unfossiliferous until much higher up from 89.5-239.5m. From 182-239.5m the presence of *N. discorbinus, N. pinfoldi, N. variolarius, N. beaumonti, Operculina* sp. and *Discocyclina* sp. warrant the designation of SBZ 15/16. Proceeding higher to 110.5-182m SBZ 17/18 is assigned based upon the presence of *N. pinfoldi* and *Discoclyclina* sp., *Silvestriella* sp. and *Heterostegina* sp.. Finally, the uppermost core from 89.5-110.5 contains *N. fabianii* and *Pellatispira* sp. of SBZ 19.

Pollen assemblages in the lower core consist of *Spinizonocolpites bulbospinous, Proxapertites, Operculatus, Acanthotricolpites achinatus* and *Acanthotricolpites kutchensis* (Fig. 2.4). Further, the dinocysts present in these samples are *Apectodinium hypercanthum, Apectodinium homomorphum, Spiniferites, Achomosphaera, Operculodinium* sp., *Polysphaeridium subtile*, and *Cordosphaeridium*. However, the *Apectodinium* sp. are only present in a single sample in which they dominate at 488m. Members of the *Apectodinium* genus are

not found in any of the samples above or below this depth despite the presence of other dinocysts. Also present above this depth are fungal fruiting bodies.

2.4.3. Compound Distributions

Overall aliphatic compound distributions remained relatively consistent throughout the core. Total ion chromatograms are dominated by a large and complex assemblage of oleanane/ursane compounds in both mono/di-unsaturated and saturated forms (Fig. 2.5). The extensive co-elution of peaks precludes the confident identification of specific structures. Other significant late eluting compounds include the C_{31} and C_{32} 17β, 21β(H)-hopanes. Further, immediately prior to the elution of pentacyclic triterpenoids appear several distinct peaks for C_{29} diasterenes. Another major feature of the chromatograms is the presence of numerous *des*-a-triterpenoids, again in unsaturated and saturated forms. Pristane (Pr) and phytane (Ph) are also usually present in high abundance. Notable however is the fact that the *n*-alkane contribution appears very low relative to other compound classes. Examination of the *m/z* 85 extracted ion chromatogram (EIC) was thus utilized to study the *n*-alkane distributions. The average chain length (ACL) of *n*-alkanes ($C_{23\text{-}35}$) remains relatively constant (average: 27.8) through most of the core (Fig. 2.3c). The carbon preference index (CPI) however rises from ~1.8 in the lower core to ~5.6 in the upper portion (Fig. 2.3b). When plotted against one another Pr/*n*-C_{17} and Ph/*n*-C_{18} reveal that the lower 100 meters of core are distinctly different that the overlying deposits (Fig. 2.6). In general this lower portion contains significantly less *n*-alkane content relative to the isoprenoidal compounds.

Examination of the aromatic fractions reveals wide variety of compounds that were not readily identifiable in the absence of authentic standards. However, their mass spectra suggested they are dominated by aromatized analogs of the oleanoid triterpenoids that occurred in the saturate hydrocarbon fraction (Fig. 2.5) and which are characteristic of angiosperm flora. Further, there is also a suite of polycyclic aromatic hydrocarbons. However, there was no evidence of retene or other markers typical of a conifer contribution.

Pyrolysis experiments on isolated kerogens afforded suites of small aromatic compounds (Fig. 2.5). Only mono- and bicyclic structures were identified and they decreased in abundance with increasing size. The most abundant compounds were toluene and phenol. Lesser amounts of methylated analogs, indenes, and napthalenes are also present. A trace of cadalene was often the last eluting, identifiable compound. Pyrolysis of the kerogens also produced elemental sulfur. Aliphatic compounds were never prominent in any of the pyrograms.

2.4.4. Compound-specific Isotope Analyses

A suite of compounds was chosen based on their prevalence throughout the sediment section, their abundances and the absence of co-eluting compounds that may have adversely affects the isotopic analysis. In the saturate fraction pristane, *n*-C_{17}, and C_{31} 17β, 21β(H)-hopanes meet these criteria (Fig. 2.3e-h). To provide a useful higher plant record the aromatic fraction was also processed due to the presence of cadalene which has a higher plant origin. These records were not accessible in the upper portion of the core as a consequence of the lower TOC values

and the absence of sufficient analyte abundances for reliable isotopic measurements.

The overall records for each of these compounds showed little consistent trend. There were numerous small anomalies but they were rarely concurrent across samples. One notable exception to this general finding was an isotope shift that occurred across all compounds and the bulk organic carbon record at 478m. The 17β, 21β(H)-homohopane record appeared to be the most 'noisy' compared to the others, likely due to the bacterial sources being prone to great variability over time.

Several samples were selected for kerogen isolation because they showed similar isotopic variability across a range of compounds. The pyrolysates of these kerogens were predominately composed of small aromatic compounds. Of these, the most prominent to provide clean isotope peaks were toluene, phenol and naphthalene. Direct comparison of the results obtained by Py-GC-IRMS to the free hydrocarbons in the same samples reveals that the kerogen components preserve the same small isotopic excursion as the compounds present in the extractable bitumen (Fig. 2.7).

2.5. Discussion

2.5.1. Biostratigraphic Age

Shallow benthic zonations have been established that provide age constraints throughout the Early Paleogene (Serra-Kiel et al., 1998). Most of the upper core is assigned to SBZs 15-19 by these fossil indices thereby providing an upper age limit

of our studied section at roughly 35 Ma. Age determinations remain consistent and well resolved until nearly halfway down core to a depth of 239.5 at SBZ 15/16. This places the lower age limit of the upper core at roughly 42-44 Ma.

The barren nature of the lower sections of the core precluded the establishment of a lower age limit. However, several samples at depths 434-443.5m fell into the SBZ 5/6 range. The boundary between the Paleocene and Eocene has already been established to have occurred at the base of SBZ 5 based upon larger benthic foraminifera index fossils from the Galala Mountains section in Egypt (Scheibner and Speijer, 2009). The age range for this lowermost zone would thus be between 55-56Ma. Therefore, if the PETM or other hyperthermal events are present in the section they would be occurring within this lowermost portion. This is corroborated by the presence of the dinocyst *Apectodinium parvum* in the bottommost section of the cored interval. This taxon is assigned to the nanoplankton zone NP9-10 which corresponds to SBZ4-8. Combined with the presence of an *Apectodinium* acme at 488m it is likely that the coring did, in fact, capture the Paleocene-Eocene transition and encompasses the hyperthermal events in the bottom 50m.

2.5.2. Depositional Environment

Examination of pollen from the lower portion of core has uncovered information on the paleofloral composition of the region. Most of the pollen identified was angiosperm in origin and of that the predominant group was the Arecaceae (Palmae). There was no evidence of any temperate flora. Further, the

presence of pollen related to extant *Nypa* was notable. *Nypa* sp. pollen has been shown to have very low productivity and their large grains are often not distributed great distances (Muller, 1968). Therefore, this pollen assemblage establishes that the sedimentary section was deposited in a coastal marsh environment. Further, the presence of fungal fruiting bodies also points to warm, humid conditions. Further, the noted pyritic nature of many of the samples (Nandi, 2014) indicates that there was marine influence during deposition. Examination of lignites in the field showed both massive pyrites and pyrite coated plant remains such as roots. This is also supported by the release of elemental sulfur during pyrolysis of isolated kerogens and the presence of benzothiophene in the pyrograms. When all factors are considered it is clear that the paleofloral composition was that of a densely vegetated tropical marsh system with marine influence. Similar conclusions have been drawn in other nearby studies (Mathews et al., 2015; Monga et al., 2015; Prasad et al., 2013; Rao et al., 2013; Samant and Phadtare, 1997).

2.5.3. Biomarker Source and Alteration

Consistent with the palynological results the extracted hydrocarbons are dominated by compounds characteristic of higher plants. The most prominent feature is the large number or saturated and unsaturated pentacyclic triterpenes including oleanoids and lupanoids, that are indicative of angiosperms. Further, it is known that the proportion of oleanoids is enhanced in systems with seawater influence during early diagenesis (Murray et al., 1997). Given the multiple lines of complementary evidence of coastal marsh environment and the pyritic nature of the

lignites in this area it is highly likely that this is the case. Analyses of the aromatic hydrocarbon fractions also revealed a number of aromatized counterparts to these molecules, as well as the presence of cadalene, a generic higher plant marker. Notably undetected in the higher plant hydrocarbon assemblage were bicadinanes which in the past have been identified from analysis of resins in this area (Dutta et al., 2009).

Analysis of the pyrolysis products from isolated kerogen corroborates the higher plant origin of the hydrocarbons. The primary dominance of phenolic and benzene type compounds over aliphatics is a key characteristic of kerogens from terrestrial sources (Horsfield, 1997, 1989; Togunwa et al., 2015). The relative proportion of xylenes, phenol and *n*-octene are often used for kerogen typing (Larter, 1984). If applied to kerogens from this core they fall within the range of type III kerogens, consistent with Rock-Eval and extractable biomarker distributions.

It is evident that the compounds present in the studied section have been affected by a high degree of bacterial degradation. Most striking is the fact that despite the heavy higher plant influence there are only minor amounts of *n*-alkanes relative to other compounds. While it is known that different plants produce varying amounts of alkanes this information does not extend to the Arecaceae to the author's knowledge. The paucity of alkanes is exemplified by the high levels of pristane and phytane relative to *n*-C_{17} and *n*-C_{18} (Fig. 2.6), though this is also influenced by the potential deposition being in a reducing environment. The

straight chain alkanes are more easily degraded that the isoprenoids and over time their relative amount will decrease under these conditions. Further, a number of bacterial lipids are present in high amounts such as the ßß-hopanes. Also, there is always a clear presence of *des*-a-triterpenoids. These are formed from bacterial degradation of the pentacyclic triterpenoids (Trendel et al., 1989) which are abundant in great variety throughout this study. Corresponding to the wide variety of intact pentacyclics, the *des*-a-triterpenoids are also present in numerous saturated, mono- and di-unsaturated forms. Additionally, the aromatic triterpenoids are also thought to be the result of biodegradation (Laflamme and Hites, 1979; Wakeham et al., 1980).

2.5.4. Potential for Hyperthermal Study

A number of hurdles exist in utilizing the acquired samples to examine hyperthermal events. The primary issue is that the original survey sampling precluded the acquisition of high resolution coverage. Samples had to be acquired at the drill site with limited time to do so and, as is customary for cores acquired for evaluation of the heat content of lignites, the remaining material was not able to be archived. Further, without prior knowledge of the potential location of the hyperthermal events it was not possible to refine the sampling resolution to accommodate. Sediment thickness in this region can vary dramatically and knowledge of potential structural features such as faulting is required also to make such a decision. However, despite these limitations some information can be

gathered that should assist in future geochemical and palynological exploration in this particular setting.

First, the establishment of age constraints has indicated that the targeted Early Eocene time interval likely was captured within the sampling window (Fig. 2.8). Since coring did not bottom out in the temporally characterized Deccan Trap the establishment of this fact is paramount for having confidence in further study at this location. Second, the presence of an *Apectodinium* acme at 488m is an indication that the PETM is possibly located around that depth. While there is no strong bulk carbon isotope excursion at that time in most parameters there is one in the bacterial record. It is therefore likely that the sampling came close to the event and while missing the main excursion captured a shoulder/recovery period instead. Finally, the presence of a small excursion soon after at 478m across all represented groups could therefore be a subsequent event such as ETM2.

2.5.5. Application of Pyrolysis-GC-IRMS

Despite the complex nature of kerogen a wealth of information may lie in the compounds formed from its pyrolysis. The results of this study indicate that individual components of kerogen also record natural isotopic excursions. Given the subset of samples chosen there is little difference in the isotopic record. While the compounds formed from the pyrolysis of the kerogens in this core are all simple aromatics, their distribution still points to a terrestrial higher plant source. Further, given the low maturity of the sedimentary section (as shown by Rock Eval and hydrocarbon biomarker maturity ratios) combined with the fact that we

analysed isolated kerogens, we can be confident that later implantation of hydrocarbons due to oil migration through the rock is unlikley. Further, this method has potential for alternative applications such as examining the biogenicity of ancient kerogens or isotopic examination of organic rich deposits such as coals or even resins.

2.6. Conclusions

The Cambay Basin in the Gujarat state of northwestern India has proven to be an area of interest for the possible study of Early Cenozoic hyperthermal events. The combination of biostratigraphic age constraints, dinocyst population dynamics, and compound-specific isotope analysis have shown that the lowermost sedimentation of the basin likely preserves these events. Further drilling and high resolution sampling of core material from this region could be extremely valuable in revealing equatorial climate dynamics across periods of rapid extreme warming.

Acknowledgements

This research was supported by the NASA Astrobiology Institute (NNA13AA90A) Foundations of Complex Life, Evolution, Preservation, and Detection on Earth and Beyond. Travel to and from India in the conduct of this collaboration was funded by the MISTI-India Innovation Seed Fund. We would like to thank Carolyn Colonero for key instrumentation support.

References

A. Banerjee, K.L.N.Rao, 1993. Geochemical Evaluation of Part of the Cambay Basin, India. Am. Assoc. Pet. Geol. Bull. 77, 29–48.

A. Banerjee, Pahari, S., Jha, M., Sinha, A.K., Jain, A.K., Kumar, N., Thomas, N.J., Misra, K.N., Chandra, K., 2002. The effective source rocks in the Cambay basin, India. Am. Assoc. Pet. Geol. Bull. 86, 433–456.

Acton, G.D., 1999. Apparent Polar Wander of India Since the Cretaceous With Implications for Regional Tectonics and True Polar Wander. Mem. Geol. Soc. India 129–175.

Ali, J.R., Aitchison, J.C., 2005. Greater India. Earth-Science Rev. 72, 169–188. doi:10.1016/j.earscirev.2005.07.005

Baczynski, A.A., McInerney, F.A., Wing, S.L., Kraus, M.J., Morse, P.E., Bloch, J.I., Chung, A.H., Freeman, K.H., 2016. Distortion of carbon isotope excursion in bulk soil organic matter during the Paleocene-Eocene thermal maximum. Geol. Soc. Am. Bull. B31389.1. doi:10.1130/B31389.1

Biswas, S.K., 1987. Regional tectonic framework, structure and evolution of the western marginal basins of India. Tectonophysics 135, 307–327. doi:10.1016/0040-1951(87)90115-6

Biswas, S.K., 1982. Rift Basins in Western Margin of India and Their Hydrocarbon Prospects with Special Reference to Kutch Basin. Am. Assoc. Pet. Geol. Bull. 6

Bowen, G.J., Beerling, D.J., Koch, P.L., Zachos, J.C., Quattlebaum, T., 2004. A humid climate state during the Palaeocene/Eocene thermal maximum. Nature 432, 495–499. doi:10.1038/nature031156, 1497–1513.

Bralower, T.J., Zachos, J.C., Thomas, E., Parrow, M., Paull, C.K., Kelly, D.C., Silva, I.P., Sliter, W. V., Lohmann, K.C., 1995. Late Paleocene to Eocene paleoceanography of the equatorial Pacific Ocean: Stable isotopes recorded at Ocean Drilling Program Site 865, Allison Guyot. Paleoceanography 10, 841–865. doi:10.1029/95PA01143

Clementz, M., Bajpai, S., Ravikant, V., Thewissen, J.G.M., Saravanan, N., Singh, I.B., Prasad, V., 2010. Early Eocene warming events and the timing of terrestrial faunal exchange between India and Asia. Geology 39, 15–18. doi:10.1130/G31585.1

Cramer, B.S., Kent, D. V., 2005. Bolide summer: The Paleocene/Eocene thermal maximum as a response to an extraterrestrial trigger. Palaeogeogr. Palaeoclimatol. Palaeoecol. 224, 144–166. doi:10.1016/j.palaeo.2005.03.040

Cramer, B.S., Wright, J.D., Kent, D. V., Aubry, M.-P., 2003. Orbital climate forcing of δ 13 C excursions in the late Paleocene-early Eocene (chrons C24n-C25n). Paleoceanography 18, n/a–n/a. doi:10.1029/2003PA000909

DeConto, R.M., Galeotti, S., Pagani, M., Tracy, D., Schaefer, K., Zhang, T., Pollard, D., Beerling, D.J., 2012. Past extreme warming events linked to massive carbon release from thawing permafrost. Nature 484, 87–91. doi:10.1038/nature10929

Dickens, G.R., O'Neil, J.R., Rea, D.K., Owen, R.M., 1995. Dissociation of oceanic methane hydrate as a cause of the carbon isotope excursion at the end of the Paleocene. Paleoceanography 10, 965–971. doi:10.1029/95PA02087

Dutta, S., Mallick, M., Bertram, N., Greenwood, P.F., Mathews, R.P., 2009. Terpenoid composition and class of Tertiary resins from India. Int. J. Coal Geol. 80, 44–50. doi:10.1016/j.coal.2009.07.006

Dutta, S., Mathews, R.P., Singh, B.D., Tripathi, S.M., Singh, A., Saraswati, P.K., Banerjee, S., Mann, U., 2011. Petrology, palynology and organic geochemistry of Eocene lignite of Matanomadh, Kutch Basin, western India: Implications to depositional environment and hydrocarbon source potential. Int. J. Coal Geol. 85, 91–102. doi:10.1016/j.coal.2010.10.003

Giraud, A., 1970. Application of Pyrolysis and Gas Chromatography to Geochemical Characterization of Kerogen in Sedimentary Rock. Am. Assoc. Pet. Geol. Bull. 54, 439–455.

González-Pérez, J.A., Jiménez-Morillo, N.T., de la Rosa, J.M., Almendros, G., González-Vila, F.J., 2015. Compound-specific stable carbon isotopic signature of carbohydrate pyrolysis products from C3 and C4 plants. J. Sci. Food Agric. doi:10.1002/jsfa.7169

Handley, L., Pearson, P.N., McMillan, I.K., Pancost, R.D., 2008. Large terrestrial and marine carbon and hydrogen isotope excursions in a new Paleocene/Eocene boundary section from Tanzania. Earth Planet. Sci. Lett. 275, 17–25.

doi:10.1016/j.epsl.2008.07.030

Higgins, J.A., Schrag, D.P., 2006. Beyond methane: Towards a theory for the Paleocene–Eocene Thermal Maximum. Earth Planet. Sci. Lett. 245, 523–537. doi:10.1016/j.epsl.2006.03.009

Horsfield, B., 1997. The Bulk Composition of First-Formed Petroleum in Source Rocks, in: Welte, D.H., Horsfield, B., Baker, D.R. (Eds.), Petroleum and Basin Evolution. Springer Berlin Heidelberg, Berlin, Heidelberg, pp. 335–402. doi:10.1007/978-3-642-60423-2

Horsfield, B., 1989. Practical criteria for classifying kerogens: Some observations from pyrolysis-gas chromatography. Geochim. Cosmochim. Acta 53, 891–901. doi:10.1016/0016-7037(89)90033-1

Jaramillo, C., Ochoa, D., Contreras, L., Pagani, M., Carvajal-Ortiz, H., Pratt, L.M., Krishnan, S., Cardona, A., Romero, M., Quiroz, L., Rodriguez, G., Rueda, M.J., de la Parra, F., Morón, S., Green, W., Bayona, G., Montes, C., Quintero, O., Ramirez, R., Mora, G., Schouten, S., Bermudez, H., Navarrete, R., Parra, F., Alvarán, M., Osorno, J., Crowley, J.L., Valencia, V., Vervoort, J., 2010. Effects of rapid global warming at the Paleocene-Eocene boundary on neotropical vegetation. Science 330, 957–61. doi:10.1126/science.1193833

Katz, M.E., 1999. The Source and Fate of Massive Carbon Input During the Latest Paleocene Thermal Maximum. Science (80-.). 286, 1531–1533. doi:10.1126/science.286.5444.1531

Kennett, J.P., Stott, L.D., 1991. Abrupt deep-sea warming, palaeoceanographic changes and benthic extinctions at the end of the Palaeocene. Nature 353, 225–229. doi:10.1038/353225a0

Laflamme, R.E., Hites, R.A., 1979. Tetra- and pentacyclic, naturally-occurring, aromatic hydrocarbons in recent sediments. Geochim. Cosmochim. Acta 43, 1687–1691. doi:10.1016/0016-7037(79)90188-1

Larter, S.R., 1984. Application of analytical pyrolysis techniques to kerogen characterization and fossil fuel exploration/exploitation, in: Analytical Pyrolysis. Elsevier, pp. 212–275. doi:10.1016/B978-0-408-01417-5.50012-3

Larter, S.R., Senftle, J.T., 1985. Improved kerogen typing for petroleum source rock analysis. Nature 318, 277–280. doi:10.1038/318277a0

Lourens, L.J., Sluijs, A., Kroon, D., Zachos, J.C., Thomas, E., Röhl, U., Bowles, J., Raffi, I., 2005. Astronomical pacing of late Palaeocene to early Eocene global warming events. Nature 435, 1083–7. doi:10.1038/nature03814

Mathews, R., Singh, H., Singh, V.P., Singh, B.D., Singh, A., 2015. Organic composition and palaeoenvironment of Valia Lignite Deposit (Cambay Basin), Gujarat, western India: inferences from palynology and petrography, in: ICCP Meeting and Symposium 2015.

McInerney, F.A., Wing, S.L., 2011. The Paleocene-Eocene Thermal Maximum: A Perturbation of Carbon Cycle, Climate, and Biosphere with Implications for the Future. Annu. Rev. Earth Planet. Sci. 39, 489–516. doi:10.1146/annurev-earth-

040610-133431

Mishra, S., Mani, D., Kavitha, S., Patil, D.J., Kalpana, M.S., Vyas, D.U., Dayal, A.M., 2015. Pyrolysis results of shales from the South Cambay basin, India: Implications for gas generation potential. J. Geol. Soc. India 85, 647–656. doi:10.1007/s12594-015-0262-z

Monga, P., Kumar, M., Prasad, V., Joshi, Y., 2015. Palynostratigraphy, palynofacies and depositional environment of a lignite-bearing succession at Surkha Mine, Cambay Basin, north-western India. Acta Palaeobot. 55, 183–207. doi:10.1515/acpa-2015-0010

Muller, J., 1968. Palynology of the Pedawan and Plateau Sandstone Formations (Cretaceous-Eocene) in Sarawak, Malaysia on JSTOR. Micropaleontology 14, 1–37.

Murray, A.P., Sosrowidjojo, I.B., Alexander, R., Kagi, R.I., Norgate, C.M., Summons, R.E., 1997. Oleananes in oils and sediments: Evidence of marine influence during early diagenesis? Geochim. Cosmochim. Acta 61, 1261–1276. doi:10.1016/S0016-7037(96)00408-5

Nandi, A., 2014. Biostratigraphy and Organic Geochemical Characterization of the Eocene Section from Valia, near Ankleshwar, Cambay Basin, Western India. Indian Institute of Technology Bombay.

Okumura, F., Mimura, K., 2011. Gradual and stepwise pyrolyses of insoluble organic matter from the Murchison meteorite revealing chemical structure and

isotopic distribution. Geochim. Cosmochim. Acta 75, 7063–7080. doi:10.1016/j.gca.2011.09.015

Pagani, M., Pedentchouk, N., Huber, M., Sluijs, A., Schouten, S., Brinkhuis, H., Sinninghe Damsté, J.S., Dickens, G.R., Backman, J., Clemens, S., Cronin, T., Eynaud, F., Gattacceca, J., Jakobsson, M., Jordan, R., Kaminski, M., King, J., Koc, N., Martinez, N.C., McInroy, D., Moore Jr, T.C., O'Regan, M., Onodera, J., Pälike, H., Rea, B., Rio, D., Sakamoto, T., Smith, D.C., St John, K.E.K., Suto, I., Suzuki, N., Takahashi, K., Watanabe, M., Yamamoto, M., 2006. Arctic hydrology during global warming at the Palaeocene/Eocene thermal maximum. Nature 442, 671–675. doi:10.1038/nature05043

Paul, S., Sharma, J., Singh, B.D., Saraswati, P.K., Dutta, S., 2015. Early Eocene equatorial vegetation and depositional environment: Biomarker and palynological evidences from a lignite-bearing sequence of Cambay Basin, western India. Int. J. Coal Geol. 149, 77–92. doi:10.1016/j.coal.2015.06.017

Prasad, V., Singh, I.B., Bajpai, S., Garg, R., Thakur, B., Singh, A., Saravanan, N., Kapur, V.V., 2013. Palynofacies and sedimentology-based high-resolution sequence stratigraphy of the lignite-bearing muddy coastal deposits (early Eocene) in the Vastan Lignite Mine, Gulf of Cambay, India. Facies 59, 737–761. doi:10.1007/s10347-012-0355-8

Rana, R.S., Kumar, K., Singh, H., 2004. Vertebrate fauna from the subsurface Cambay Shale (Lower Eeocene), Vastan Lignite Mine, Gujarat, India. Curr. Sci.

87, 1726–1733.

Rao, M.R., Sahni, A., Rana, R.S., Verma, P., 2013. Palynostratigraphy and depositional environment of Vastan Lignite Mine (Early Eocene), Gujarat, western India. J. Earth Syst. Sci. 122, 289–307. doi:10.1007/s12040-013-0280-4

Reeves, C., de Wit, M., 2000. Making ends meet in Gondwana: retracing the transforms of the Indian Ocean and reconnecting continental shear zones. Terra Nov. 12, 272–280. doi:10.1046/j.1365-3121.2000.00309.x

Rose, K.D., Rana, R.S., Sahni, A., Kumar, K., Singh, L., Smith, T., 2009. First Tillodont from India: Additional Evidence for an Early Eocene Faunal Connection between Europe and India? Acta Palaeontol. Pol. 54, 351–355. doi:10.4202/app.2008.0067

Rose, K.D., Smith, T., Rana, R.S., Sahni, A., Singh, H., Missiaen, P., Folie, A., 2006. Early Eocene (Ypresian) continental vertebrate assemblage from India, with description of a new anthracobunid (Mammalia, Tethytheria). J. Vertebr. Paleontol. 26, 219–225. doi:10.1671/0272-4634(2006)26[219:EEYCVA]2.0.CO;2

Samant, B., Phadtare, N.R., 1997. Stratigraphic palynoflora of the Early Eocene Rajpardi lignite, Gujarat andthe lower age limit of the Tarkeswar Formation of South Cambay Basin, India. Palaeontogr. Abteilung B 1–108.

Samanta, A., Bera, M.K., Ghosh, R., Bera, S., Filley, T., Pande, K., Rathore, S.S., Rai, J., Sarkar, A., 2013a. Do the large carbon isotopic excursions in terrestrial organic matter across Paleocene–Eocene boundary in India indicate

intensification of tropical precipitation? Palaeogeogr. Palaeoclimatol. Palaeoecol. 387, 91–103. doi:10.1016/j.palaeo.2013.07.008

Samanta, A., Sarkar, A., Bera, M.K., Rai, J., Rathore, S.S., 2013b. Late Paleocene–early Eocene carbon isotope stratigraphy from a near-terrestrial tropical section and antiquity of Indian mammals. J. Earth Syst. Sci. 122, 163–171. doi:10.1007/s12040-012-0259-6

Scheibner, C., Speijer, R.P., 2009. Recalibration of the Tethyan shallow-benthic zonation across the Paleocene-Eocene boundary: the Egyptian record. Geol. Acta. doi:10.1344/105.000000267

Sephton, M.A., Gilmour, I., 2001. Pyrolysis–gas chromatography–isotope ratio mass spectrometry of macromolecular material in meteorites. Planet. Space Sci. 49, 465–471. doi:10.1016/S0032-0633(00)00163-X

Serra-Kiel, J., Hottinger, L., Caus, E., Drobne, K., Ferrandez, C., Jauhri, A.K., Less, G., Pavlovec, R., Pignatti, J., Samso, J.M., Others, A., 1998. Larger foraminiferal biostratigraphy of the Tethyan Paleocene and Eocene. Bull. la Société Géologique Fr. 169, 281–299.

Singh, A., Thakur, O.P., Singh, B.D., 2012. Petrographic and depositional characteristics of Tadkeshwar lignite deposits (Cambay Basin), Gujarat. J. Geol. Soc. India 80, 329–340. doi:10.1007/s12594-012-0151-7

Singh, P.K., Singh, M.P., Singh, A.K., 2010. Petro-chemical characterization and evolution of Vastan Lignite, Gujarat, India. Int. J. Coal Geol. 82, 1–16.

doi:10.1016/j.coal.2010.01.003

Smith, F.A., Wing, S.L., Freeman, K.H., 2007. Magnitude of the carbon isotope excursion at the Paleocene–Eocene thermal maximum: The role of plant community change, Earth and Planetary Science Letters. doi:10.1016/j.epsl.2007.07.021

Svensen, H., Planke, S., Malthe-Sørenssen, A., Jamtveit, B., Myklebust, R., Rasmussen Eidem, T., Rey, S.S., 2004. Release of methane from a volcanic basin as a mechanism for initial Eocene global warming. Nature 429, 542–5. doi:10.1038/nature02566

Tewari, H.C., Dixit, M.M., Sarkar, D., 1995. Relationship of the Cambay rift basin to the Deccan volcanism. J. Geodyn. 20, 85–95. doi:10.1016/0264-3707(94)00025-Q

Thakur, O.P., Singh, A., Singh, B.D., 2010. Petrographic characterization of Khadsaliya lignites, Bhavnagar district, Gujarat. J. Geol. Soc. India 76, 40–46. doi:10.1007/s12594-010-0079-8

Tipple, B.J., Pagani, M., Krishnan, S., Dirghangi, S.S., Galeotti, S., Agnini, C., Giusberti, L., Rio, D., 2011. Coupled high-resolution marine and terrestrial records of carbon and hydrologic cycles variations during the Paleocene–Eocene Thermal Maximum (PETM). Earth Planet. Sci. Lett. 311, 82–92. doi:10.1016/j.epsl.2011.08.045

Togunwa, O.S., Abdullah, W.H., Hakimi, M.H., Barbeito, P.J., 2015. Organic geochemical and petrographic characteristics of Neogene organic-rich sediments from the onshore West Baram Delta Province, Sarawak Basin: Implications for source rocks and hydrocarbon generation potential. Mar. Pet. Geol. 63, 115–126. doi:10.1016/j.marpetgeo.2015.02.032

Trendel, J.M., Lohmann, F., Kintzinger, J.P., Albrecht, P., Chiarone, A., Riche, C., Cesario, M., Guilhem, J., Pascard, C., 1989. Identification of des-A-triterpenoid hydrocarbons occurring in surface sediments. Tetrahedron 45, 4457–4470. doi:10.1016/S0040-4020(01)89081-5

Wakeham, S.G., Schaffner, C., Giger, W., 1980. Poly cyclic aromatic hydrocarbons in Recent lake sediments—II. Compounds derived from biogenic precursors during early diagenesis. Geochim. Cosmochim. Acta 44, 415–429. doi:10.1016/0016-7037(80)90041-1

Zachos, J.C., Dickens, G.R., Zeebe, R.E., 2008. An early Cenozoic perspective on greenhouse warming and carbon-cycle dynamics. Nature 451, 279–283. doi:10.1038/nature06588

Zachos, J.C., Wara, M.W., Bohaty, S., Delaney, M.L., Petrizzo, M.R., Brill, A., Bralower, T.J., Premoli-Silva, I., 2003. A transient rise in tropical sea surface temperature during the Paleocene-Eocene thermal maximum. Science 302, 1551–4. doi:10.1126/science.1090110

Zeebe, R.E., Ridgwell, A., Zachos, J.C., 2016. Anthropogenic carbon release rate

unprecedented during the past 66 million years. Nat. Geosci. 9, 325–329. doi:10.1038/ngeo2681

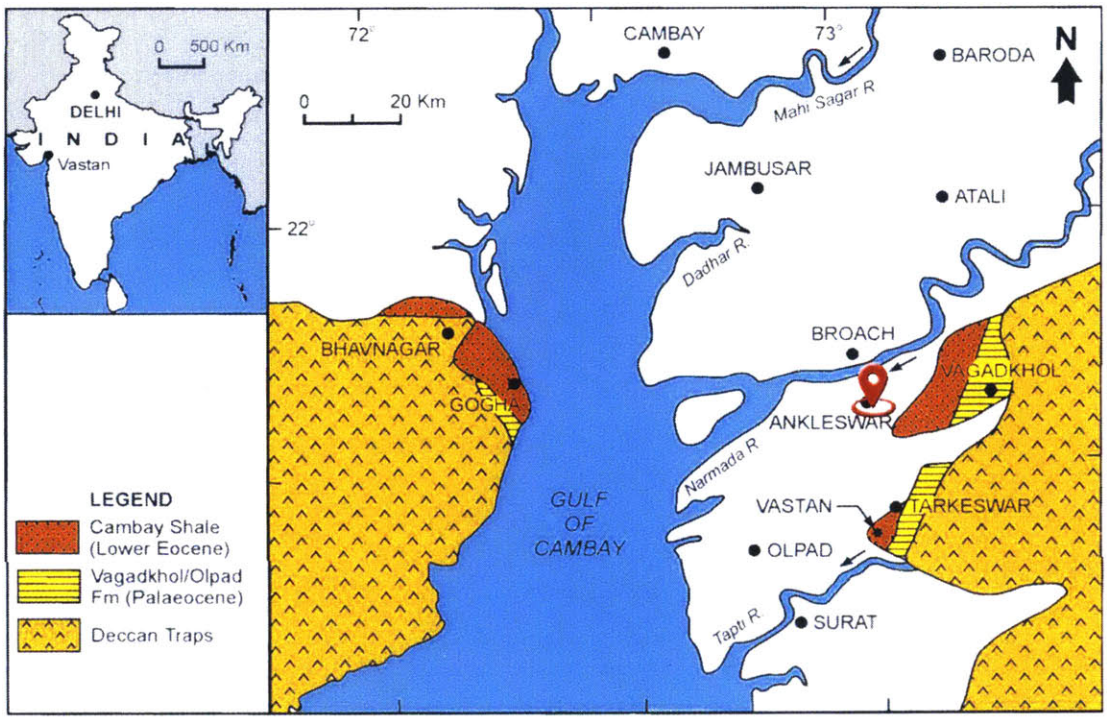

Figure 2.1: Map of the study area with drill site marked. Regional outcroppings of Cretaceous-Eocene deposits are illustrated. Adapted from Rana et al., 2004.

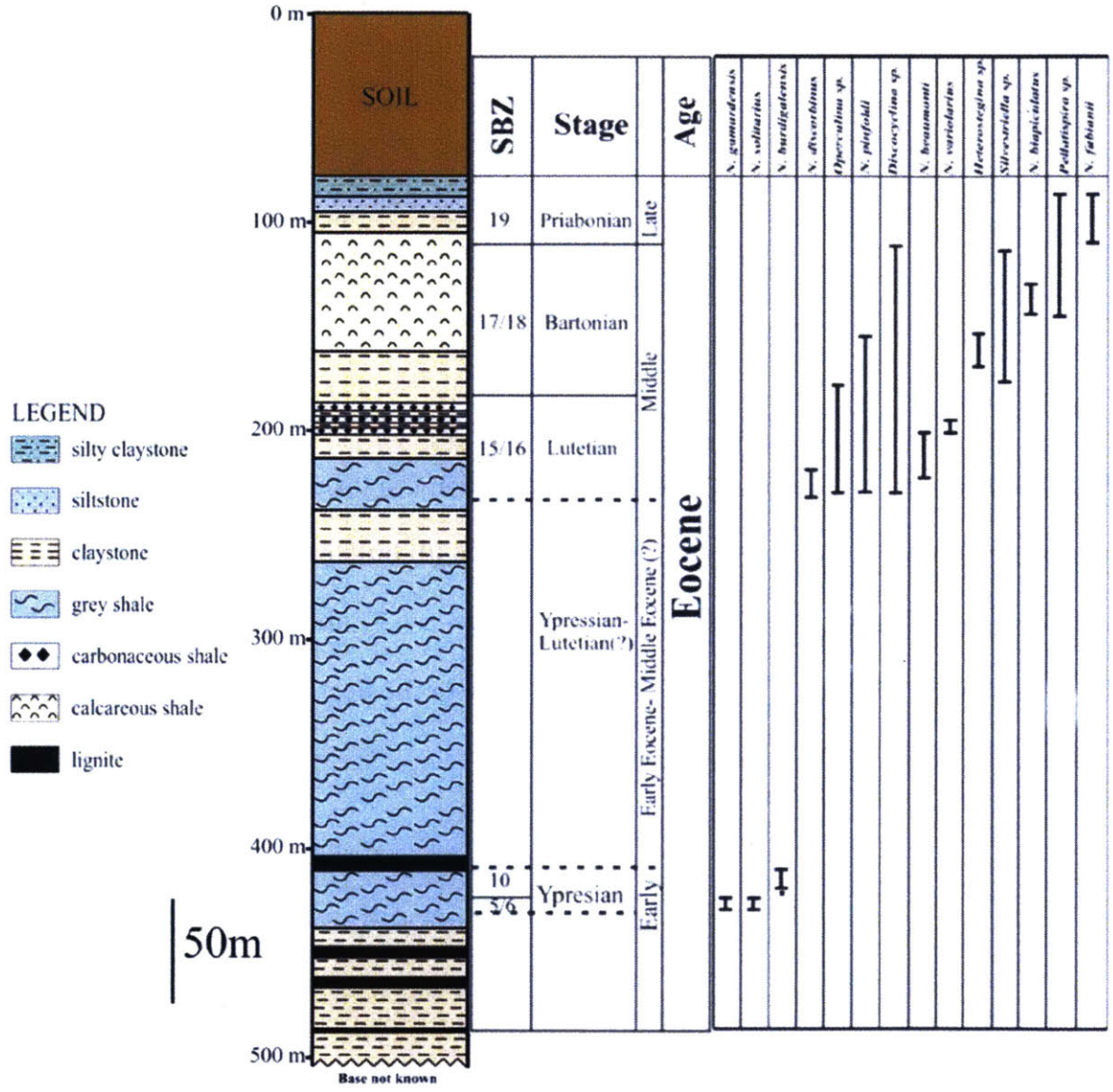

Figure 2.2: Lithology of the sampled core with attached benthic foraminifera based biostratigraphy. Age assignments are based upon the determined shallow benthic zones (SBZ) which are assigned based upon the illustrated first and last appearances of specific taxa.Modified from Nandi, 2014.

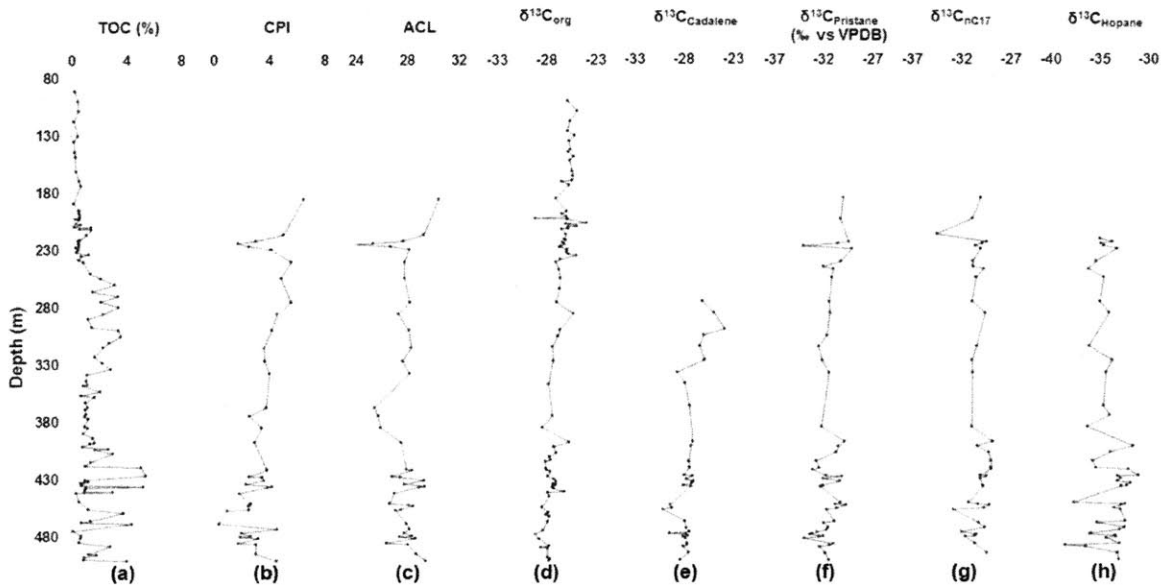

Figure 2.3: Core profiles of (a) total organic carbon (%) (excluding lignites), (b) carbon preference index, (c) average chain length, (d) bulk organic carbon $\delta^{13}C$ and (e-h) compound-specific $\delta^{13}C$ of cadalene, pristane, *n*-C17 and hopane respectively. Upper portions of several profiles are absent due to the decrease in organic content preventing their reliable measurement.

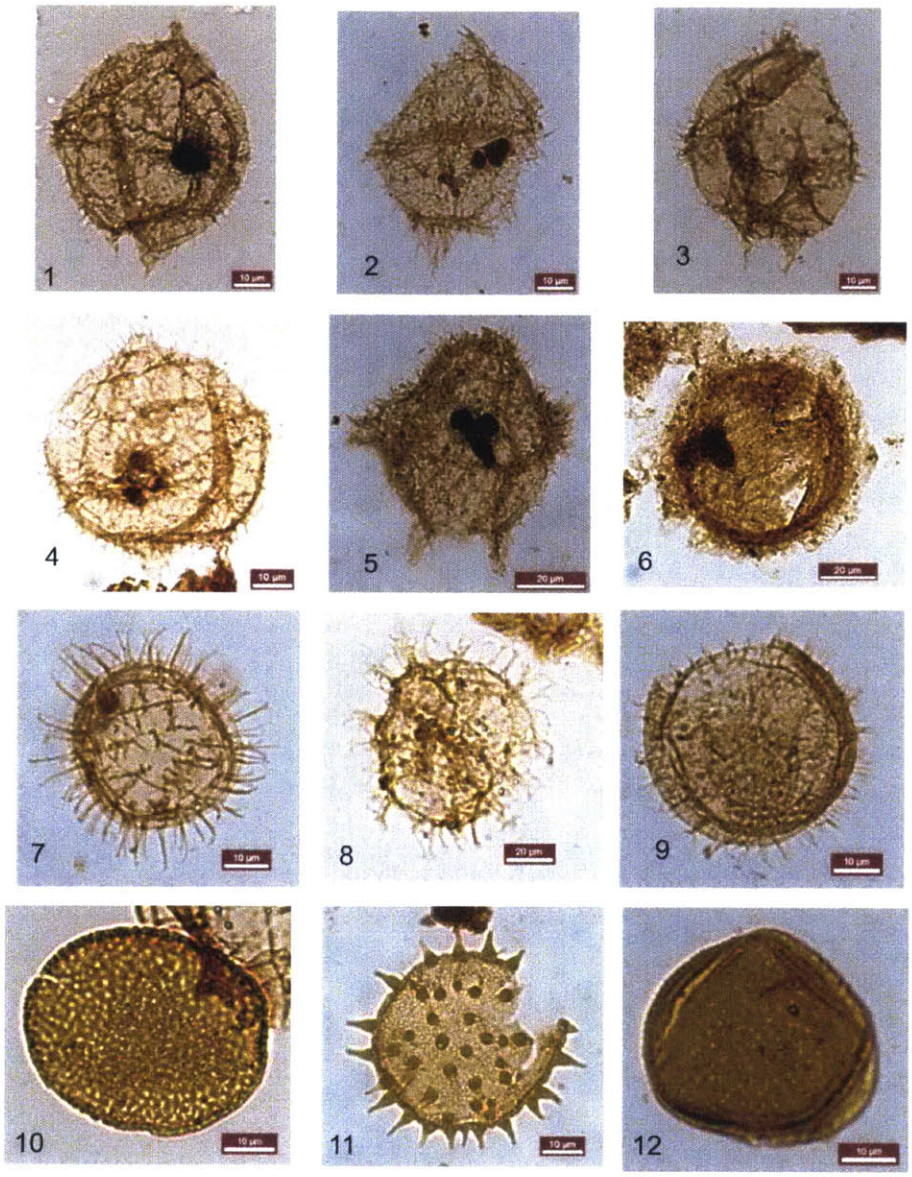

Figure 2.4: Various palynomorphs from the examined core material. 1. *Apectodinium* sp.; 2. *Apectodinium hypercanthum* ; 3. *Apectodinium homomorphum;* 4. *Apectodinium parvum;* 5. *Apectodinium paniculatum*; 6. *Cordosphaeridium* sp.;7. *Polysphaeridium subtile;* 8.*Achomosphaera* sp.; 9. *Operculodinium* sp.*;* 10. *Proxapertites cursus* 11. *Spinizonocolpites bulbospinous* 12. *Proxapertites* sp.

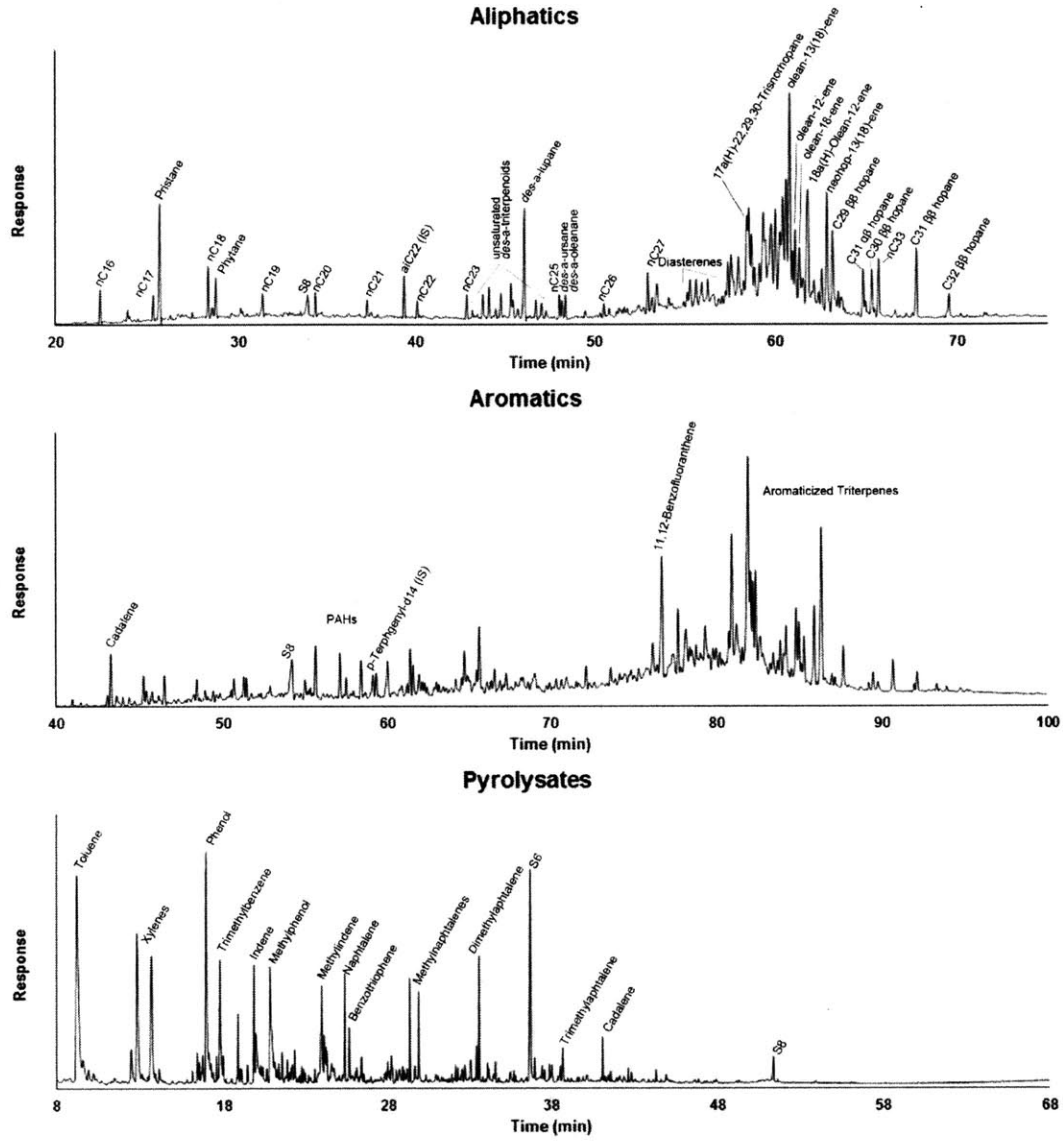

Figure 2.5: Representative chromatograms and pyrogram of the (top) aliphatic, (middle) aromatic fractions and (bottom) pyrolysates. Where individual compound identifications were not possible compound groups are labelled instead.

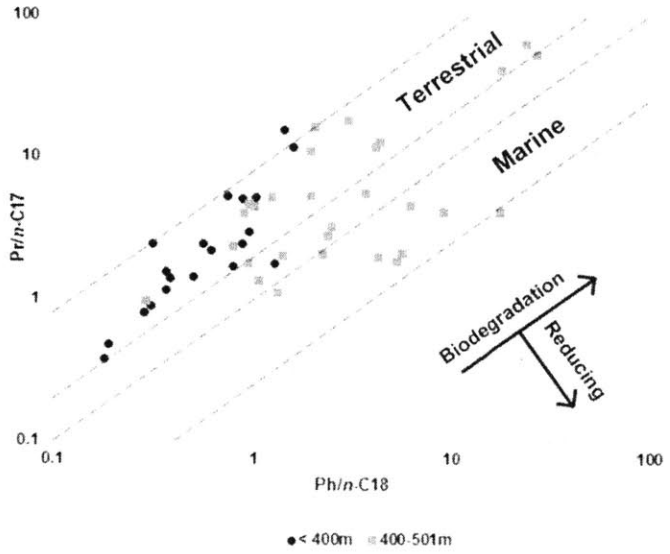

Figure 2.6: Pristante/*n*-C17 vs. Phytane/*n*-C18 log plot illustrating the different relative abundance of n-alkanes in the lower 100 meters of core.

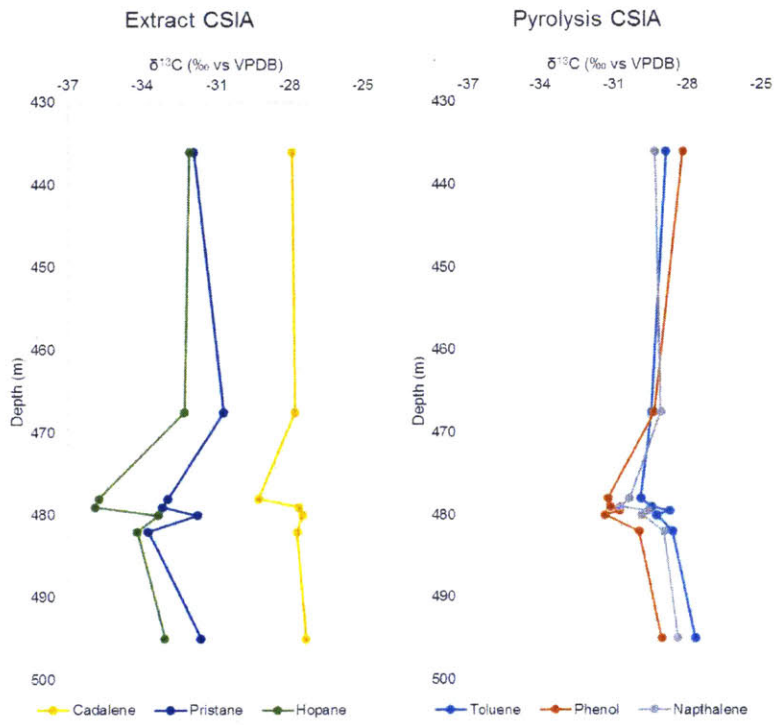

Figure 2.7: Compound-specific isotope profiles of several compounds from (left) extracted free hydrocarbons and (right) pyrolysis released compounds from isolated kerogens.

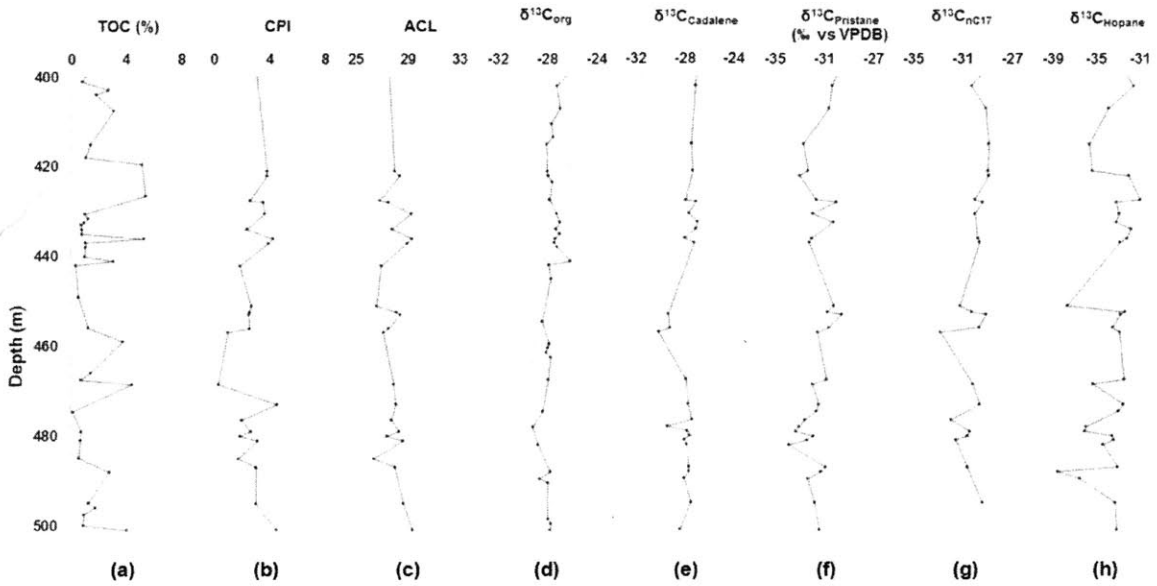

Figure 2.8: Close up profiles of the lowermost 100 meters of core where any hyperthermal events would be located. Profile descriptions the same as Figure 3.

Table 2.1: Bulk rock properties from Rock-Eval and EA-IRMS.

Sample Depth (m)	TOC (%)	T_{max} (°C)	HI	OI	S2	$\delta^{13}C_{org}$ (‰ vs. VPDB)
91.3	0.23	428	43	478	0.1	-25.7
96.5						-25.2
100.5	0.47	421	32	211	0.15	-25.8
102	0.2	420	45	170	0.09	
106						-24.5
109	0.5	411	100	600	0.05	-24.9
115						-24.7
118	0.19	397	53	442	0.11	-25.6
126.5						-25.8
130.5	0.46	401	28	230	0.1	-25.2
135.5	0.16	420	81	800	0.13	-25.7
142.5						-25.5
145	0.22	413	36	282	0.13	-25.7
149	0.29	423	31	286	0.08	-25.2
152						-25.6
161.5	0.36	424	39	214	0.09	-25.3
165.5						-25.3
169.5	0.59	418	34	249	0.14	-25.4
170.5						-26.5
174	0.68	420	32	207	0.2	-25.7
185.5						-27.0
189.5	0.19	453	42	505	0.22	-25.1
195.5	0.55	436	25	324	0.24	-24.3
196.5	0.58	432	29	297	1.1	-25.9
198.5	0.65	440	25	325	0.14	-26.4
201.5	0.65	436	23	306	0.17	-25.9
202.5	0.29	443	45	455	0.16	-29.1
203.5	0.58	436	29	316	0.15	-25.8
206.5	0.37	463	32	505	0.12	-23.9
207.5	0.68	431	25	231	0.17	-26.0
209.5	0.24	433	29	296	0.17	-24.9
210.5	1.46	436	36	137	0.07	-25.8
211.5	0.64	433	44	145	0.52	-25.7
212.5	1.46	433	27	96	0.28	-26.4
217	1.15	429	23	117	0.4	-26.0
221	0.62	424	26	205	0.26	-26.2
222	0.52	426	35	175	0.41	-26.0
224	0.6	424	37	137	0.16	-26.3

225	0.57	416	32	174	0.18	-26.1
227	0.55	433	29	173	0.22	-26.5
228	0.33	412	24	139	0.18	-26.6
230	0.51	418	22	206	0.16	-25.9
231.5	0.43	426	28	279	0.08	-25.9
234	1.33	428	23	123	0.11	-25.8
235.5	0.74	437	59	161	0.12	-24.9
238.5	0.56	415	25	246	0.3	-26.6
240.5	0.93	423	26	138	0.44	-27.0
246.5		436	310	38	0.14	
247.5						-26.7
250.5	1.41	436	31	94	0.24	
254.5	2.17	437	37	82	34.05	-26.6
260	3.21	441	46	62	0.44	
264						-26.6
266	1.6	437	39	76	0.81	
270	3.41	442	54	61	1.43	
275	2.2	440	39	109	0.63	
275.5						-27.0
280	3.47	431	36	64	1.85	
285.5	2.34	445	45	68	0.85	-25.2
290	1.23	439	44	92	1.25	
295						-27.3
297.5	1.54	443	49	69	1.06	
300	3.48	441	64	61	0.54	-26.5
305.5	3.66	444	46	70	0.75	-26.8
310.5	2.8	444	49	64	2.24	
315	2.39	441	51	59	1.69	-27.3
323	1.77	435	34	70	1.38	
327						-27.3
328.5	2.29	435	36	68	1.23	
333.5	2.9	437	45	153	0.61	
337.5						-28.6
338.5	1.19	432	35	72	0.83	
343.5	1.15	432	40	87	1.31	
347	1.18	436	45	97	0.42	-27.7
348	0.91	437	45	73	0.46	
353	2.14	441	54	56	0.53	
356.5	0.75	435	43	117	0.41	-28.9
358	1.74	443	74	56	1.15	
363	1.06	434	30	81	0.32	

367	1.24	435	52	78	1.29	-28.8
368.5	1.09	436	30	110	0.32	
373	1.13	441	31	82	0.64	
375	1.01	435	40	87	0.33	-27.3
377	1.32	439	36	73	0.35	
383.5	1.01	437	45	73	0.4	
385	1.22	437	53	74	0.48	-28.3
389.5	0.89	436	47	61	0.45	
393.5	1.62	437	80	52	0.65	
397.5	1.73	435	103	51	0.42	-25.6
398.5	1.42	438	62	53	1.29	
402						-27.2
404	1.81	441	106	51	1.91	
407						-26.9
407.5	3.11	436	194	34	6.04	
410.5						-27.6
413.5		418	250	27	92.82	-27.5
415	1.46	430	108	63	1.57	-28.0
418	1.1	437	55	53	0.95	
419.5	5.18	433	77	47	0.61	
421						-27.9
422						-27.8
423.5						-27.6
426.5	5.49	374	533	39	3.99	
427.5						-27.8
430.5	1.06	425	81	56	0.86	-27.2
431						-27.4
431.5	1.29	432	34	81	0.44	-27.1
432.5	1	432	27	96	0.27	-27.0
433	0.76	428	25	107	0.19	
434	0.83	426	36	110	0.3	-27.2
435	0.82	426	34	105	0.28	-26.9
436	5.35	427	49	50	2.64	-27.3
437	1.13	443	38	83	0.43	-27.4
438	1.08	434	43	147	0.46	-27.2
440	1.04	441	32	137	0.33	
441	3.1	416	138	51	4.28	-26.1
442	0.39	417	46	136	0.18	-27.8
445.1		416	249	28	104.32	-27.6
449	0.62	545	21	90	0.13	
454.6		420	189	29	65.39	-28.3

456	1.32	428	88	73	1.16	
459	3.87	436	103	37	3.98	
459.5		414	160	43	26.72	-27.7
460.4						-27.9
461.4						-28.0
462.4		416	255	27	116.65	-27.7
466	1.49	428	55	89	0.82	
467.5	0.78	425	73	123	0.57	-27.8
468.5	4.49	434	109	42	4.9	
474.5	0.21	418	52	95	0.11	-28.3
478						-29.0
479	0.81	425	54	58	0.44	
481	0.75	429	55	65	0.41	
482						-28.6
485	0.64	431	58	77	0.37	
488	2.91	430	88	42	2.56	-27.6
489.5		420	236	25	103.75	-28.5
490.5						-27.8
495	1.38	420	130	41	1.8	
496	1.9	436	49	36	0.93	
497.5	1.05	428	33	54	0.35	
498.6						-27.8
499.6						-27.6
500	0.98	427	31	79	0.3	
501	4.16	433	108	32	4.51	-27.6

Chapter 3

A Biogeochemical Survey of the Early Paleogene Eureka Sound Group of the Canadian High Arctic

A Biogeochemical Survey of the Early Paleogene Eureka Sound Group of the Canadian High Arctic

Ross H. WILLIAMS[1]*, David A. EBERTH[2], Jaelyn J. EBERLE[3], Sabine MEHAY[4], Katherine H. FREEMAN[5] and Roger E. SUMMONS[1]

1. Department of Earth, Atmospheric and Planetary Sciences, Massachusetts Institute of Technology, 77 Massachusetts Avenue, Cambridge, MA 02139-4307, USA

2. Royal Tyrrell Museum, Box 7500, Drumheller, AB T0J 0Y0, Canada

3. Museum of Natural History and Department of Geological Sciences, University of Colorado at Boulder, Boulder, Colorado 80309, USA

4. Schlumberger, Reservoir Laboratory, Jebel Ali, 16818 Dubai, UAE

5. Department of Geosciences, Pennsylvania State University, University Park, PA 16802, USA

*rosshw@mit.edu

Abstract

In order to better understand how polar amplification will affect the Arctic in future climatic scenarios, it is instructive to study what records exist of geologically-recent events there. During the Early Cenozoic, Earth was significantly warmer with tropical flora and fauna evident at high latitude locations. Here we present a biomarker and isotopic survey of the Eureka Sound Group in the Canadian High Arctic. Biomarker distributions combined with lithology from Strathcona Fiord have indicated significant changes in the composition and source of hydrocarbons across the Paleocene-Eocene transition. During the Paleocene, *n*-alkane distributions follow the standard terrestrial higher plant signal found within extensive marine deposits while the Eocene strata are characterized by coastal lithologies and leaf waxes with a shorter chain length dominance. Further, biomarker proxy estimates for mean air temperature from this site, along with paleosols from Banks Island, demonstrate clear evidence for warming trends, albeit with significantly cooler values than expected in some sites. Sea surface temperature estimates based upon TEX_{86} measurements of shales from Strathcona Fiord confirm prior studies that identify substantially higher values than at present (16-19°C). Finally, the compound-specific hydrogen isotope data for leaf waxes has shown that the ice-free conditions previously inferred for the middle Eocene can be extended back to the early Eocene and likely the late Paleocene. All of these factors, combined, confirm the existence of a significantly warmer Eocene Arctic with biomarker records that readily lend themselves to further detailed investigation of the region.

3.1. Introduction

In the near future, climate change will result in dramatic differences in conditions worldwide including the polar amplification that leads to relatively greater warming in the Arctic regions. Recent changes in the Arctic have revealed that temperature increases in those regions have already far surpassed global averages (Serreze et al., 2009). To better predict conditions in the Arctic we must turn to periods in Earth's past during which temperatures rose rapidly and of a comparable magnitude to future predictions. In that respect the early Paleogene provides a useful analog. For many years it has been known from fossil evidence that during this time 'tropical' flora and fauna thrived at high latitudes (Dawson et al., 1976, Estes and Hutchison, 1980, McIver and Basinger, 1999). Here we report compound-specific isotopic records and biomarker analyses of both paleosols and shales from the Early Paleogene portion of the Eureka Sound Group that pertain to the Arctic climate of that time.

Numerous studies have been conducted regarding the Early Paleogene Arctic, but the bulk of the biomarker analyses has been conducted solely on marine deposits (Krishnan et al., 2014; McCarren et al., 2008; Schouten et al., 2007; Speelman et al., 2009; Weller and Stein, 2008). The biogeochemical work that has been done confirms what has been recorded in the record of physical fossils; that exceedingly warm temperatures persisted throughout this period. Fossil evidence

has demonstrated that fauna such as alligators and turtles once thrived in this region (Dawson et al., 1976) as well as sand tiger sharks whose modern relatives inhabit warm coastal waters (Padilla et al., 2014).

Paleobotanical evidence has further reinforced the idea of a warm wet Arctic environment during the Paleogene. Most striking is the presence of a fossil forest on Axel Heiberg Island which preserves macrofossil and palynological records of what was a dense conifer rainforest with an angiosperm component (Jahren, 2007). Studies of this floral community reveal mean annual precipitation (MAP) and mean annual temperature (MAT) that reinforce the Arctic rainforest paradigm (Greenwood et al., 2010). Further isotopic analysis of tree rings narrowed the nearest modern analogue to be forests from eastern Asia where most of the precipitation occurs during the summer (Schubert et al., 2012) which was later reinforced by leaf physiognomy (West et al., 2015).

Over the past decade, the microbial membrane lipids known as glycerol dialkyl glycerol tetraethers (GDGTs) have proven to have value for reconstructing paleoenvironmental conditions. GDGTs occur in two main forms distinguished by the nature of their alkyl chains, isoprenoidal and non-isoprenoidal (aka branched). Isoprenoidal GDGTs are produced by various archaea while the non-isoprenoidal variety is commonly found in soils and are thought to be produced by soil bacteria (Weijers et al., 2006) or possibly acidobacteria (Damsté et al., 2011). In the marine realm, the proxy TEX_{86} is based on the numbers of cyclic moieties within the hydrocarbon chains of isoprenoidal GDGTs and has been shown to correlate with

sea surface temperatures (SSTs) (Schouten et al., 2002). The isoprenoidal GDGT proxies have been supplemented by two indices derived from the composition of bacterial, non-isoprenoidal GDGT. These are based on the methylation of branched tetraether (MBT) and cyclization of branched tetraethers (CBT). The combined MBT/CBT ratio shows correlation with MAT (Weijers et al., 2007b).

Since its development, carbon compound-specific isotope analysis (CSIA) has been utilized in a myriad of studies of biogeochemical processes (Matthews and Hayes, 1978). It has been particularly useful in petroleum studies (Murray et al., 1994), determination of vegetation types (Tanner et al., 2007), and even extended to the global carbon cycle itself (Dal Corso et al., 2011). Extending this technique further, methods were developed to study the hydrogen isotopic content of individual compounds (Burgoyne and Hayes, 1998; Hilkert et al., 1999; Sachse et al., 2012). This has allowed CSIA studies to infer conditions such as paleoelevation (Jia et al., 2008; Polissar et al., 2009) as well as paleohydrology (Pagani et al., 2006; Schefuss et al., 2005) and ecosystem evolution pertaining to early human habitats (Magill et al., 2016, 2013a, 2013b).

A further application of hydrogen CSIA of plant alkyl lipids is as a paleotemperature proxy. However, this can only be utilized when the many various other factors such as further environmental conditions or biochemistry affecting the δD_{alkane} can be accounted for (Schimmelmann et al., 2006). It has been demonstrated that a primary control on the isotopic composition of long chain n-alkanes is the composition of the source water (Pedentchouk et al., 2008; Sessions et al., 1999).

Further, the composition of the source water for a particular region is often in turn linked to the temperature. This has been shown to be true especially in high latitude regions where the isotopic composition is closely linked to the variation of temperature with latitude (Dansgaard, 1964; Feakins et al., 2012; Jahren et al., 2009), and established for Canada in particular (Birks and Edwards, 2009). The veracity of this paleotemperature proxy has been assessed through comparison with other established biomarker based proxies such as the MBT/CBT of arctic paleosols (Pautler et al., 2014) or modeled results utilizing TEX_{86} record (Speelman et al., 2010).

3.2. Geologic Setting

The Late Cretaceous to Early Tertiary Eureka Sound Group is an extensive sequence of deposits across the Canadian Arctic Archipelago. While notably dominated by terrestrial deposits, the heterogeneity of depositional environments across the Arctic provides the ability to sample both terrestrial and marine sections. The Eureka Sound Group was subdivided independently on the basis of lithofacies assemblage correlation (Miall, 1986) and by a regional transgressive marker formation (Ricketts, 1986). While both methodologies have their advantages, the terminology of Miall will be utilized in this study.

Shale samples were collected from exposures along Strathcona Fiord on Ellesmere Island (Fig. 3.1). Collection began at roughly the base of the Mt. Moore Formation and extended 810 meters into the Mt. Margaret Formation. The

boundary between these formations occurs around the transition from the Paleocene to the Eocene and roughly divides the section in half while definite upper and lower bounds remain unknown (Fig. 3.2). The Mt. Moore Formation is dominated by marine deposits of shale and carbonate while the Margaret Formation is composed of a more diverse series of transgressive events (Miall, 1979) (Fig. 3.3).

Several paleosols were chosen for sampling on Banks Island, Canadian Northwest Territories within the Aulavik National Park. Paleosols from this location belong to the Cyclic Member, which corresponds to the Margaret Formation samples at Strathcona Fiord. This correlation is confirmed by the presence of vertebrate fossils and palynology, with several samples recently ascribed to the early Eocene (Sweet, 2012). Four different paleosols were studied from various portions of the exposure which contains cyclic deltaic sequences of shale-silt-sand-paleosol-lignite (Miall, 1979) (Fig 3.4). Exact locations of three of the paleosols are known while paleosol H is known to occur within 50 meters of the base of the measured section.

3.3. Methods

In all cases samples were obtained by exposing fresh material and storing in combusted foil in whirl-pak bags or combusted jars for transport. Total lipid extracts (TLEs) were obtained by extracting approximately 50 grams of sample with a Dionex ASE-200 extractor using a solvent mixture of dichloromethane:methanol (DCM:MeOH 9:1). The resulting TLE was separated by compound class utilizing

silica gel column chromatography. Five fractions were collected with the corresponding eluents: saturates (hexane), aromatics (hexane:DCM 8:2), ketones (DCM), alcohols (DCM:EtOAc 1:1) and acids/diols (EtOAc). The latter two fractions were combined prior to further analyses. Samples were screened via GC-MS with an Agilent 7890A gas chromatograph coupled with an Agilent 5975C mass selective detector. Those sites which exhibited presence of elemental sulfur were desulfurized with the addition of activated copper shot. Due to the limited amount of sample extracts were consumed by analysis precluding further analyses.

The saturate fractions were initially run for compositional analysis by GC-MS on an Agilent 7890A gas chromatograph equipped with a DB-1MS or DB-5MS column (Agilent J&W 60m length, 0.25mm diameter, 0.25µm film) interfaced to an Agilent 5975C mass selective detector. For carbon CSIA the samples were injected into a ThermoFinnigan TraceGC coupled to a Finnigan DELTA^{plus} XP via a combustion furnace and water removal interface. Delta values were calculated relative to a gas standard calibrated to Vienna Pee Dee Belemnite (VPDB). Compounds resulting in signals greater than 100mV and displaying no irresolvable co-elution with other compounds were accepted for interpretation. Deuterium CSIA was conducted at Pennsylvania State University on an Agilent 6890A GC with a high temperature pyrolysis furnace coupled to a Finnigan DELTA^{plus} XP. Results were determined using a reference gas calibrated to VPDB. The H_3^+ factor was monitored daily and averaged 0.732±0.015. A suite of n-alkanes (Mix A; *n*-C_{16} to *n*-C_{30} alkanes; Arndt Schimmelmann; Indiana University) was utilized as external

standards to monitor performance and provide a linear correction based on peak area.

Tetraether lipids were identified using a 1200 series Agilent HPLC coupled with an Agilent QTOF 6520 mass spectrometer. Separation of compounds was achieved using an Agilent ZORBAX CN (cyano) column with an eluent gradient between 100% Hexane:IPA 99:1 and 15% Hexane:IPA 9:1. MBT/CBT proxy ratios were calculated using extracted ion chromatograms. Further biomarker characterization of the saturate fraction was conducted by gas chromatography-multiple reaction monitoring-mass spectrometry (GC-MRM-MS) on an Agilent 6890N gas chromatograph interfaced with a Micromass Autospec Ultima. Compound identification was accomplished by comparison with an AGSO standard oil.

3.4. Results

3.4.1. Aliphatic Compound Distributions

Normal alkane distributions for Paleosol E and the Strathcona Fiord have been examined in detail. In all samples a strong odd over even preference was seen. In Paleosol E, the dominant chain lengths were *n*-C_{25} and *n*-C_{27} with an average Paq value of 0.68. In the Strathcona Fiord, a very clear shift is seen in the Margaret vs. Mt. Moore Formations. In the Mt. Moore Formation the *n*-alkane distribution is the typical higher plant distribution with a dominance of *n*-C_{29}. However, in the Margaret Formation this dominance waivers in favor of the slightly shorter chains

such as n-C_{23-27}. The average Paq value of the Mt. Moore Formation is 0.32 while the Margaret Formation is 0.98 (Fig. 3.5a).

Other compounds in the Strathcona Fiord aliphatic fractions are 17ß,21ß-hopanes and unsaturated hopenes (Fig. 3.6). The Mt. Moore formation has hop-17(21)-ene as the most prevalent compound in the m/z 191 extracted ion chromatogram and also contained a strong trisnorneohop-13(18)-ene. While the compound variety does not change in the Margaret Formation, the relative abundances do, with the ßß hopanes increasing in dominance.

The Paleosols have hopanes in the biological configuration as well, but also have significant unsaturated pentacyclic triterpenoids such as olean-12-ene and taraxer-14-ene. Some minor contribution of diterpenoids is also evident (Fig. 3.7). Examination of the m/z 123 extracted ion chromatogram reveals a suite of C19-20 structures. In the absence of authentic standards only tentative structures are proposed based on spectral library comparisons and retention patterns.

Analyses by MRM of Strathcona Fiord and Paleosol E provided useful hopane and sterane parameters (Fig. 3.8) (Tables 3.1 & 3.2). As with the isotopic data the results from the multiple samples of Paleosol E are binned. For the C35 homohopane index and dinorhopane/hopane (DNH/H) there is a marked decrease from the Mount Moore to Margaret Formations of Strathcona Fiord. In both cases the lower values seen in the Margaret formation are consistent with the average values from Paleosol E. The moretane/hopane ratio shows only a slight increase over time and the C29/C30 hopane ratio is relatively constant. The homohopane

S/(S+R) ratios show a very distinct difference between the C31 and the extended C32-35 values in the fiord as well as paleosol. While the C31 value is always consistently low, C33-35 are always elevated. C32 however is interesting in that it appears elevated in the Mt. Moore formation but then drops lower in the Margaret formation. Comparison of Ts/(Ts+Tm) and Dia/(Dia+Reg) C27 Steranes shows very distinct groupings between the two fiord formations and the paleosol (Fig. 3.9).

3.4.2. Carbon and Hydrogen Isotopic Data for Hydrocarbons

Isotopic measurements were taken of numerous *n*-alkanes at every sampling site (Fig. 3.10a) (Table 3.3 & 3.4). For the sake of consistency, the peak with the least amount of co-elution that was abundant at every site was *n*-C_{27} and will be discussed herein. To address the fact that *n*-C_{27} is not as desirable as *n*-C_{29} for such approaches it was compared to *n*-C_{29} where available and showed the same overall trends supporting its use throughout the sections. Paleosol sections were largely homogenous and in the absence of a detailed classification scheme in place are treated in the present study as binned samples instead of profiles. The distribution of carbon isotopic values for the paleosols are all very similar with the exception of paleosol A. Here a much broader range of values were measured that are slightly heavier (1.5‰) than the other sites. In the Strathcona Fiord section little variation in isotopic composition is seen over the 800m record (2.7‰) (Fig 3.5b).

Hydrogen isotopic measurements were only possible at Strathcona Fiord and one paleosol site, Paleosol E, due to the higher compound abundances necessary

for this measurement (Fig 3.10b). In Strathcona Fiord only a couple of measurements were possible from the Mt. Moore Formation while most of the samples from the Margaret Formation were amenable to analysis (Fig 3.5c). While spanning a much longer depositional history, the samples from the Margaret Formation are actually closer in value than the highly variable results from the paleosol (45‰ vs. 83‰).

3.4.3. Tetraether Membrane Lipids

For all sites MAT was calculated using the terrestrial MBT/CBT proxy (Fig. 3.11). The Strathcona Fiord samples have a BIT index >0.6 for all samples indicating a high proportion of riverine organic matter input. Temperatures calculated from the paleosols vary greatly, with average values ranging by 9.3°C (Table 3.3). In Strathcona Fiord, the Mt. Moore Formation has an average temperature of 2.2°C while the Margaret Formation is 7.9°C, with a clear warming trend over time (Fig. 3.5d) (Table 3.4). It is worth noting that the paleosols recording cooler temperatures are in close agreement with the Eocene Margaret Formation temperatures. While only possible to calculate from a subset (1/3) of the samples, Strathcona Fiord TEX_{86} gives SST values averaging 16.4°C.

3.5. Discussion

It is evident from the aliphatic compound distribution that the sites presented here have excellent preservation of organic matter. Numerous unsaturated hopanoids and other pentacyclic triterpenoids are present that would

be altered in the early stages of diagenesis (Mackenzie et al., 1982). The primary source of the higher plant input to the paleosols record is likely angiosperm in origin due to significant amounts of oleanane type compounds in all samples. Such compounds have been shown to be closely linked with the diversification of angiosperms (Moldowan et al., 1994) though a few exceptions to this have been noted (Taylor et al., 2006). Prior studies of coals from the Eureka Sound Group also contained angiosperm biomarkers but contrast in the fact that they also contained a significant amount of conifer diterpenoids while the sites studied herein only contain minor contributions (Kalkreuth et al., 1998, 1996). However, it was recently noted that despite the overwhelming evidence for gymnosperm dominated floral communities in the coals the interbedded mudstones-siltstones contained abundant angiosperm input (Harrington et al., 2012). The results presented here further indicate that the role of angiosperms in the Early Eocene High Arctic may be underestimated.

The most striking information revealed is the alteration of *n*-alkane distributions in Strathcona Fiord between the Paleocene Mt. Moore Formation and the Eocene Margaret Formation. This shift from higher chain length maxima to lower indicates a change in the source of plant material at this boundary. During the Paleocene, deposition of leaf waxes in this region was predominantly by terrestrial vascular plants while the Eocene sees a shift to more aquatic vegetation. Interestingly, this coincides with a stark lithology change that goes from marine deposition to a more near shore environment with extensive sandstone deposits.

However, interbedded with these sandstones are numerous coal deposits that were not present in the Paleocene and may point to an alternative source for the *n*-alkane signal. Therefore, the increase in n-C_{23} is likely due to an increase in sphagnum due to the development of coastal peat deposits (Inglis et al., 2015).

A general increase in the oxicity of the water from the Paleocene into the Eocene is evident by the decrease both in the C35 homohopane index and the DNH/H ratio. The C31 homohopane S/(S+R) remains low and consistent throughout this time indicating no change in the immaturity consistent with the established immaturity of the section. Therefore, the slight changes in the C30 moretane/hopane ratio is likely due to the source of the organic matter and not a changing maturity as it has been shown to increase with increasing terrestrial input (Isaksen and Bohacs, 1995). Most striking is the great dissimilarity between the C30 vs C32-35 homohopane S/(S+R) values. However, it has been noted that elevated S/(S+R) values have been seen in immature sediments deposited under hypersaline conditions (Haven et al., 1986). This interpretation is corroborated by the increase in Ts/(Ts+Tm) in the Mt.Moore formation despite apparent constant maturity as this too can be indicative of hypersaline conditions (Rullkötter and Marzi, 1988). The fact that the C32 homohopane S/(S+R) value drops across the transition from Paleocene into Eocene when the Ts/(Ts+Tm) value drops as well may indicate a decrease in salinity. If this was the case it would suggest that there is a chain length sensitivity to salinity in terms of isomerization though it is unclear at this time why this would occur. It is also unclear why the distribution would be

such in the paleosol and likely means that there is an alternative cause for the discrepancy beyond hypersalinity.

It is important to note that very few of the calculated parameters for Paleosol E differ greatly from the Margaret Formation despite significantly different depositional history. The main difference is in the C29/C30 hopane ratio likely due to the difference in lithology. Further, the Dia/(Dia+Reg) C27 sterane ratio is higher in the paleosol. This may be due to a higher oxicity in the paleosol or alternatively be due to differences in clay content.

The GDGT-based temperature estimates confirm the significantly warmer conditions of the early Cenozoic Arctic compared to today. Furthermore, the long-term temperature estimates from the Strathcona Fiord section display a clear warming over time, consistent with the established Early Paleogene climatic paradigm. The paleosol GDGT data also shows a very significant warming. Due to the spatial separation of the individual paleosol sites, and the absence of any means to correlate them, significant amounts of time may have elapsed between each. While the observed trends are clear, one additional insight that can be drawn this study is that a significant amount of variability occurs within a single paleosol deposit. Therefore, it is evident that a significant amount of caution should be followed in the study of paleosol biogeochemistry and a thorough classification scheme of paleosol types (i.e. soil taxonomy) should be utilized.

While these records reveal useful climatic trends, the absolute values differ from those presented in past studies. Prior work from Lomonosov Ridge

calculated MBT/CBT based temperature of 18-20°C (Weijers et al., 2007a). These values agree well with the reconstructed temperatures at sites C and E (Average MATs 17°C) but sites A and H are significantly lower (Average MATs 8°C). It is likely that the paleosols are recording the warming trend through the Early Eocene into the Early Eocene Climatic Optimum (EECO). The Strathcona Fiord section provides lower temperatures that are in agreement with those of Paleosols A and H in the Paleocene base and rise as expected into the Eocene, though not as high as those from Paleosols C and E. However, caution must be taken when interpreting these absolute temperature estimates due to a number of factors. The first of these is the calibration error of the proxy (~5°C), which may account for a portion of the discrepancy. Further, the Strathcona Fiord deposits are likely integrating a much larger area, while paleosols would provide more of a localized snapshot. Despite the uncertainty of the magnitude of the temperature the overall trend of a warming Eocene-Paleocene world is reaffirmed by our data. Marine samples from Strathcona Fiord also provided TEX_{86} based SSTs of 16-19°C, consistent with past studies in the region (Sluijs et al., 2006).

By utilizing established fractionation factors it is possible to back calculate the δD of environmental water using terrestrially sourced *n*-alkanes (Jahren et al., 2009; Sachse et al., 2012). Our average $\delta D_{n\text{-}C27}$ value for Paleosol E was -268‰ and -246‰ for the Margaret Formation. In the absence of a precise plant community composition the apparent fractionation for dicotyledons (-113‰ ± 31‰) was used given the established arctic rainforest paradigm. Therefore the

environmental water values for Paleosol E around -155‰ and for the Margaret Formation of around -133‰. These isotopic values coincide with those found in prior studies in this region (Jahren et al., 2009) as well as modelling studies of the distribution of environmental water isotopic values during the Early/Middle Eocene (Speelman et al., 2010). Jahren et al. (2009) concluded based on their data that during the middle Eocene the Arctic lacked snowfall and ice cover. Therefore given the similarities demonstrated here it is likely that the same holds true for the Early Eocene. While only two data points are available from the Paleocene deposits, they are similar in value and indicate that this conclusion could also be extended further with additional study. Further, despite the uncertainty of the apparent fractionation of ± 31‰ these measurements do not overlap with modern meteoric water measurements from nearby Axel Heiberg Island (<-200‰) (Jahren et al., 2009).

3.6. Conclusions

A detailed characterization of the early Cenozoic Canadian High Arctic has been established. Aliphatic hydrocarbon distributions have revealed that the area has remained unaffected by geothermal heating and is a good candidate for biomarker studies and highlight the presence of angiosperms in the floral community. Further, deposits from Strathcona Fiord have indicated an environment shift from marine to near coastal across the Paleocene-Eocene boundary through biomarkers and lithology. Environmental proxies based on GDGTs, despite uncertainties of absolute values, have reinforced the known

warming during this time period. Finally, the hydrogen isotopic composition of n-alkanes has illustrated that the isotopic composition of environmental water agrees with prior results that have indicated a snow free Arctic.

Acknowledgements

We thank Hope Jahren for her invaluable insights and suggestions at an early stage of this work. The research conducted at MIT was supported by an award (NNA13AA90A) from the NASA Astrobiology Institute.

References

Birks, S.J., Edwards, T.W.D., 2009. Atmospheric circulation controls on precipitation isotope-climate relations in western Canada. Tellus B 61, 566–576. doi:10.1111/j.1600-0889.2009.00423.x

Burgoyne, T.W., Hayes, J.M., 1998. Quantitative Production of H 2 by Pyrolysis of Gas Chromatographic Effluents. Anal. Chem. 70, 5136–5141. doi:10.1021/ac980248v

Dal Corso, J., Mietto, P., Newton, R.J., Pancost, R.D., Preto, N., Roghi, G., Wignall, P.B., 2011. Discovery of a major negative 13C spike in the Carnian (Late Triassic) linked to the eruption of Wrangellia flood basalts. Geology 40, 79–82. doi:10.1130/G32473.1

Damsté, J.S.S., Rijpstra, W.I.C., Hopmans, E.C., Weijers, J.W.H., Foesel, B.U., Overmann, J., Dedysh, S.N., 2011. 13,16-Dimethyl octacosanedioic acid (iso-diabolic acid), a common membrane-spanning lipid of Acidobacteria subdivisions 1 and 3. Appl. Environ. Microbiol. 77, 4147–54. doi:10.1128/AEM.00466-11

Dansgaard, W., 1964. Stable isotopes in precipitation. Tellus 16, 436–468. doi:10.1111/j.2153-3490.1964.tb00181.x

Dawson, M.R., West, R.M., Langston, W., Hutchison, J.H., 1976. Paleogene terrestrial vertebrates: northernmost occurrence, ellesmere island, Canada. Science 192, 781–2. doi:10.1126/science.192.4241.781

Estes, R., Howard Hutchison, J., 1980. Eocene lower vertebrates from Ellesmere Island, Canadian Arctic Archipelago. Palaeogeogr. Palaeoclimatol. Palaeoecol. 30, 325–347. doi:10.1016/0031-0182(80)90064-4

Feakins, S.J., Warny, S., Lee, J.-E., 2012. Hydrologic cycling over Antarctica during the middle Miocene warming. Nat. Geosci. 5, 557–560. doi:10.1038/ngeo1498

Greenwood, D.R., Basinger, J.F., Smith, R.Y., 2010. How wet was the Arctic Eocene rain forest? Estimates of precipitation from Paleogene Arctic macrofloras. Geology 38, 15–18. doi:10.1130/G30218.1

Harrington, G.J., Eberle, J., Le-Page, B.A., Dawson, M., Hutchison, J.H., 2012. Arctic plant diversity in the Early Eocene greenhouse. Proc. Biol. Sci. 279, 1515–21. doi:10.1098/rspb.2011.1704

Haven, H.L.T., Leeuw, J.W.D., Peakman, T.M., Maxwell, J.R., 1986. Anomalies in steroid and hopanoid maturity indices. Geochim. Cosmochim. Acta 50, 853–855. doi:10.1016/0016-7037(86)90361-3

Hilkert, A., Douthitt, C., Schlüter, H., Brand, W., 1999. Isotope ratio monitoring gas chromatography/Mass spectrometry of D/H by high temperature conversion isotope ratio mass spectrometry. Rapid Commun. Mass Spectrom. 13, 1226–1230. doi:10.1002/(SICI)1097-0231(19990715)13:13<1226::AID-RCM575>3.0.CO;2-9

Inglis, G.N., Collinson, M.E., Riegel, W., Wilde, V., Robson, B.E., Lenz, O.K., Pancost, R.D., 2015. Ecological and biogeochemical change in an early

Paleogene peat-forming environment: Linking biomarkers and palynology. Palaeogeogr. Palaeoclimatol. Palaeoecol. 438, 245–255. doi:10.1016/j.palaeo.2015.08.001

Isaksen, G.H., Bohacs, K.M., 1995. Geological Controls of Source Rock Geochemistry Through Relative Sea Level; Triassic, Barents Sea, in: Petroleum Source Rocks. Springer Berlin Heidelberg, Berlin, Heidelberg, pp. 25–50. doi:10.1007/978-3-642-78911-3

Jahren, A.H., 2007. The Arctic Forest of the Middle Eocene. Annu. Rev. Earth Planet. Sci. 35, 509–540. doi:10.1146/annurev.earth.35.031306.140125

Jahren, A.H., Byrne, M.C., Graham, H. V., Sternberg, L.S.L., Summons, R.E., 2009. The environmental water of the middle Eocene Arctic: Evidence from δD, δ18O and δ13C within specific compounds. Palaeogeogr. Palaeoclimatol. Palaeoecol. 271, 96–103. doi:10.1016/j.palaeo.2008.09.016

Jia, G., Wei, K., Chen, F., Peng, P., 2008. Soil n-alkane δD vs. altitude gradients along Mount Gongga, China. Geochim. Cosmochim. Acta 72, 5165–5174. doi:10.1016/j.gca.2008.08.004

Kalkreuth, W., Keuser, C., Fowler, M., Li, M., Mcintyre, D., Püttmann, W., Richardson, R., 1998. The petrology, organic geochemistry and palynology of Tertiary age Eureka Sound Group coals, Arctic Canada. Org. Geochem. 29, 799–809. doi:10.1016/S0146-6380(98)00122-3

Kalkreuth, W.D., Riediger, C.L., McIntyre, D.J., Richardson, R.J.H., Fowler, M.G.,

Marchioni, D., 1996. Petrological, palynological and geochemical characteristics of Eureka Sound Group coals (Stenkul Fiord, southern Ellesmere Island, Arctic Canada). Int. J. Coal Geol. 30, 151–182. doi:10.1016/0166-5162(96)00005-5

Krishnan, S., Pagani, M., Huber, M., Sluijs, A., 2014. High latitude hydrological changes during the Eocene Thermal Maximum 2. Earth Planet. Sci. Lett. 404, 167–177. doi:10.1016/j.epsl.2014.07.029

Mackenzie, A.S., Brassell, S.C., Eglinton, G., Maxwell, J.R., 1982. Chemical fossils: the geological fate of steroids. Science 217, 491–504. doi:10.1126/science.217.4559.491

Magill, C.R., Ashley, G.M., Domínguez-Rodrigo, M., Freeman, K.H., 2016. Dietary options and behavior suggested by plant biomarker evidence in an early human habitat. Proc. Natl. Acad. Sci. U. S. A. 113, 2874–2879. doi:10.1073/pnas.1507055113

Magill, C.R., Ashley, G.M., Freeman, K.H., 2013a. Water, plants, and early human habitats in eastern Africa. Proc. Natl. Acad. Sci. U. S. A. 110, 1175–80. doi:10.1073/pnas.1209405109

Magill, C.R., Ashley, G.M., Freeman, K.H., 2013b. Ecosystem variability and early human habitats in eastern Africa. Proc. Natl. Acad. Sci. U. S. A. 110, 1167–74. doi:10.1073/pnas.1206276110

Matthews, D.E., Hayes, J.M., 1978. Isotope-ratio-monitoring gas chromatography-mass spectrometry. Anal. Chem. 50, 1465–1473. doi:10.1021/ac50033a022

McCarren, H., Thomas, E., Hasegawa, T., Röhl, U., Zachos, J.C., 2008. Depth dependency of the Paleocene-Eocene carbon isotope excursion: Paired benthic and terrestrial biomarker records (Ocean Drilling Program Leg 208, Walvis Ridge). Geochemistry, Geophys. Geosystems 9, n/a–n/a. doi:10

McIver, E.E., Basinger, J.F., 1999. Early Tertiary Floral Evolution in the Canadian High Arctic. Ann. Missouri Bot. Gard. 86, 523. doi:10.2307/2666184.1029/2008GC002116

Miall, A.D., 1986. The Eureka Sound Group (Upper Cretaceous - Oligocene), Canadian Arctic Islands. Bull. Can. Pet. Geol. 34, 240–270.

Miall, A.D., 1979. Mesozoic and Tertiary geology of Banks Island, Arctic Canada: The history of an unstable craton margin. Geological Survey of Canada, Memoir 387. doi:doi:10.4095/105620

Moldowan, J.M., Dahl, J., Huizinga, B.J., Fago, F.J., Hickey, L.J., Peakman, T.M., Taylor, D.W., 1994. The molecular fossil record of oleanane and its relation to angiosperms. Science 265, 768–71. doi:10.1126/science.265.5173.768

Murray, A.P., Summons, R.E., Boreham, C.J., Dowling, L.M., 1994. Biomarker and n-alkane isotope profiles for Tertiary oils: relationship to source rock depositional setting. Org. Geochem. 22, 521–IN6. doi:10.1016/0146-6380(94)90124-4

Padilla, A., Eberle, J.J., Gottfried, M.D., Sweet, A.R., Hutchison, J.H., 2014. A sand tiger shark–dominated fauna from the Eocene Arctic greenhouse. J. Vertebr.

Paleontol. 34, 1307–1316. doi:10.1080/02724634.2014.880446

Pagani, M., Pedentchouk, N., Huber, M., Sluijs, A., Schouten, S., Brinkhuis, H., Sinninghe Damsté, J.S., Dickens, G.R., Backman, J., Clemens, S., Cronin, T., Eynaud, F., Gattacceca, J., Jakobsson, M., Jordan, R., Kaminski, M., King, J., Koc, N., Martinez, N.C., McInroy, D., Moore Jr, T.C., O'Regan, M., Onodera, J., Pälike, H., Rea, B., Rio, D., Sakamoto, T., Smith, D.C., St John, K.E.K., Suto, I., Suzuki, N., Takahashi, K., Watanabe, M., Yamamoto, M., 2006. Arctic hydrology during global warming at the Palaeocene/Eocene thermal maximum. Nature 442, 671–675. doi:10.1038/nature05043

Pautler, B.G., Reichart, G.-J., Sanborn, P.T., Simpson, M.J., Weijers, J.W.H., 2014. Comparison of soil derived tetraether membrane lipid distributions and plant-wax δD compositions for reconstruction of Canadian Arctic temperatures. Palaeogeogr. Palaeoclimatol. Palaeoecol. 404, 78–88. doi:10.1016/j.palaeo.2014.03.038

Pedentchouk, N., Sumner, W., Tipple, B., Pagani, M., 2008. δ13C and δD compositions of n-alkanes from modern angiosperms and conifers: An experimental set up in central Washington State, USA. Org. Geochem. 39, 1066–1071. doi:10.1016/j.orggeochem.2008.02.005

Polissar, P.J., Freeman, K.H., Rowley, D.B., McInerney, F.A., Currie, B.S., 2009. Paleoaltimetry of the Tibetan Plateau from D/H ratios of lipid biomarkers. Earth Planet. Sci. Lett. 287, 64–76. doi:10.1016/j.epsl.2009.07.037

Ricketts, B., 1986. New formations in the Eureka Sound Group, Canadian Arctic

Islands [WWW Document]. Curr. Res. Part B; Geol. Surv. Canada. URL ftp://s5-bsc-faisan.cits.rncan.gc.ca/pub/geott/ess_pubs/120/120661/cr_1986_120661.pdf (accessed 8.3.15).

Rullkötter, J., Marzi, R., 1988. Natural and artificial maturation of biological markers in a Toarcian shale from northern Germany. Org. Geochem. 13, 639–645. doi:10.1016/0146-6380(88)90084-8

Sachse, D., Billault, I., Bowen, G.J., Chikaraishi, Y., Dawson, T.E., Feakins, S.J., Freeman, K.H., Magill, C.R., McInerney, F.A., van der Meer, M.T.J., Polissar, P., Robins, R.J., Sachs, J.P., Schmidt, H.-L., Sessions, A.L., White, J.W.C., West, J.B., Kahmen, A., 2012. Molecular Paleohydrology: Interpreting the Hydrogen-Isotopic Composition of Lipid Biomarkers from Photosynthesizing Organisms. Annu. Rev. Earth Planet. Sci. 40, 221–249. doi:10.1146/annurev-earth-042711-105535

Schefuss, E., Schouten, S., Schneider, R.R., 2005. Climatic controls on central African hydrology during the past 20,000 years. Nature 437, 1003–6. doi:10.1038/nature03945

Schimmelmann, A., Sessions, A.L., Mastalerz, M., 2006. HYDROGEN ISOTOPIC (D/H) COMPOSITION OF ORGANIC MATTER DURING DIAGENESIS AND THERMAL MATURATION. Annu. Rev. Earth Planet. Sci. 34, 501–533. doi:10.1146/annurev.earth.34.031405.125011

Schouten, S., Hopmans, E.C., Schefuß, E., Sinninghe Damsté, J.S., 2002. Distributional variations in marine crenarchaeotal membrane lipids: a new tool

for reconstructing ancient sea water temperatures? Earth Planet. Sci. Lett. 204, 265–274. doi:10.1016/S0012-821X(02)00979-2

Schouten, S., Woltering, M., Rijpstra, W.I.C., Sluijs, A., Brinkhuis, H., Sinninghe Damsté, J.S., 2007. The Paleocene–Eocene carbon isotope excursion in higher plant organic matter: Differential fractionation of angiosperms and conifers in the Arctic. Earth Planet. Sci. Lett. 258, 581–592. doi:10.1016/j.epsl.2007.04.024

Schubert, B.A., Jahren, A.H., Eberle, J.J., Sternberg, L.S.L., Eberth, D.A., 2012. A summertime rainy season in the Arctic forests of the Eocene. Geology 40, 523–526. doi:10.1130/G32856.1

Serreze, M.C., Barrett, A.P., Stroeve, J.C., Kindig, D.N., Holland, M.M., 2009. The emergence of surface-based Arctic amplification. Cryosph. 3, 11–19. doi:10.5194/tc-3-11-2009

Sessions, A.L., Burgoyne, T.W., Schimmelmann, A., Hayes, J.M., 1999. Fractionation of hydrogen isotopes in lipid biosynthesis. Org. Geochem. 30, 1193–1200. doi:10.1016/S0146-6380(99)00094-7

Sluijs, A., Schouten, S., Pagani, M., Woltering, M., Brinkhuis, H., Damsté, J.S.S., Dickens, G.R., Huber, M., Reichart, G.-J., Stein, R., Matthiessen, J., Lourens, L.J., Pedentchouk, N., Backman, J., Moran, K., 2006. Subtropical Arctic Ocean temperatures during the Palaeocene/Eocene thermal maximum. Nature 441, 610–613. doi:10.1038/nature04668

Speelman, E.N., Reichart, G.-J., de Leeuw, J.W., Rijpstra, W.I.C., Sinninghe

Damsté, J.S., 2009. Biomarker lipids of the freshwater fern Azolla and its fossil counterpart from the Eocene Arctic Ocean. Org. Geochem. 40, 628–637. doi:10.1016/j.orggeochem.2009.02.001

Speelman, E.N., Sewall, J.O., Noone, D., Huber, M., der Heydt, A. von, Damsté, J.S., Reichart, G.-J., 2010. Modeling the influence of a reduced equator-to-pole sea surface temperature gradient on the distribution of water isotopes in the Early/Middle Eocene. Earth Planet. Sci. Lett. 298, 57–65. doi:10.1016/j.epsl.2010.07.026

Sweet, A.R., 2012. Applied research report on 5 outcrop samples collected by Andrew Miall from northern Banks Island.

Tanner, B.R., Uhle, M.E., Kelley, J.T., Mora, C.I., 2007. C3/C4 variations in salt-marsh sediments: An application of compound-specific isotopic analysis of lipid biomarkers to late Holocene paleoenvironmental research. Org. Geochem. 38, 474–484. doi:10.1016/j.orggeochem.2006.06.009

Taylor, D.W., Li, H., Dahl, J., Fago, F.J., Zinniker, D., Moldowan, J.M., 2006. Biogeochemical evidence for the presence of the angiosperm molecular fossil oleanane in Paleozoic and Mesozoic non-angiospermous fossils. Paleobiology 32, 179–190. doi:10.1666/0094-8373(2006)32[179:BEFTPO]2.0.CO;2

Vandenberghe, N., Hilgen, F.J., Speijer, R.P., Ogg, J.G., Gradstein, F.M., Hammer, O., Hollis, C.J. and Hooker, J.J., 2012. The Paleogene Period. The geologic time scale, 2012, pp.855-921.

Weijers, J.W.H., Schouten, S., Sluijs, A., Brinkhuis, H., Sinninghe Damsté, J.S., 2007a. Warm arctic continents during the Palaeocene–Eocene thermal maximum. Earth Planet. Sci. Lett. 261, 230–238. doi:10.1016/j.epsl.2007.06.033

Weijers, J.W.H., Schouten, S., Spaargaren, O.C., Sinninghe Damsté, J.S., 2006. Occurrence and distribution of tetraether membrane lipids in soils: Implications for the use of the TEX86 proxy and the BIT index. Org. Geochem. 37, 1680–1693. doi:10.1016/j.orggeochem.2006.07.018

Weijers, J.W.H., Schouten, S., van den Donker, J.C., Hopmans, E.C., Sinninghe Damsté, J.S., 2007b. Environmental controls on bacterial tetraether membrane lipid distribution in soils. Geochim. Cosmochim. Acta 71, 703–713. doi:10.1016/j.gca.2006.10.003

Weller, P., Stein, R., 2008. Paleogene biomarker records from the central Arctic Ocean (Integrated Ocean Drilling Program Expedition 302): Organic carbon sources, anoxia, and sea surface temperature. Paleoceanography 23, n/a–n/a. doi:10.1029/2007PA001472

West, C.K., Greenwood, D.R., Basinger, J.F., 2015. Was the Arctic Eocene "rainforest" monsoonal? Estimates of seasonal precipitation from early Eocene megafloras from Ellesmere Island, Nunavut. Earth Planet. Sci. Lett. 427, 18–30. doi:10.1016/j.epsl.2015.06.036

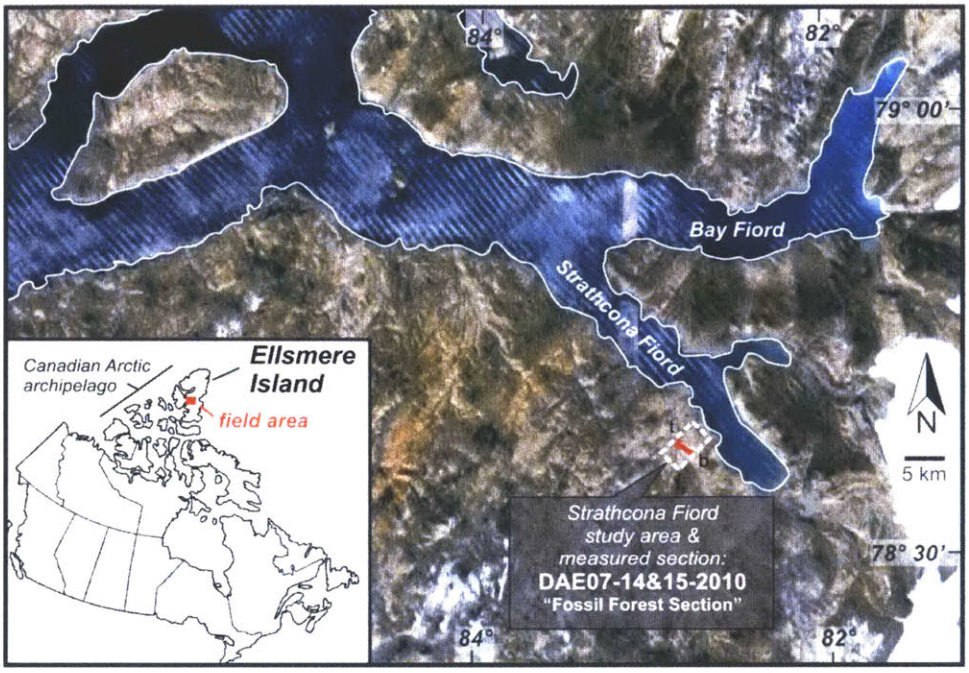

Figure 3.1: Map showing the sampling area within Strathcona Fiord on Ellesmere Island, Nunavut, Canada. Sampling covered 810m from the bottom (b) to the top (t) of the outcrop.

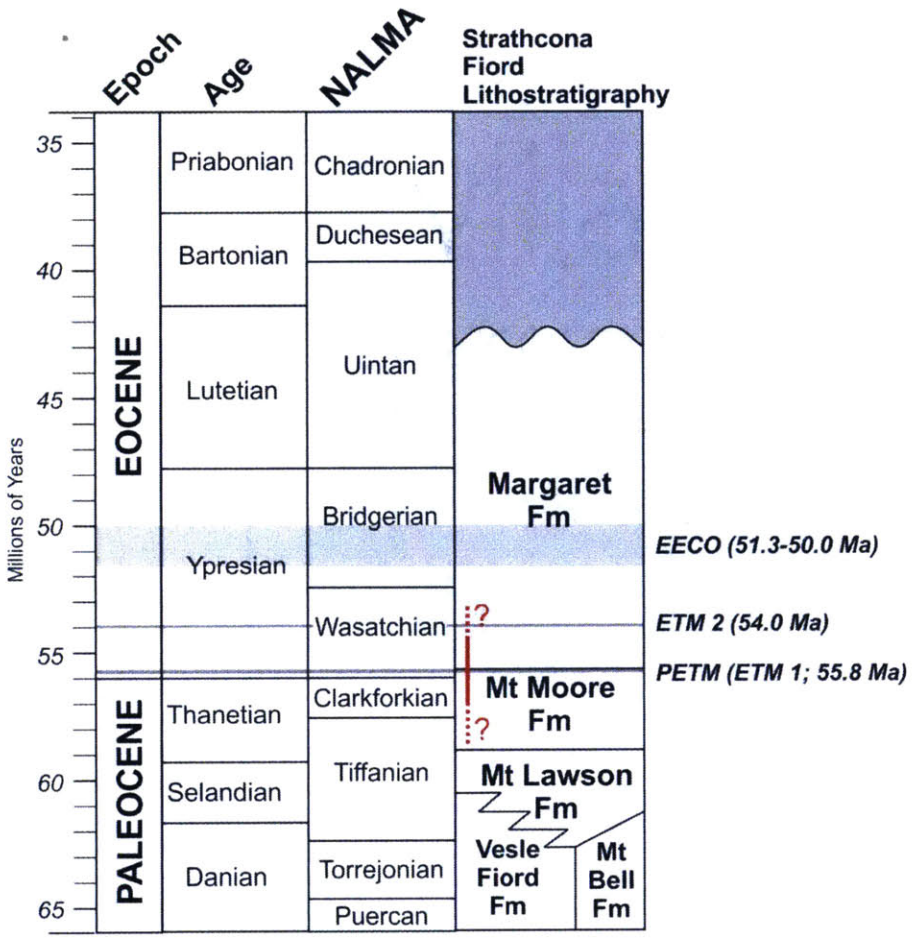

Figure 3.2: Inferred age range of the Strathcona Fiord section. Range is anchored based upon the formational contact in the middle of the section. Dashed lines illustrate the uncertainty of extent at the limits of the section. Modifed from Eberle and Greenwood (2012) and updated chronostratigraphically using Vandenberghe et al. (2012).

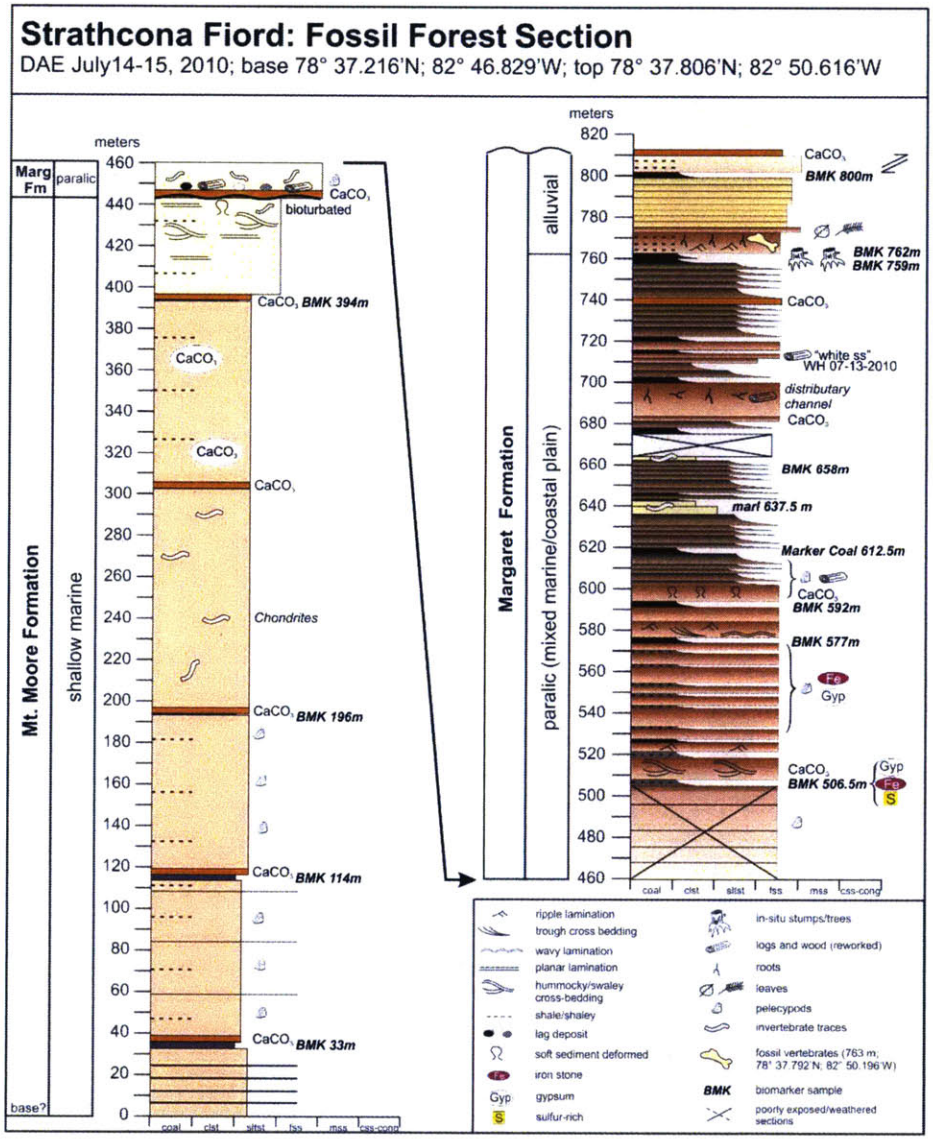

Figure 3.3: Lithostratigraphy of the Strathcona Fiord outcrop. Samples taken for biomarker analysis denoted BMK.

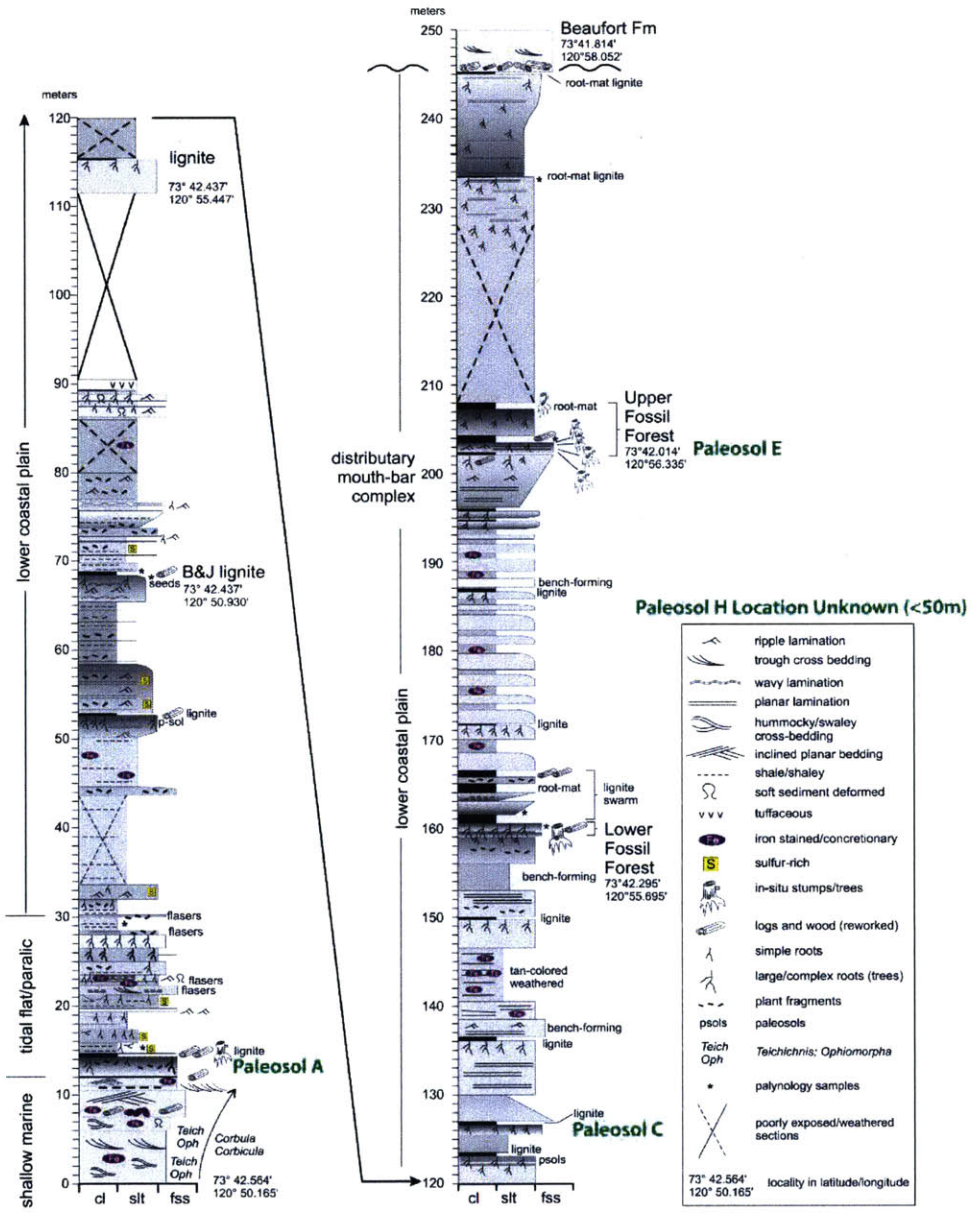
meters
lignite
73° 42.437'
120° 55.447'
B&J lignite
73° 42.437'
120° 50.930'
seeds
p-sol
flasers
Paleosol A
Teich Oph
Corbula Corbicula
73° 42.564'
120° 50.165'
lower coastal plain
tidal flat/paralic
shallow marine
cl
slt
fss
Beaufort Fm
73°41.814'
120°58.052'
root-mat lignite
root-mat
Upper Fossil Forest
73°42.014'
120°56.336'
Paleosol E
distributary mouth-bar complex
bench-forming lignite
Paleosol H Location Unknown (<50m)
lignite swarm
Lower Fossil Forest
73°42.295'
120°55.695'
tan-colored weathered
Paleosol C
psols
ripple lamination
trough cross bedding
wavy lamination
planar lamination
hummocky/swaley cross-bedding
inclined planar bedding
shale/shaley
soft sediment deformed
tuffaceous
iron stained/concretionary
sulfur-rich
in-situ stumps/trees
logs and wood (reworked)
simple roots
large/complex roots (trees)
plant fragments
paleosols
Teich Oph
Teichichnis; Ophiomorpha
palynology samples
poorly exposed/weathered sections
73° 42.564'
120° 50.165'
locality in latitude/longitude

Figure 3.4: Composite measured section through the exposures of the Eureka Sound Formation at Musk Ox River, north eastern Banks Island. Section transect is indicated by latitude and longitude coordinates at various localities highlighted in the section. Overall, the section records deposition in a lower coastal plain setting characterized by distributary mouth-bar complexes and extensive wetlands (Miall 1979).

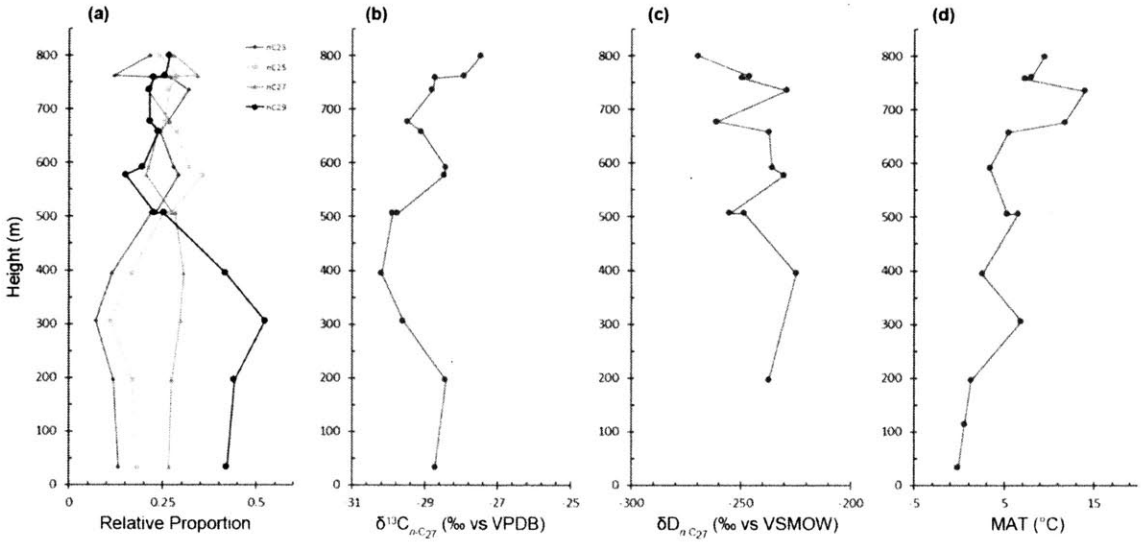

Figure 3.5: Strathcona Fiord profiles illustrating the **(a)** relative proportion of major long chain *n*-alkanes, **(b+c)** *n*-C_{27} carbon and hydrogen isotopes and **(d)** MBT/CBT based mean air temperatures (MAT).

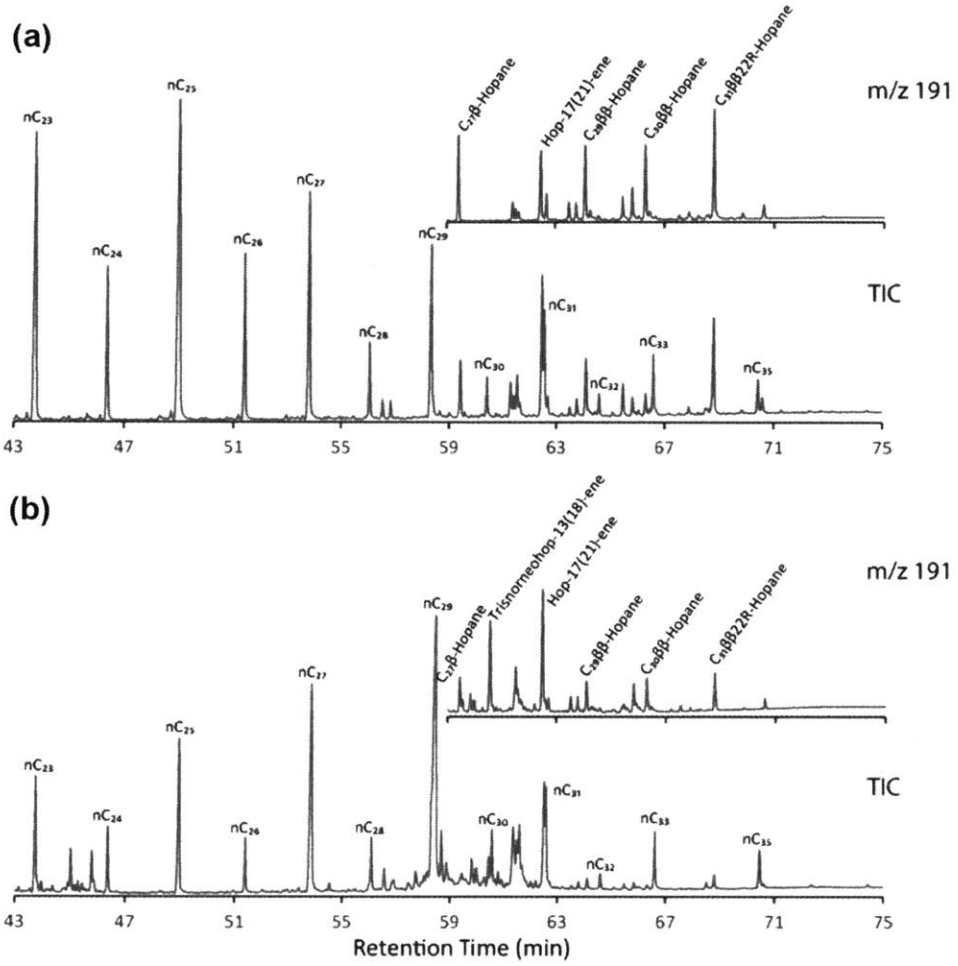

Figure 3.6: Representative distributions of aliphatic hydrocarbons from the **(a)** Margaret Formation and **(b)** Mt. Moore Formation at Strathcona Fiord. Peaks amplitudes are displayed relative to the largest. Total ion chromatograms (TICs) are given with inset extracted ion chromatograms (EICs) of m/z 191 to illustrate the hopanoid components.

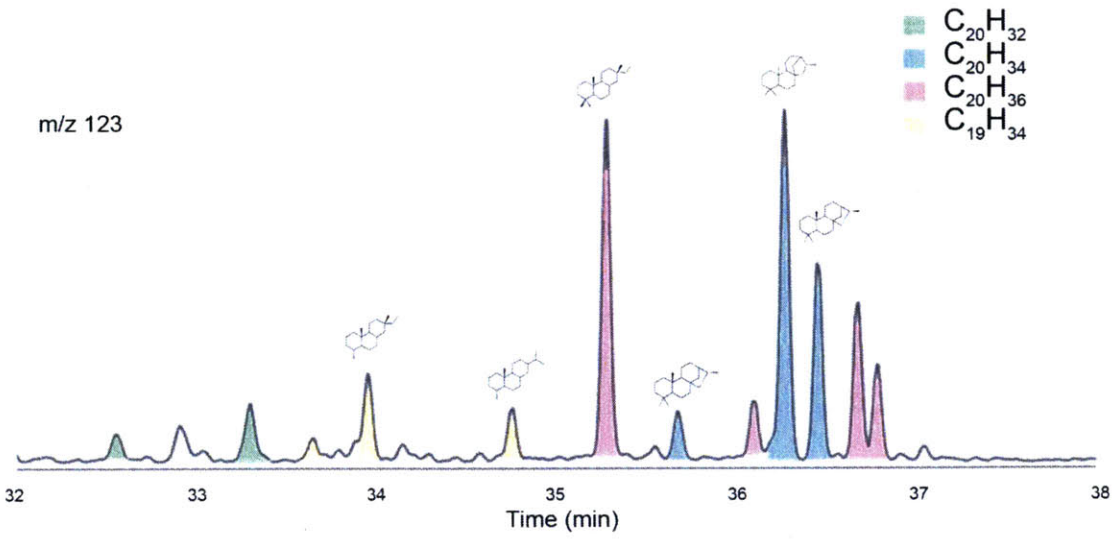

Figure 3.7: Distribution of diterpenoids in a m/z 123 extracted ion chromatogram from Paleosol E. Structures placed above peaks are tentative due to the lack of availability of authentic standards to confirm identification.

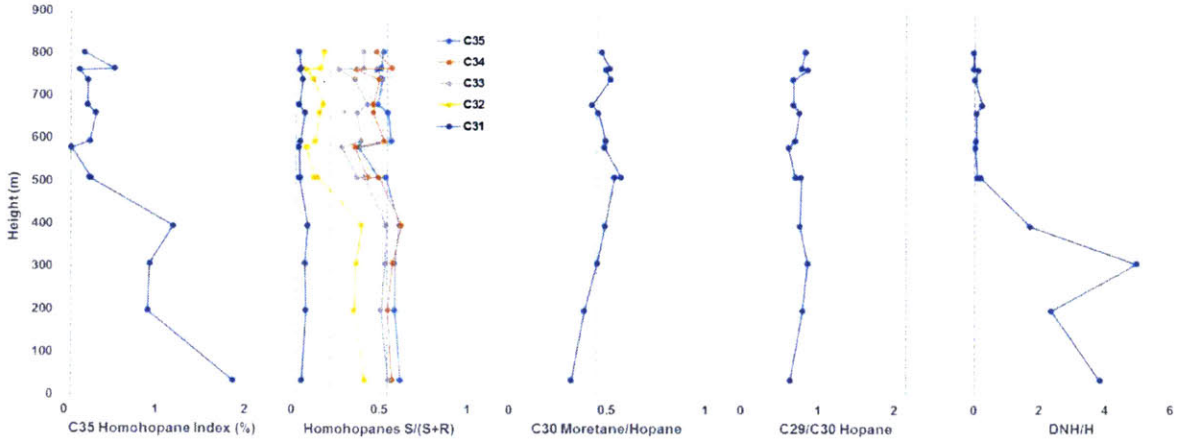

Figure 3.8: Characteristic parameters based upon hopane and sterane distributions: (a) the homohopane index (%), (b) the homohopane isomerization series, (c) the C30 moretane/hopane ratio, (d) the norhopane/hopane ratio and (e) the 28,30-dinorhopane/hopane ratio. Dashed color lines indicate average values of Paleosol E. Standard deviations of paleosol measurements (n=10) are (a) ±0.05, (b) ±0.04, (c) ±0.08, (d) ±0.58 and (e) ±0.03.

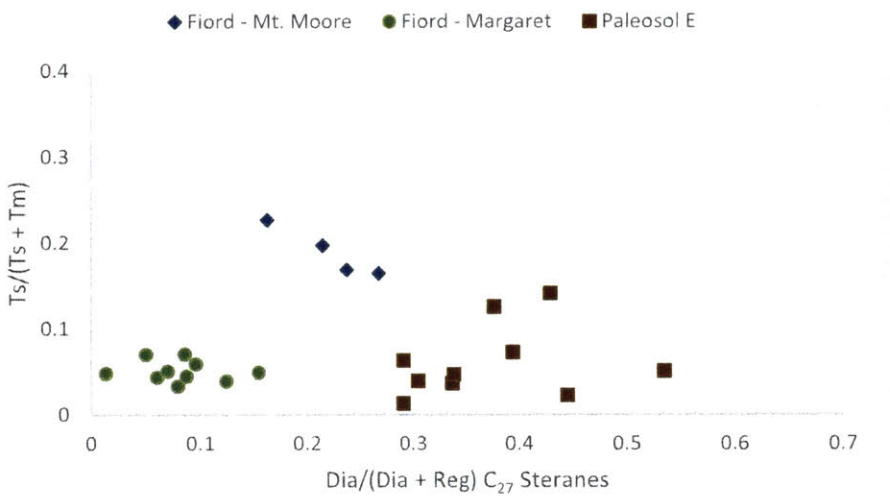

Figure 3.9: 18α-trisnorhopane/(18α-trisnorhopane + 17α-trisnorhopane) vs. C27 diasteranes/(diasteranes + steranes) illustrating distinct groupings by formation within Strathcona Fiord and Paleosol E.

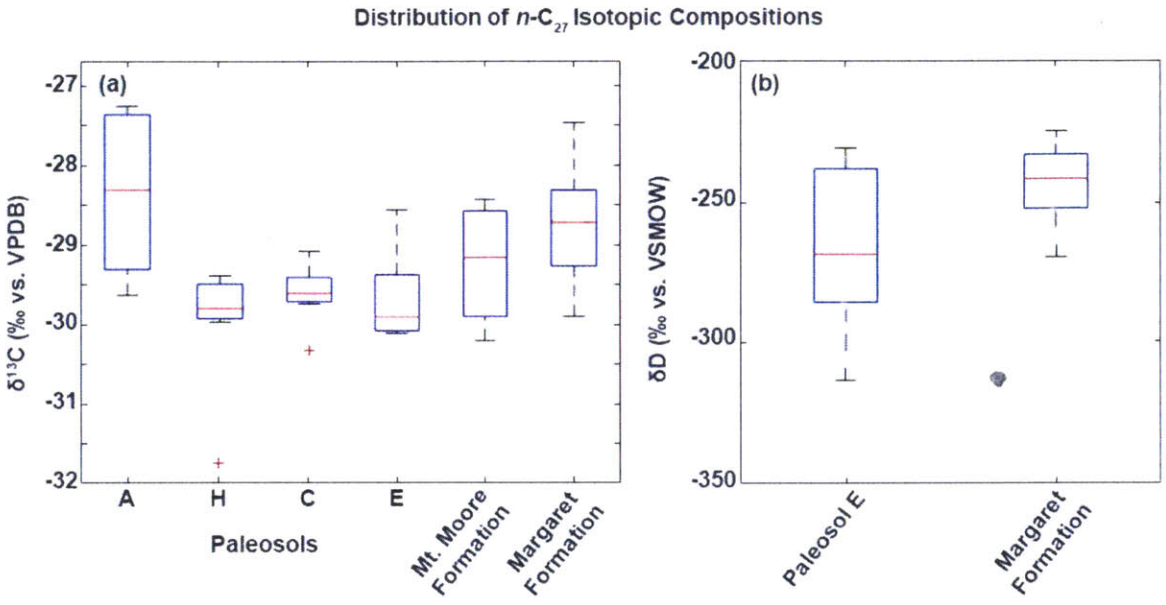

Figure 3.10: (a) Carbon and **(b)** hydrogen isotopic distributions across all sample sites for n-C_{27}.

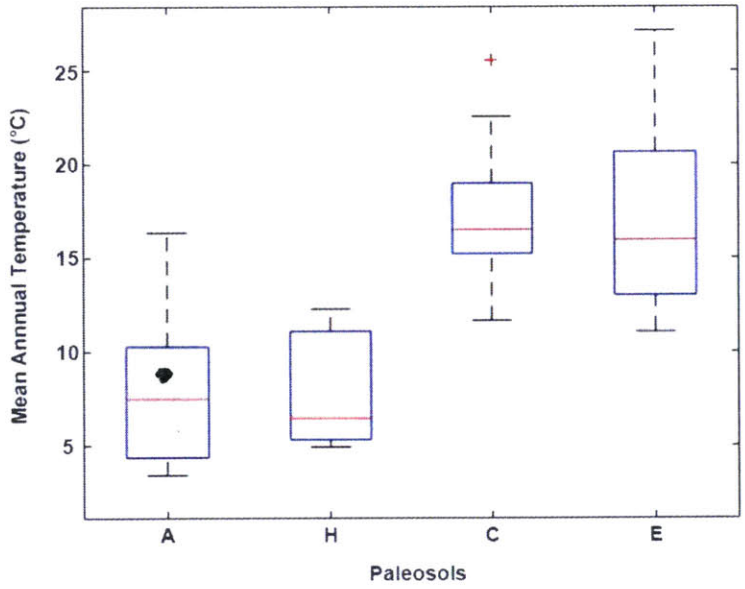

Figure 3.11: MBT/CBT based mean air temperatures (MATs) for paleosol sections.

Table 3.1: Homohopane based indices of the Strathcona Fiord section

Sample Height (m)	C_{35} Homohopane Index	C_{35} Homohopane S/(S+R)	C_{34} Homohopane S/(S+R)	C_{33} Homohopane S/(S+R)	C_{32} Homohopane S/(S+R)	C_{31} Homohopane S/(S+R)
33.0	1.87	0.62	0.57	0.55	0.42	0.06
196.0	0.92	0.59	0.55	0.51	0.36	0.08
306.0	0.94	0.59	0.58	0.54	0.37	0.08
394.0	1.20	0.62	0.63	0.54	0.40	0.09
506.5	0.28	0.54	0.50	0.41	0.15	0.04
506.5	0.30	0.50	0.43	0.37	0.13	0.05
577.0	0.08	0.38	0.36	0.28	0.08	0.04
592.0	0.29	0.57	0.53	0.40	0.13	0.05
658.0	0.35	0.55	0.47	0.37	0.16	0.08
677.0	0.26	0.49	0.47	0.43	0.18	0.04
736.0	0.27	0.52	0.50	0.36	0.13	0.06
759.0	0.17	0.49	0.37	0.27	0.08	0.05
762.0	0.56	0.51	0.57	0.41	0.17	0.05
800.0	0.23	0.52	0.49	0.41	0.19	0.04

Table 3.2: Hopane and sterane indices of the Strathcona Fiord section

Sample Height (m)	C_{30} moretane/ hopane	C_{29} /C_{30} hopane	dinorhopane/ hopane	Ts/(Ts+Tm)	Dia/(Dia+Reg) C_{27} Steranes
33.0	0.32	0.64	3.86	0.23	0.16
196.0	0.39	0.81	2.38	0.17	0.24
306.0	0.45	0.87	4.98	0.16	0.27
394.0	0.49	0.77	1.74	0.20	0.21
506.5	0.54	0.79	0.23	0.07	0.05
506.5	0.57	0.71	0.12	0.05	0.01
577.0	0.49	0.62	0.04	0.04	0.06
592.0	0.49	0.70	0.08	0.07	0.09
658.0	0.46	0.76	0.08	0.04	0.12
677.0	0.43	0.68	0.27	0.06	0.10
736.0	0.52	0.68	0.04	0.05	0.07
759.0	0.50	0.88	0.14	0.03	0.08
762.0	0.52	0.79	0.00	0.04	0.09
800.0	0.47	0.84	0.00	0.05	0.15

Table 3.3: MBT/CBT based mean annual temperature and *n*-C27 carbon and hydrogen isotopic composition of Banks Island paleosols.

Site	Depth (cm)	MAT (°C)	$\delta^{13}C_{n\text{-}C27}$ (‰ vs. VPDB)	$\delta^{2}H_{n\text{-}C27}$ (‰ vs. VSMOW)
Paleosol A	4	16	-29.6	-
	12	3	-29.2	-
	20	10	-27.7	-
	28	7	-27.3	-
	36	4	-28.3	-
	44	8	-27.4	-
Paleosol C	4	26	-30.3	-
	12	23	-29.6	-
	20	17	-29.6	-
	28	18	-	-
	36	16	-29.6	-
	44	16	-29.1	-
	52	16	-29.7	-
	60	12	-29.4	-
	68	12	-29.4	-
Paleosol E	4	27	-30.3	-260.8
	12	21	-29.8	-231.0
	20	14	-31.7	-233.9
	28	21	-28.6	-279.7
	36	13	-30.0	-291.4
	44	19	-29.3	-276.8
	52	12	-30.1	-313.8
	60	15	-30.1	-242.7
	68	16	-29.4	-287.1
Paleosol H	2	5	-31.8	-
	11	5	-29.4	-
	26	6	-30.0	-
	36	11	-30.2	-
	40.5	12	-29.8	-

Table 3.4: MBT/CBT based mean annual temperature and *n*-C27 carbon and hydrogen isotopic composition of the Strathcona Fiord section.

Site	Height (m)	MAT (°C)	$\delta^{13}C_{n\text{-}C27}$ (‰ vs. VPDB)	$\delta^{2}H_{n\text{-}C27}$ (‰ vs. VSMOW)
Strathcona Fiord	800	9	-27.5	-269.7
	762	8	-27.9	-246.1
	759	7	-28.7	-249.5
	736	14	-28.8	-229.0
	677	12	-29.5	-261.2
	658	5	-29.1	-237.1
	592	3	-28.4	-235.8
	577	5	-28.5	-230.2
	506.5	3	-29.9	-248.5
	506.5	6	-29.8	-255.2
	394	7	-30.2	-224.7
	306	1	-29.6	-
	196	1	-28.4	-237.1
	33	0	-28.7	-

Chapter 4

The recent history of high elevation Lagunas Miscanti and Miñiques, Chilean Altiplano, as revealed by biomarker study

The recent history of high elevation Lagunas Miscanti and Miñiques, Chilean Altiplano, as revealed by biomarker study

Ross H. WILLIAMS[a]*, Jiaynaer BOLATI[b], Blas E. VALERO–GARCÉS[c], David MCGEE[a] and Roger E. SUMMONS[a]

a. Department of Earth, Atmospheric and Planetary Sciences, Massachusetts Institute of Technology, 77 Massachusetts Avenue, Cambridge, MA 02139-4307, USA
b. School of Earth and Space Sciences, University of Science and Technology of China, 96 Jinzhai Road, Hefei, Anhui Province, China 230026
c. Instituto Pirenaico de Ecología, CSIC, Aptdo. 13034, 50080 Zaragoza, Spain

*rosshw@mit.edu

Abstract

Situated in the Chilean Altiplano, the neighboring lakes of Miscanti and Miñiques are of interest due to their unique location and ability to furnish detailed continuous high elevation biogeochemical records. Accordingly, sediment cores were acquired for centennial scale investigation of regional climates of this region of South America over the Holocene. Coring in the two lakes spanned two different but overlapping time periods that extend from ~2500 BCE to 1905 CE as determined by ^{14}C dating supported by U/Th and $^{210}Pb/^{137}Cs$ measurements. Our study has revealed distinct limnological phases within the lakes that are characterized by markedly different biomarker contents. The contributions of macrophytes and algae were determined by the relative contributions of multiple source-diagnostic compounds (i.e. n-C_{17} and n-C_{23}). Further, core glycerol dialkyl glycerol tetraethers (GDGTs) were used to examine physical changes in the lake such as salinity (ACE index) and lake level (%thaum). Finally, periods of likely euxinic conditions were identified based on the presence of recently described S-GDGTs.

In Laguna Miñiques, the earliest period (~2500-1910 BCE) studied was characterized by a transition from low to high lake levels ending with a sharp increase in salinity and collapse of stratification and euxinia. This time was followed by an extended period (1910-139 BCE) of high salinity that saw a decline of aquatic macrophytes and rise of unicellular algae. This picture reversed in the final period (139 BCE-1670 CE) where the molecular records suggest that salinity dropped sharply and stabilized, macrophytes recovered, and the relative

contributions from algae declined. Complementing this record, Laguna Miscanti displays just two limnologically distinct periods. The first (212-920 CE) is revealed to be physically and chemically stable as in Miñiques, but with potential variations in productivity. The most recent time period (920-1905 CE) is shown to be a period of increasing salinity with episodic events of lake level change and euxinia.

4.1. Introduction

Over the past millennia our planet has experienced a number of centennial scale climate fluctuations. While these are well established in numerous Northern Hemisphere climate records, complementary data from the Southern Hemisphere is sparse. In particular, South America's diverse climatic zones suffer from the absence of extensive well dated high resolution climatic records. It is important to remedy this as the region is subject to economically important climatic events such as El Niño.

High altitude lakes are of particular interest for paleoenvironmental studies. Their locations, remote from centers of population density, mean that they are less likely to have experienced pollution and other forms of anthropogenic perturbation. Further, extreme locations can furnish unique settings in terms of ecological complexity and lake chemistry that are useful interpreting past climatic variations. Other high altitude lakes in the region have been studied in the past to elucidate changes in climate features such as ENSO events (Baker et al., 2001; Moy et al., 2002; Rowe et al., 2002) including studies involving Laguna Miscanti itself (Schwalb et al., 1999; Valero-Garcés et al., 2003, 1999, 1996). However, no detailed lipid biomarker studies of either Laguna Miscanti or neighboring Laguna Miñiques have been conducted.

While most often employed in the marine realm, lipid biomarker records are becoming ever more important in limnologic studies that include climatic reconstructions. While the marine records serve as invaluable long term climatic

records, lakes have significant benefits as well. While their records are not as lengthy, the high production levels and sedimentation rates allow for the study of local and regional effects at much greater temporal resolution. In lakes there are a number of prevalent biomarker classes that can be utilized to establish the primary sources of organic matter. These include sterols (Nishimura, 1977; Wen-Yen and Meinschein, 1976), alkanoic acids (Rielley et al., 1991), *n*-alkanes (Cranwell, 1973) n-alkanols, and diols (Volkman et al., 1999), for example.

Beyond identifying the source of organic matter, biomarkers can also furnish information about past environmental conditions. Of particular interest in studies utilizing biomarkers for this is the application of proxies that utilize the membrane-spanning ether lipids known as glycerol-dialkyl-glycerol tetraethers (GDGTs) produced by archaea and some bacteria. Most common are the TEX_{86} and MBT/CBT based temperature proxies. The first, TEX_{86}, employs GDGTs with an isoprenoidal backbone formed by various archaea and is widely applied in the marine realm to reconstruct sea surface temperatures (Schouten et al., 2002). While clearly a measurement specifically suited to the marine realm, successful attempts have been made in a few large lacustrine settings as well (Kaiser et al., 2015; Kraemer et al., 2015; Powers et al., 2005; Wang et al., 2015).

In contrast, the MBT/CBT proxy uses non-isoprenoidal (a.k.a. branched) GDGTs with varying degrees of methylation and cyclization on their alkyl chains to reconstruct mean air temperature (MAT) (Weijers et al., 2007). This class of compounds is formed by soil bacteria (Weijers et al., 2006), and possibly

acidobacteria (Damsté et al., 2011). Similar to TEX_{86}, this proxy was initially used in marine deposits with terrestrial organic matter inputs but then expanded to include studies of lakes (Sinninghe Damsté et al., 2012). However, caution must be exercised in such studies due to the infancy of this research. *In-situ* production of these compounds is, for example, one process that could significantly impact the interpretation of any results (Tierney and Russell, 2009).

In both cases, the temperature proxies based upon GDGTs require proper application of calibrations. The question of applicability of TEX_{86} in polar oceans led to separate calibration lines for low temperature environments, TEX^{L}_{86}, and high temperature environments, TEX^{H}_{86} (Kim et al., 2010). Further, observed offsets in temperature reconstruction led to the development of at least one lacustrine-specific calibration (Powers et al., 2010). To address discrepancies in the MBT/CBT measurements several adjustments were proposed for application to lakes (Pearson et al., 2011; Tierney et al., 2010) including regional calibrations (Foster et al., 2016). Recent isotopic investigation has also revealed complexity in possible GDGT sources that reinforces that caution must be taken in interpreting results based upon them (Pearson et al., 2016).

4.2. Regional Setting

The Altiplano plateau is second only to Tibet in elevation above sea level and areal extent. Included in its boundaries are portions of Chile, Argentina, Bolivia, and Peru. However, unlike Tibet, the Altiplano did not form from continental collision but instead predominantly due to horizontal shortening of crust leading to

thickening (Allmendinger et al., 1997). Often defined by its internally draining basins, the plateau is associated with several active volcanic ranges. An area of extreme climatic gradients, the Amazon rainforest lies to the northeast just over the Andes Mountains while the Atacama, the world's driest desert, overlaps the southwestern portion.

Two lakes, Miscanti and Miñiques, lie in the driest region of the Atacama Altiplano (Fig. 4.1). Situated at 4120-4140 meters above sea level, these two lakes are the largest and deepest lakes in the region. As such, they have been identified as the only potentially reliable local sources for records of continuous paleolimnologic (Valero-Garcés et al., 2003, 1996) and palynologic features (Grosjean, 2001). The lakes are separated by a ~1km wide rise although numerous paleoshorelines indicate they constituted a single body of water during past times of elevated lake levels. Immediately to the west, the lakes are bounded by a ridge along the Quebrada Nacimiento Fault. The regional geology is dominated by Miocene to recent volcanic deposits.

Mean temperatures in this area are only ~2°C and rainfall amounts to just 200mm/yr (Grosjean, 2001). Vegetation is sparse around the lakes due to the limited precipitation. Further, no major human settlements exist nearby and, as they are part of the Los Flamencos National Reserve, public access to the lakes themselves is restricted. The dominant fauna in the area are small herds of the cameloid vicuña which congregate around the salt deposits rimming the lakes.

The larger lake, Laguna Miscanti, lies to the north and is about 13.5km^2 and up to 10m deep. With a pH ~8 the lake is presently mildly alkaline and brackish (6.4–6.9 mS cm−1) (Grosjean, 2001). With no input or output by rivers, the closed lake is fed by groundwater flow through its large catchment area (320km^2). The lake also has two exposed springs along its shoreline. On the northern shore lies a freshwater spring while a thermal spring flows into the northeastern region. Expansive green and orange microbial mats are present in the warm waters at that point.

Laguna Miñiques is very similar to L. Miscanti in lacking permanent surface inflow/outflow channels. Due to its close proximity, it also has a similar catchment and surrounding ecology. However, L. Miñiques is much smaller at only 1.6 km^2 (Crespo and De los Rios, 2004) and 7m deep. As such, it is likely more prone to dramatic changes in response to shifting climates. While L. Miñiques does not have any springs, it is believed to be fed from L. Miscanti, possibly along the nearby fault. Due to its more limited size, far fewer studies have been conducted on L. Miñiques as compared to L. Miscanti.

4.3 Methods

Both lakes were cored in April of 2013 using a gravity corer. Cores were kept sealed and were shipped to Spain where they were kept in cold storage. There they were split, imaged, and samples taken using solvent clean spatulas and combusted glass jars. For L. Miscanti, one core was sampled at 10 cm intervals to a depth of 110 cm. In L. Miñiques, three cores from the same hole were combined to make a

composite profile which was sampled at 15cm intervals to a depth of 175cm. Once exposed to the air, samples were kept frozen prior to analysis.

Samples were freeze-dried and crushed prior to lipid extraction and spiked with a mix of appropriate standard compounds (3-Methylheneicosane, 1-Nonadecanol and 2-Methyloctadecanoic acid; 1000 ng each). Procedural blanks of combusted sand revealed no contamination during the work-up. A modified Bligh-Dyer method was utilized for extraction (Sturt et al., 2004). Samples were first extracted 3 times via sonication in a phosphate buffer solution (PBS), dichloromethane (DCM) and methanol mix (PBS:DCM:MeOH 0.8:1:2) then again with trichloroacetic acid in place of the PBS (TCA:DCM:MeOH 0.8:1:2). Finally it was extracted once with DCM:MeOH 3:1. All extracts of a sample were pooled in a separatory funnel and the organic phase removed by liquid-liquid extraction. Silica gel column chromatography was then used to separate the extracts into four compound classes: aliphatic hydrocarbons, aromatic hydrocarbons, ketones, and a combined acids and alcohols fraction (henceforth termed 'polar' fraction).

Gas chromatography-mass spectrometry (GC-MS) of aliphatic and polar fractions was obtained on an Agilent 7890A gas chromatograph equipped with a programmable temperature vaporizing (PTV) injector operated in splitless mode and a DB-1MS column (Agilent J&W 60m length, 0.25mm diameter, 0.25μm film) interfaced to an Agilent 5975C mass selective detector. The temperature program for the GC oven at an initial temperature of 60°C for 2 minutes then ramped at 10°C/min to 150°C followed by 3°C/min to 330°C where it was maintained for 19 minutes. Prior to this analysis,

the polar fractions were derivatized with 20 μL each of N,O-Bis(trimethylsilyl)trifluoroacetamide (BSTFA) and pyridine at 80°C for 2 hours to make the compounds amenable to gas chromatography. Compound identification was based upon comparison to spectral libraries and published spectra. When definitive identification was not possible they were assigned to compound classes based upon characteristic fragment ions and relative retention times.

For analysis of core GDGTs an aliquot of the polar fraction was taken for analysis by liquid chromatography-mass spectrometry (LC-MS) on an Agilent 1260 Infinity series high performance liquid chromatograph (HPLC) coupled with an Agilent 6130 single quadrupole mass spectrometer via an air pressure chemical ionization (APCI) interface. APCI source conditions were positive ion mode, drying gas (N2) temperature 350 °C, vaporizer temperature 380 °C, drying gas flow rate 6 L/min, nebulizer gas (N2) pressure 30 psi, capillary voltage 2000 V, corona current 5 μA. The detector was run in selected ion monitoring (SIM) mode targeting core GDGT masses as well as archaeol and a C46 GDGT standard used for response factor determination and compound quantification (Huguet et al., 2006). Separation of compounds was achieved using a slightly modified version of the tandem amide column method of Becker et al. (2013). Two Acquity UPLC BEH HILIC amide columns (2.1 x 150 mm, 1.7 μm, Waters, Milford, U.S.A.) were used in tandem and maintained at 45 °C. Eluents A (n-hexane) and B (n-hexane:isopropyl alcohol, 80:20 v:v) were applied with a flow rate of 0.4ml/min and the following linear gradients: 2% B constant for 10 minutes, to 6% B in 10 minutes, to 15% B in 15 minutes, to

45% B in 15 minutes, to 55% B in 20 minutes, to 70% B in 15 minutes, then returning to 2% B in 0.1 minutes and held there for 9.9 minutes.

4.4 Results

4.4.1 Chronology

Chronology of the cores was established through ^{14}C, $^{210}Pb/^{137}Cs$ and U/Th dating. The 14C and 210Pb/137Cs dating was conducted by coauthor Blas Valero-Garces while the U/Th dating was done by Christine Chen and Justin Stroup in the McGee lab at MIT. The ^{14}C reservoir effects can be quite large at 3750-4544 years for L. Miscanti and 2965 years for L. Miñiques. The reservoir effect in L. Miñiques was held constant while L. Miscanti's was 3750 years in the upper portion based on Pb dating and 4544 years in the lower portion based upon the U/Th dating. These effects are constrained by the $^{210}Pb/^{137}Cs$ dating and U/Th dating. An age model, based on the calculated dates, was then established for each lake. Each individual sample taken for biomarker analysis was 2 cm in depth, therefore the age assigned to each sample is thus the midpoint of a time window spanning several decades. Further, the bottommost sample from L. Miñiques fell just outside the modelled ages and is thus an estimate based on the nearest accumulation rates based upon the lowermost modelled depths. Results indicate very different chronologies between the two lakes with lower sediment accumulation rates in Miñiques. The age of the L. Miscanti samples in this study extend back 1,800 years while the L. Miñiques samples go back approximately 4,500 years. Both core tops are modern and no hiatuses were observed. The analyzed timespan of Miñiques does not extend

to the present as the core top sample for biomarker analysis was compromised during shipping. Average sedimentation rates are 0.21 cm/yr in L. Miscanti and 0.08 cm/yr in L. Miñiques. A consequence of this disparity is that despite similar sampling resolution, the cores overlap only for two data points. However, the two lakes should be hydrologically similar so the higher resolution recent record from L. Miscanti actually complements the longer term record from Miñiques.

4.4.2 Aliphatic Compounds

The aliphatic hydrocarbon fractions of the extractable lipids from both lakes generally display very simple distributions of n-alkanes (Fig. 4.2a). The long chain n-alkanes have a maximum at carbon length 23. This can be demonstrated by the Paq ratio, which is a proxy for the presence of submerged/emergent macrophytes (Ficken et al., 2000). In both lakes the high Paq values remain high over the course of deposition indicating a consistent macrophyte presence in the lakes and lack of significant terrestrial plant matter input (Fig. 4.3). However, there is an interesting decrease in L. Miñiques from the period of 1910 BCE to 139 BCE. Traces of long chain alkanes, such as isononacosane, with additional methylation are evident during this time period. These compounds were not present outside of this period or in L. Miscanti. A very strong odd chain length preference typical of higher plants is evident in all samples.

Laguna Miscanti also differs from L. Miñiques in that hopanoid hydrocarbons are present in the saturate fraction including hop-17(21)-ene, 17β, 21β(H)-hopane, 17β, 21β(H)-homohopane and diploptene. The one exception to this contrast is the uppermost sample from L. Miñiques which shows a very significant diploptene presence compared to other depths (149 ng/g dry weight vs. 90 ng/g dry weight). Another major contrast between the two lakes is in respect to the n-C_{17} abundance. In L. Miscanti this hydrocarbon is always a minor component that varies along with the overall amount of organic matter as represented by the TLE/Mass Extracted ratio, used here due to the absence of total organic carbon values (Fig. 4.4d) (Table 4.1). However, in L. Miñiques there is a clear rise of n-C_{17} from 1671 BCE to a maximum at 567 BCE before reverting to lower levels (Fig. 4.5d). This maximum actually represents a time when n-C_{17} surpassed n-C_{23} as the most dominant n-alkane.

4.4.3. Polar Compounds

The polar components of the TLE are dominated by several compound classes common to lacustrine settings (Table 4.1). For both lakes we find fatty acids, alkanols, alkane diols and sterols/stanols (collectively referred to as sterols henceforth). Other compounds of interest in the lakes are archaeol, O-alkylglycerols and tetrahymanol. The fatty acids and alkanols in both lakes are both dominated by their n-C_{24}. Sterols present in both lakes include stigmastanol, β-sitosterol, stigmasterol, campestanol and campesterol. L. Miñiques also has spongesterol, brassicasterol, cholestanol and cholesterol (Fig. 4.2b).

In L. Miscanti (Fig. 4.4), the archaeol and alkylglycerol concentrations are both very low with the exception of a spike in concentration at 233 CE. This spike is also present to a lesser extent in the tetrahymanol and n-C_{17} records. Diols are present for most of the core with only minor variations in concentration. The long chain fatty acids, alkanols, tetrahymanol and sterols all tend to fluctuate together with two maxima occurring at 365 CE and 920 CE. The earlier maxima at 365 CE is also displayed by n-C_{23} and the overall extractable lipid concentration but they have a second maxima earlier than the other compounds at 688 CE. There is also a very dramatic increase in n-C16 fatty acid at the most recent time point, 1905 CE, from background levels of ~4 μg/g dry weight to ~570 μg/g dry weight.

L. Miñiques differs foremost from L. Miscanti by the fact that none of the measured compound concentrations match the overall extracted lipid concentration (Fig. 4.5). Once again the long chain fatty acids, alkanols, tetrahymanol and sterols all co-vary, this time rising from low background levels to a maximum at 536 CE before dropping again, though not to background levels. The diols are very minor compounds for much of the core but have a very pronounced presence at the base. From the lake's earliest point to 1910 BCE there is a decrease from 51 μg/g dry weight to <1 μg/g dry weight without any recovery. Finally, there is an interesting period from 1671 BCE to 139 BCE where there is an increase in archaeol and alkylglycerols.

4.4.4. Tetraether Lipids

At all measured samples in both lakes the BIT index is always high (~0.98) indicating a significant proportion of branched (i.e. nonisoprenoidal) GDGTs (Table 4.2). Given the lack of riverine input and low precipitation it is likely that these compounds are being produced in situ within the water or sediment of the lake. As such, it is unlikely that any temperature reconstruction based upon these samples would be accurate. The calculated MATs based upon the lake calibrations of Tierney et al., 2010 and Pearson et al., 2011 return values that far overestimate reasonable temperatures for the area by 10-20°C. However the original calibration of Schouten et al., 2002 does return reasonable values of 0.1-0.2°C that vary little over time as expected (actual estimates are 2°C) (Fig. 4.6a,f). This may be entirely coincidental and is not meant to imply the calibration is robust in other lake settings. However it does illustrate the benefit of applying multiple calibrations to generated datasets.

In the isoprenoidal GDGT pool there is always a strong predominance of GDGT-0 (caldarchaeol) over the cyclic GDGTs (Fig. 4.6b,g). At most times caldarchaeol alone represents >75% of the total isoprenoidal GDGTs. The ACE index is a measure of the relative proportions of GDGT-0 and archaeol proposed to be a salinity proxy (Turich and Freeman, 2011). Due to the lack of established response factors during acquisition of the data the approach of Wang et al., 2013 was used in this study. While archaeol was observed by GC-MS, for use in the ACE index it was measured in the same LC-MS runs as GDGT-0. In L. Miscanti, there is a general increase of the index over time with its maximum value in the most recent sediments (Fig. 4.6c). Laguna Miñiques differs in displaying a pronounced increase

from 1910 BCE to 567 BCE before dropping again though not to values as low as prior to 1910 BCE (Fig. 4.6h).

Another recently proposed proxy for lakes is the relationship between the relative amount of thaumarcheaol (previously crenarchaeol) to the total isoprenoidal GDGT pool expressed as %thaum (Wang et al., 2014). This proxy is based on the idea that thaumarcheota prefer deeper waters and thus an increase in the produced thaumarcheaol may indicate an increase in lake level for medium sized lakes. A relatively new tool, it has been successfully applied in Lake Qinghai on the Tibetan plateau (Wang et al., 2014). In both lakes there are times of variation in %thaum which may be linked to changing lake levels (Fig. 4.6d,i)

A new class of isoprenoidal GDGTs was recently discovered with a cyclohexyl ring on the alkyl chain instead of the conventional cyclopentyl ring (Liu et al., 2016). These compounds were found in sulfidic environments and are termed "S-GDGTs" for their six-membered rings and sulfidic locales. They were initially found in Fayetteville Green Lake, a permanently stratified water body fed by groundwater through gypsum rich rocks. Both L. Miscanti and L. Miñiques are also groundwater fed with high presence of gypsum (Grosjean, 2001) making them ideal candidates for the presence of similar conditions. In this study S-GDGT-1 was found in both lakes at certain times (Fig. 4.6e,j). In L. Miscanti it was present from 212 CE to 920 CE and with a brief resurgence at 1454 CE. In L. Miñiques it was present in high amounts at the earliest times before mostly disappearing by 1910 BCE then displaying a slight increase from 567 BCE to 536 BCE.

4.5 Discussion

4.5.1 Compound Sources

Examination of fluctuations in compound concentrations through time illuminates those which have related sources within this lake system. Many of the major compound classes co-vary in their abundances, and these are likely from the aquatic plant life, namely submerged macrophytes. Long chain fatty acids and *n*-alkanes, alkanols, and major sterols show strikingly similar patterns. Further, the presence of alkylglycerols in many samples always correlates with the presence of archaeol suggesting that they reflect related microbial processes. Elevated levels of these microbial lipids only occurs when long chain methyl-substituted alkanes are found in the saturate fraction pointing toward a possible microbial origin for these as well. The overwhelming dominance of GDGT-0 over the other isoprenoidal GDGTs, and its anti-correlation with crenarchaeol indicates that it is possibly being produced by methanogens (Schouten et al., 2007).

4.5.2. Laguna Miñiques

2500-1910 BCE

The biomarker data measured here suggest the earliest ~600 years record dramatic changes in the biogeochemistry of L. Miñiques. High levels of S-GDGT-1 at the basal sampling point suggests an initial euxinic condition. The possibility of euxinia in these lakes is not surprising given the brackish conditions and presence of gypsum in the lake sediments and around the surrounding catchment. During

this initial state the highest abundance of long chain diols is also observed. Diols occur in many settings and are commonly attributed to eustigmatophyte microalgae (Volkman et al., 1999, 1992) or, perhaps, other types of algae (Gelin et al., 1997). The occurrence of diols during deposition of sapropels from euxinic waters of the Pliocene Mediterranean Sea has been noted before (Menzel et al., 2003). Both of these markers decrease over time as lake level, as suggested by %thaum, increased. Overall, this period is shown to be a transition from a shallower stratified lake with euxinic conditions to a deeper well-mixed lake by 1910 BCE.

1910-139 BCE

Around 1910 BCE lake levels had apparently begun to drop with a corresponding increase in salinity as indicated by the ACE index. Salinity remains high for the next approximately 1,750 years. This time period represents the only drop in P_{aq} values indicating a lower contribution from submerged macrophytes compared to emergent or non-aquatic plants. This change in water chemistry clearly appears to have favored cyanobacteria as demonstrated by the abundance increase of *n*-C_{17} over this time period. The compound 5-methylheptadecane is also present, likely indicative of cyanobacteria, at the point of highest concentration of *n*-C_{17} (Dembitsky et al., 2001; Shiea et al., 1990). One possible scenario is that increasing blooms of phytoplankton led to a shading effect that adversely affected the submerged macrophytes (Sand-Jensen and Søndergaard, 1981). Alternatively, and more likely, increasing salinity suppressed growth of macrophytes (Hammer

and Heseltine, 1988) which could lead to less nutrient competition and resulting expansion of cyanobacteria and microalgae.

139BC – 1670 CE

After 139 BCE there was an apparent drop in salinity which subsequently reversed the changes of the previous 1,750 years with a shift back towards submerged macrophytes in place of algae. P_{aq} values rose again while n-C_{17} concentrations decreased. Further, the n-C_{23} produced by macrophytes gradually increased to the highest levels observed in this study. This is complemented by an increase in sterol content and predominantly in the C_{29} sterols likely derived from the macrophytes. Coupled to these compounds the alkanols and long chain fatty acids likely have the same source. Increases in tetrahymanol at this time likely indicate an increase in bacteriovous ciliates in the lake (Harvey and Mcmanus, 1991). However, tetrahymanol may be formed by some purple non-sulfur bacteria and other taxa (Kleemann et al., 1990). Recent combined genetic-lipid analysis revealed that its production may be more widespread than previously thought (Banta et al., 2015). Despite this, an origin from ciliates may be justified due to the reappearance of S-GDGT-1 and possible times of increased salinity stratification and euxinia in the lake. This could lead to the establishment of a chemocline and layer of enhanced bacterial activity which is the primary food source for the ciliates (Sinninghe Damsté et al., 1995).

4.5.3. Laguna Miscanti

212-920AD

During the earliest studied time period recorded in sediments of L. Miscanti the GDGT based proxies all indicate relatively stable conditions of hydrology and water chemistry. No variations in the ACE index or %thaum point to a lake with relatively constant lake level and salinity. This earliest period corresponds to the most recent period from L. Miñiques where these proxies are also fairly constant indicating this to be a time of regional climatic stability. S-GDGT-1 is present at all time points except 501 CE possibly indicating the long term presence of stratification and euxinia. Lipids derived from macrophytes fluctuate throughout this time with maxima at 365 CE 688-920 CE. Interestingly, all compounds drop at 501 CE including the relative amount of extractable lipids in the sediment. Therefore, it is likely a general decrease in productivity that causes the changes seen at that time than major physical changes to lake level or chemistry.

920-1905 CE

In contrast to the lower half of the record, major changes appear to have occurred in the lake over the last millennium and approaching modern day. Over this time the ACE index rises indicating increasing salinity in the lake. Periodic increases in %thaum indicate episodic increases in lake level while simultaneous absences of S-GDGT-1 point to loss of euxinic conditions. This relationship between deepening of the lake and loss of euxinia is similar to the oldest changes recorded in L. Miñiques. Contrary to L. Miñiques, the presence of euxinia does not seem to enhance production of tetrahymanol in L. Miscanti as tetrahymanol rises steadily

across this time while S-GDGT-1 decreases. Macrophyte lipids are relatively stable in their abundances and composition during this time period despite the physical changes in the lake. However, during a period where lake level dropped and euxinia returned at 1454 CE there is a decrease in P_{aq} possibly indicating a detrimental effect on the submerged macrophytes.

4.5.4 Comparison to Regional Records

Recent studies have been undertaken to address the relative lack of high resolution climate records over the Holocene in the southern hemisphere. Prior geochemical, sedimentological, and palynological examination of L. Miscanti revealed arid conditions during the mid-Holocene with a nonlinear progression to modern conditions by 1,000 BCE (Grosjean, 2001; Valero-Garcés et al., 1996). By that time, our record indicates a relatively stable water depth in L. Miñiques. The ACE Index record shows that this time falls during the period of elevated salinity but conditions freshened within a few centuries after. The proposed pattern of gradual deepening in the late Holocene is also confirmed by the records established here with the exception of the potential deepening episode from 2,500-1910 BCE in L. Miñiques.

Further records of South American climate have been shown to vary significantly on regional levels. Study of Laguna del Negro Francisco provided a record that revealed a different paleohydrology than L. Miscanti (Grosjean et al., 1997). There, conditions were shown to be the wettest in a period from 3,000-1,800 BP. Farther to the south, temperature reconstruction from Laguna Chepical

indicates a stable warm period from 700 BCE – 800 CE (de Jong et al., 2013). This period roughly coincides with the period of stability shown by the GDGT proxy data from L. Miscanti 212 CE (start of record) to 900 CE. In L. Chepical, cooler and wetter conditions occurred during the Little Ice Age (LIA) but no Medieval Climate Anomaly (MCA) was found. Cooler conditions during the LIA were also shown in recent records from the high elevation Laguna del Maule in Central Chile (Carrevedo et al. 2015). This study indicates that a change occurred between 920-1182 CE, which corresponds to the MCA. At this time salinity of L. Miscanti is shown to increase and water level/euxinia variations begin. However, these conditions extend many centuries and are not likely to be a direct representation of the MCA.

4.6. Conclusions

Detailed biomarker examination of dated cores from Lagunas Miscanti and Miñiques has allowed for the establishment of a recent (2500 BCE-1905 CE) record of lake and biological community changes. It has been established that there are multiple periods where euxinia may have existed in the lakes and how that relates to possible changes in lake level. Further, an extended period of relative quiescence has been identified from 139 BCE-920 CE. It has been shown that even on short time scales the lakes of the Chilean Altiplano have an interesting and varied history. Future analyses of pigments and bacteriohopanepolyols will enhance the results presented here. It has been established that coring in these lakes is possible to significantly greater depths indicating the possibility of a longer term high

resolution biogeochemical study of Holocene climate and ecological changes at these lakes.

Acknowledgements

Funding for this study was provided by NASA Astrobiology Institute (NNA13AA90A) and the NASA Exobiology Program. Travel support was provided by the MISTI-Chile and the MIT-USTC summer intern program. We would like to thank the numerous team members from the Instituto Pirenaico de Ecología of the Consejo Superior de Investigaciones Científicas involved in the field campaign and sample preparation.

References

Allmendinger, R.W., Jordan, T.E., Kay, S.M., Isacks, B.L., 1997. The evolution of the Altiplano-Puna plateau of the Central Andes. Annu. Rev. Earth Planet. Sci. 25, 139–174. doi:10.1146/annurev.earth.25.1.139

Baker, P.A., Seltzer, G.O., Fritz, S.C., Dunbar, R.B., Grove, M.J., Tapia, P.M., Cross, S.L., Rowe, H.D., Broda, J.P., 2001. The history of South American tropical precipitation for the past 25,000 years. Science 291, 640–3. doi:10.1126/science.291.5504.640

Banta, A.B., Wei, J.H., Welander, P. V, 2015. A distinct pathway for tetrahymanol synthesis in bacteria. Proc. Natl. Acad. Sci. U. S. A. 112, 13478–83. doi:10.1073/pnas.1511482112

Carrevedo, M.L., Frugone, M., Latorre, C., Maldonado, A., Bernardez, P., Prego, R., Cardenas, D., Valero-Garces, B., 2015. A 700-year record of climate and environmental change from a high Andean lake: Laguna del Maule, central Chile (36 S). The Holocene 25, 956–972. doi:10.1177/0959683615574584

Cranwell, P.A., 1973. Chain-length distribution of n-alkanes from lake sediments in relation to post-glacial environmental change. Freshw. Biol. 3, 259–265. doi:10.1111/j.1365-2427.1973.tb00921.x

Crespo, J., De los Rios, P., 2004. Salinity Effects on the Abundance of Boeckella Poopoensis (copepoda, Calanoida) in Saline Ponds in the Atacama Desert, Northern Chile. Crustaceana 77, 417–423. doi:10.1163/1568540041643328

Damsté, J.S.S., Rijpstra, W.I.C., Hopmans, E.C., Weijers, J.W.H., Foesel, B.U., Overmann, J., Dedysh, S.N., 2011. 13,16-Dimethyl octacosanedioic acid (iso-diabolic acid), a common membrane-spanning lipid of Acidobacteria subdivisions 1 and 3. Appl. Environ. Microbiol. 77, 4147–54. doi:10.1128/AEM.00466-11

de Jong, R., von Gunten, L., Maldonado, A., Grosjean, M., 2013. Late Holocene summer temperatures in the central Andes reconstructed from the sediments of high-elevation Laguna Chepical, Chile (32° S). Clim. Past 9, 1921–1932. doi:10.5194/cp-9-1921-2013

Dembitsky, V.M., Dor, I., Shkrob, I., Aki, M., 2001. Branched Alkanes and Other Apolar Compounds Produced by the Cyanobacterium Microcoleus vaginatusfrom the Negev Desert. Russ. J. Bioorganic Chem. 27, 110–119. doi:10.1023/A:1011385220331

Ficken, K.., Li, B., Swain, D.., Eglinton, G., 2000. An n-alkane proxy for the sedimentary input of submerged/floating freshwater aquatic macrophytes. Org. Geochem. 31, 745–749. doi:10.1016/S0146-6380(00)00081-4

Foster, L.C., Pearson, E.J., Juggins, S., Hodgson, D.A., Saunders, K.M., Verleyen, E., Roberts, S.J., 2016. Development of a regional glycerol dialkyl glycerol tetraether (GDGT)–temperature calibration for Antarctic and sub-Antarctic lakes. Earth Planet. Sci. Lett. 433, 370–379. doi:10.1016/j.epsl.2015.11.018

Gelin, F., Volkman, J.K., De Leeuw, J.W., Sinninghe Damsté, J.S., 1997. Mid-chain

hydroxy long-chain fatty acids in microalgae from the genus Nannochloropsis. Phytochemistry 45, 641–646. doi:10.1016/S0031-9422(97)00068-X

Grosjean, M., 2001. A 22,000 14C year BP sediment and pollen record of climate change from Laguna (23°S), northern Chile. Glob. Planet. Change 28, 35–51. doi:10.1016/S0921-8181(00)00063-1

Grosjean, M., Valero-Garces, B.L., Geyh, M.A., Messerli, B., Schotterer, U., Schreier, H., Kelts, K., 1997. Mid- and late-Holocene limnogeology of Laguna del Negro Francisco, northern Chile, and its palaeoclimatic implications. The Holocene 7, 151–159. doi:10.1177/095968369700700203

Hammer, U.T., Heseltine, J.M., 1988. Aquatic macrophytes in saline lakes of the Canadian prairies. Hydrobiologia 158, 101–116. doi:10.1007/BF00026269

Harvey, H.R., Mcmanus, G.B., 1991. Marine ciliates as a widespread source of tetrahymanol and hopan-3ß-ol in sediments. Geochim. Cosmochim. Acta 55, 3387–3390. doi:10.1016/0016-7037(91)90496-R

Kaiser, J., Schouten, S., Kilian, R., Arz, H.W., Lamy, F., Sinninghe Damsté, J.S., 2015. Isoprenoid and branched GDGT-based proxies for surface sediments from marine, fjord and lake environments in Chile. Org. Geochem. 89-90, 117–127. doi:10.1016/j.orggeochem.2015.10.007

Kim, J.-H., van der Meer, J., Schouten, S., Helmke, P., Willmott, V., Sangiorgi, F., Koç, N., Hopmans, E.C., Damsté, J.S.S., 2010. New indices and calibrations derived from the distribution of crenarchaeal isoprenoid tetraether lipids:

Implications for past sea surface temperature reconstructions. Geochim. Cosmochim. Acta 74, 4639–4654. doi:10.1016/j.gca.2010.05.027

Kleemann, G., Poralla, K., Englert, G., Kjosen, H., Liaaen-Jensen, S., Neunlist, S., Rohmer, M., 1990. Tetrahymanol from the phototrophic bacterium Rhodopseudomonas palustris: first report of a gammacerane triterpene from a prokaryote. J. Gen. Microbiol. 136, 2551–2553. doi:10.1099/00221287-136-12-2551

Kraemer, B.M., Hook, S., Huttula, T., Kotilainen, P., O'Reilly, C.M., Peltonen, A., Plisnier, P.-D., Sarvala, J., Tamatamah, R., Vadeboncoeur, Y., Wehrli, B., McIntyre, P.B., 2015. Century-Long Warming Trends in the Upper Water Column of Lake Tanganyika. PLoS One 10, e0132490. doi:10.1371/journal.pone.0132490

Liu, X., De Santiago Torio, A., Bosak, T., Summons, R.E., 2016. Novel archaeal tetraether lipids with a cyclohexyl ring identified in Fayetteville Green Lake, NY, and other sulfidic lacustrine settings. Rapid Commun. Mass Spectrom. 30, 1197–1205. doi:10.1002/rcm.7549

Menzel, D., van Bergen, P.F., Schouten, S., Sinninghe Damsté, J.S., 2003. Reconstruction of changes in export productivity during Pliocene sapropel deposition: a biomarker approach. Palaeogeogr. Palaeoclimatol. Palaeoecol. 190, 273–287. doi:10.1016/S0031-0182(02)00610-7

Moy, C.M., Seltzer, G.O., Rodbell, D.T., Anderson, D.M., 2002. Variability of El

Niño/Southern Oscillation activity at millennial timescales during the Holocene epoch. Nature 420, 162–5. doi:10.1038/nature01194

Nishimura, M., 1977. Origin of stanols in young lacustrine sediments. Nature 270, 711–712. doi:10.1038/270711a0

Pearson, A., Hurley, S.J., Shah Walter, S.R., Kusch, S., Lichtin, S., Zhang, Y.G., 2016. Stable carbon isotope ratios of intact GDGTs indicate heterogeneous sources to marine sediments. Geochim. Cosmochim. Acta 181, 18–35. doi:10.1016/j.gca.2016.02.034

Pearson, E.J., Juggins, S., Talbot, H.M., Weckström, J., Rosén, P., Ryves, D.B., Roberts, S.J., Schmidt, R., 2011. A lacustrine GDGT-temperature calibration from the Scandinavian Arctic to Antarctic: Renewed potential for the application of GDGT-paleothermometry in lakes. Geochim. Cosmochim. Acta 75, 6225–6238. doi:10.1016/j.gca.2011.07.042

Powers, L., Werne, J.P., Vanderwoude, A.J., Sinninghe Damsté, J.S., Hopmans, E.C., Schouten, S., 2010. Applicability and calibration of the TEX86 paleothermometer in lakes. Org. Geochem. 41, 404–413. doi:10.1016/j.orggeochem.2009.11.009

Powers, L.A., Johnson, T.C., Werne, J.P., Casteneda, I.S., Hopmans, E.C., Sinninghe Damsté, J.S., Schouten, S., 2005. Large temperature variability in the southern African tropics since the Last Glacial Maximum. Geophys. Res. Lett. 32, L08706. doi:10.1029/2004GL022014

Rielley, G., Collier, R.J., Jones, D.M., Eglinton, G., 1991. The biogeochemistry of Ellesmere Lake, U.K.—I: source correlation of leaf wax inputs to the sedimentary lipid record. Org. Geochem. 17, 901–912. doi:10.1016/0146-6380(91)90031-E

Rowe, H.D., Dunbar, R.B., Mucciarone, D.A., Seltzer, G.O., Baker, P.A., Fritz, S., 2002. Insolation, Moisture Balance and Climate Change on the South American Altiplano Since the Last Glacial Maximum. Clim. Change 52, 175–199. doi:10.1023/A:1013090912424

Sand-Jensen, K., Søndergaard, M., 1981. Phytoplankton and Epiphyte Development and Their Shading Effect on Submerged Macrophytes in Lakes of Different Nutrient Status. Int. Rev. der gesamten Hydrobiol. und Hydrogr. 66, 529–552. doi:10.1002/iroh.19810660406

Schouten, S., Hopmans, E.C., Schefuß, E., Sinninghe Damsté, J.S., 2002. Distributional variations in marine crenarchaeotal membrane lipids: a new tool for reconstructing ancient sea water temperatures? Earth Planet. Sci. Lett. 204, 265–274. doi:10.1016/S0012-821X(02)00979-2

Schouten, S., van der Meer, M.T.J., Hopmans, E.C., Rijpstra, W.I.C., Reysenbach, A.-L., Ward, D.M., Sinninghe Damsté, J.S., 2007. Archaeal and bacterial glycerol dialkyl glycerol tetraether lipids in hot springs of yellowstone national park. Appl. Environ. Microbiol. 73, 6181–91. doi:10.1128/AEM.00630-07

Schwalb, A., Burns, S.J., Kelts, K., 1999. Holocene environments from stable isotope

stratigraphy of ostracods and authigenic carbonate in Chilean Altiplano Lakes. Palaeogeogr. Palaeoclimatol. Palaeoecol. 148, 153–168. doi:10.1016/S0031-0182(98)00181-3

Shiea, J., Brassell, S.C., Ward, D.M., 1990. Mid-chain branched mono- and dimethyl alkanes in hot spring cyanobacterial mats: A direct biogenic source for branched alkanes in ancient sediments? Org. Geochem. 15, 223–231. doi:10.1016/0146-6380(90)90001-G

Sinninghe Damsté, J.S., Kenig, F., Koopmans, M.P., Köster, J., Schouten, S., Hayes, J.M., de Leeuw, J.W., 1995. Evidence for gammacerane as an indicator of water column stratification. Geochim. Cosmochim. Acta 59, 1895–1900. doi:10.1016/0016-7037(95)00073-9

Sinninghe Damsté, J.S., Ossebaar, J., Schouten, S., Verschuren, D., 2012. Distribution of tetraether lipids in the 25-ka sedimentary record of Lake Challa: extracting reliable TEX86 and MBT/CBT palaeotemperatures from an equatorial African lake. Quat. Sci. Rev. 50, 43–54. doi:10.1016/j.quascirev.2012.07.001

Sturt, H.F., Summons, R.E., Smith, K., Elvert, M., Hinrichs, K.-U., 2004. Intact polar membrane lipids in prokaryotes and sediments deciphered by high-performance liquid chromatography/electrospray ionization multistage mass spectrometry--new biomarkers for biogeochemistry and microbial ecology. Rapid Commun. Mass Spectrom. 18, 617–28. doi:10.1002/rcm.1378

Tierney, J.E., Russell, J.M., 2009. Distributions of branched GDGTs in a tropical lake system: Implications for lacustrine application of the MBT/CBT paleoproxy. Org. Geochem. 40, 1032–1036. doi:10.1016/j.orggeochem.2009.04.014

Tierney, J.E., Russell, J.M., Eggermont, H., Hopmans, E.C., Verschuren, D., Sinninghe Damsté, J.S., 2010. Environmental controls on branched tetraether lipid distributions in tropical East African lake sediments. Geochim. Cosmochim. Acta 74, 4902–4918. doi:10.1016/j.gca.2010.06.002

Turich, C., Freeman, K.H., 2011. Archaeal lipids record paleosalinity in hypersaline systems. Org. Geochem. 42, 1147–1157. doi:10.1016/j.orggeochem.2011.06.002

Valero-Garcés, B.L., Delgado-Huertas, A., Navas, A., Edwards, L., Schwalb, A., Ratto, N., 2003. Patterns of regional hydrological variability in central-southern Altiplano (18°–26°S) lakes during the last 500 years. Palaeogeogr. Palaeoclimatol. Palaeoecol. 194, 319–338. doi:10.1016/S0031-0182(03)00284-0

Valero-Garcés, B.L., Grosjean, M., Kelts, K., Schreier, H., Messerli, B., 1999. Holocene lacustrine deposition in the Atacama Altiplano: facies models, climate and tectonic forcing. Palaeogeogr. Palaeoclimatol. Palaeoecol. 151, 101–125. doi:10.1016/S0031-0182(99)00018-8

Valero-Garcés, B.L., Grosjean, M., Schwalb, A., Geyh, M., Messerli, B., Kelts, K., 1996. Limnogeology of Laguna Miscanti: evidence for mid to late Holocene moisture changes in the Atacama Altiplano (Northern Chile). J. Paleolimnol.

16. doi:10.1007/BF00173268

Volkman, J.K., Barrett, S.M., Blackburn, S.I., 1999. Eustigmatophyte microalgae are potential sources of C29 sterols, C22–C28 n-alcohols and C28–C32 n-alkyl diols in freshwater environments. Org. Geochem. 30, 307–318. doi:10.1016/S0146-6380(99)00009-1

Volkman, J.K., Barrett, S.M., Dunstan, G.A., Jeffrey, S.W., 1992. C30-C32 alkyl diols and unsaturated alcohols in microalgae of the class Eustigmatophyceae. Org. Geochem. 18, 131–138. doi:10.1016/0146-6380(92)90150-V

Wang, H., Dong, H., Zhang, C.L., Jiang, H., Liu, Z., Zhao, M., Liu, W., 2015. Deglacial and Holocene archaeal lipid-inferred paleohydrology and paleotemperature history of Lake Qinghai, northeastern Qinghai–Tibetan Plateau. Quat. Res. 83, 116–126. doi:10.1016/j.yqres.2014.10.003

Wang, H., Dong, H., Zhang, C.L., Jiang, H., Zhao, M., Liu, Z., Lai, Z., Liu, W., 2014. Water depth affecting thaumarchaeol production in Lake Qinghai, northeastern Qinghai–Tibetan plateau: Implications for paleo lake levels and paleoclimate. Chem. Geol. 368, 76–84. doi:10.1016/j.chemgeo.2014.01.009

Wang, H., Liu, W., Zhang, C.L., Jiang, H., Dong, H., Lu, H., Wang, J., 2013. Assessing the ratio of archaeol to caldarchaeol as a salinity proxy in highland lakes on the northeastern Qinghai–Tibetan Plateau. Org. Geochem. 54, 69–77. doi:10.1016/j.orggeochem.2012.09.011

Weijers, J.W.H., Schouten, S., Spaargaren, O.C., Sinninghe Damsté, J.S., 2006.

Occurrence and distribution of tetraether membrane lipids in soils: Implications for the use of the TEX86 proxy and the BIT index. Org. Geochem. 37, 1680–1693. doi:10.1016/j.orggeochem.2006.07.018

Weijers, J.W.H., Schouten, S., van den Donker, J.C., Hopmans, E.C., Sinninghe Damsté, J.S., 2007. Environmental controls on bacterial tetraether membrane lipid distribution in soils. Geochim. Cosmochim. Acta 71, 703–713. doi:10.1016/j.gca.2006.10.003

Wen-Yen, H., Meinschein, W.., 1976. Sterols as source indicators of organic materials in sediments. Geochim. Cosmochim. Acta 40, 323–330. doi:10.1016/0016-7037(76)90210-6

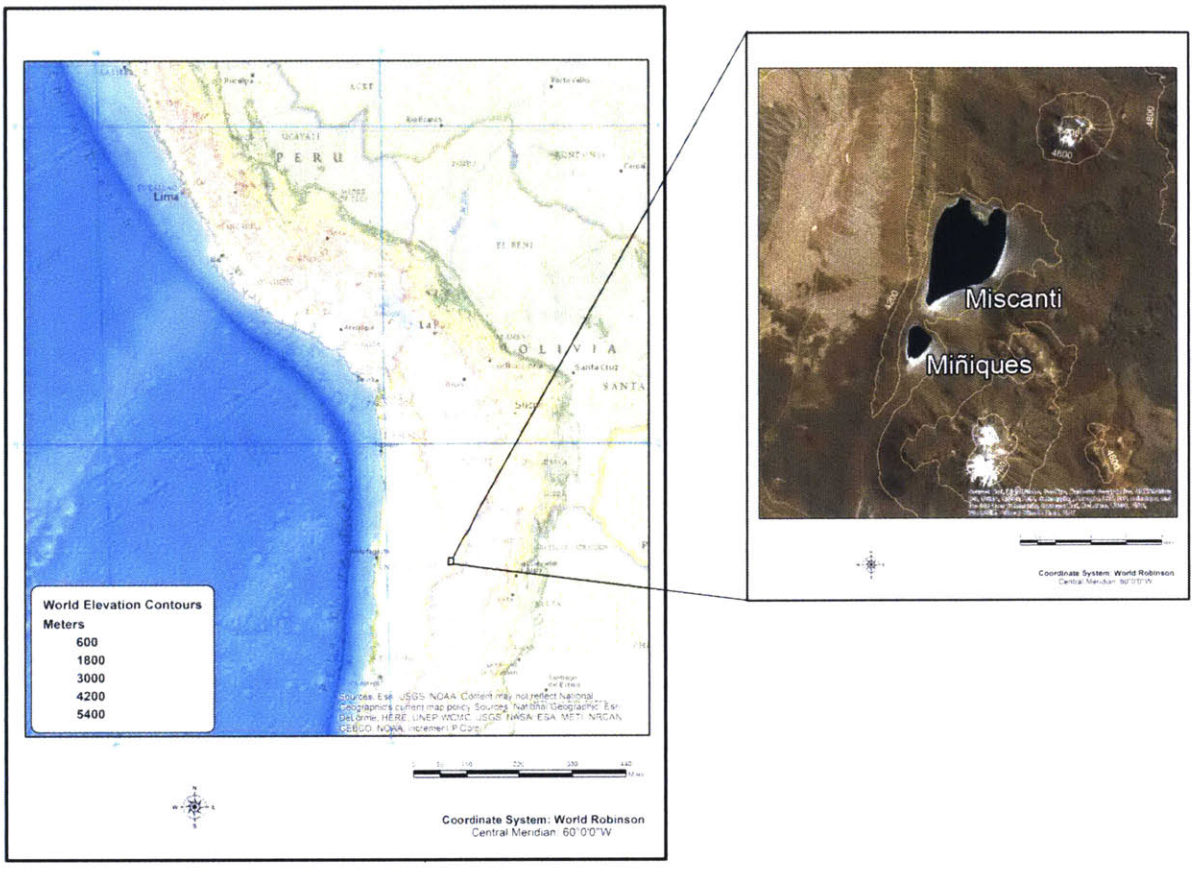

Figure 4.1: Regional map illustrating the location of Lagunas Miscanti and Miñiques with close up imagery of the site locale.

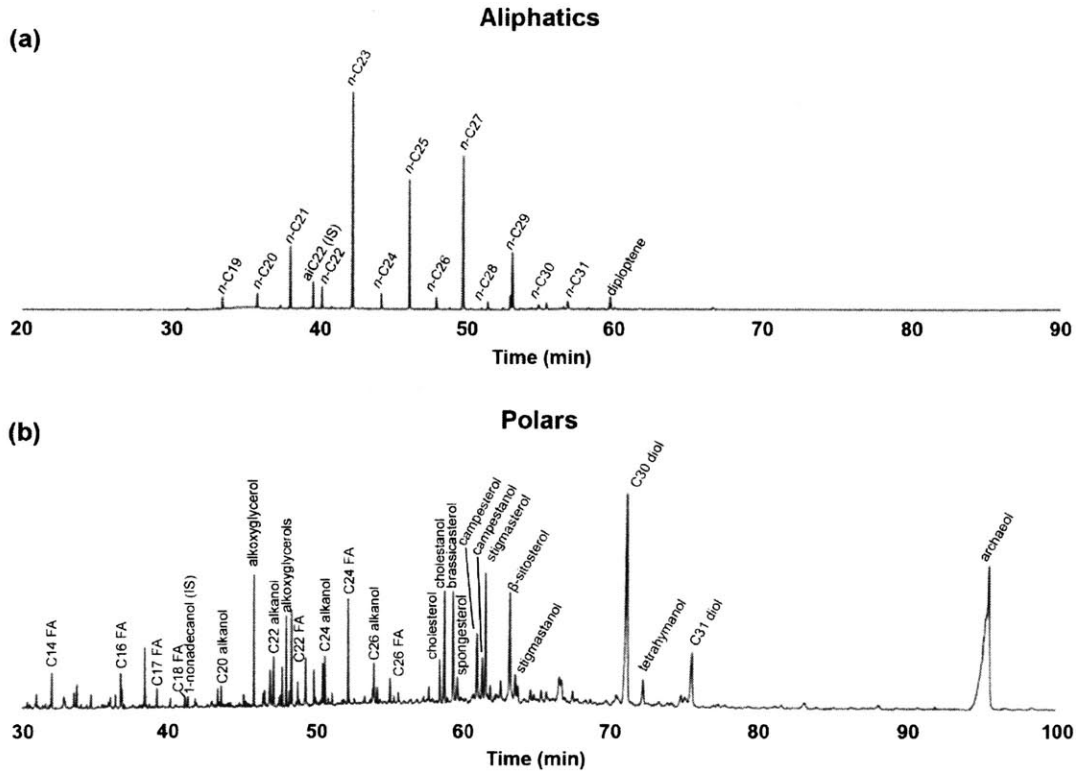

Figure 4.2: Typical total ion chromatograms of (a) aliphatic compounds and (b) polar compounds (BSTFA derivatized).

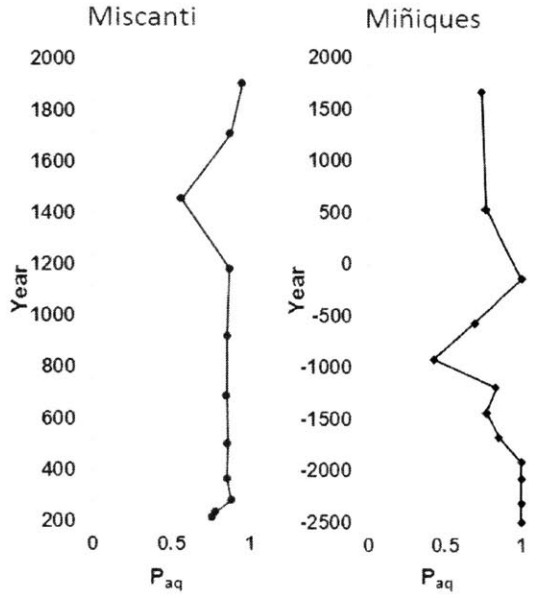

Figure 4.3: Plots of the P_{aq} proxy (Ficken et al., 2000) for macrophytes over time in Lagunas Miscanti and Miñiques. Higher values indicate the presence of submerged macrophytes.

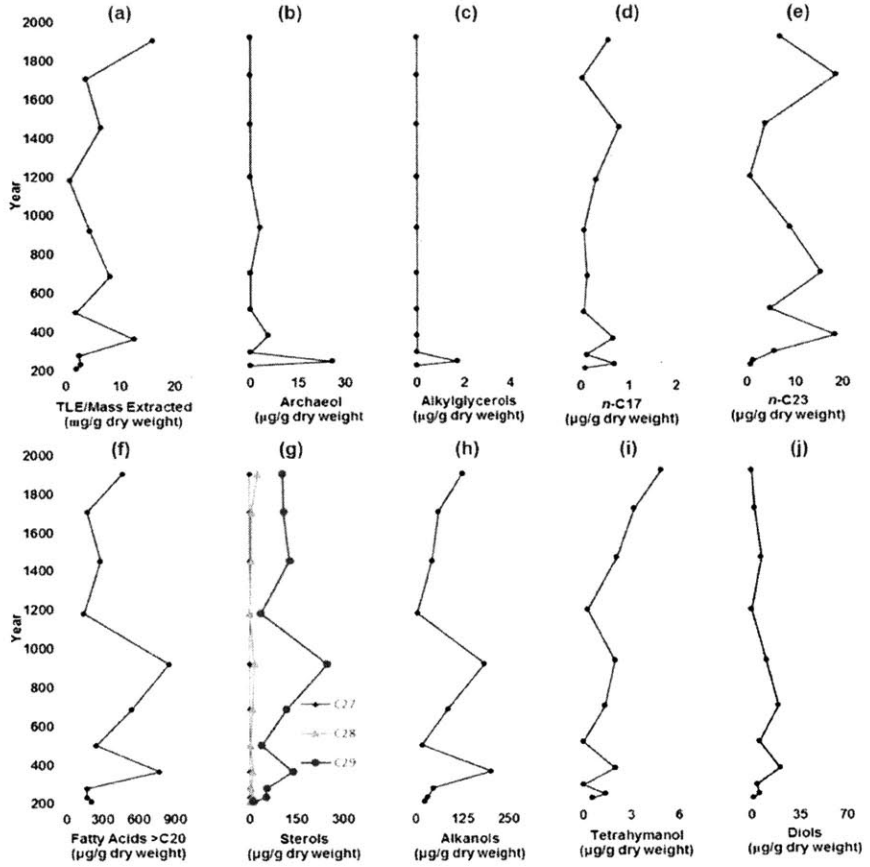

Figure 4.4: Laguna Miscanti records normalized to the amount of dried sediment extracted of (a) amount of extractable lipids, (b) archaeol, (c) alkylglycerols, (d) *n*-C_{17}, (e) *n*-C_{23}, (f) long chain fatty acids, (g) sterol groups, (h) total alkanols, (i) tetrahymanol and (j) total diols. Shading marks different time periods discussed in the text.

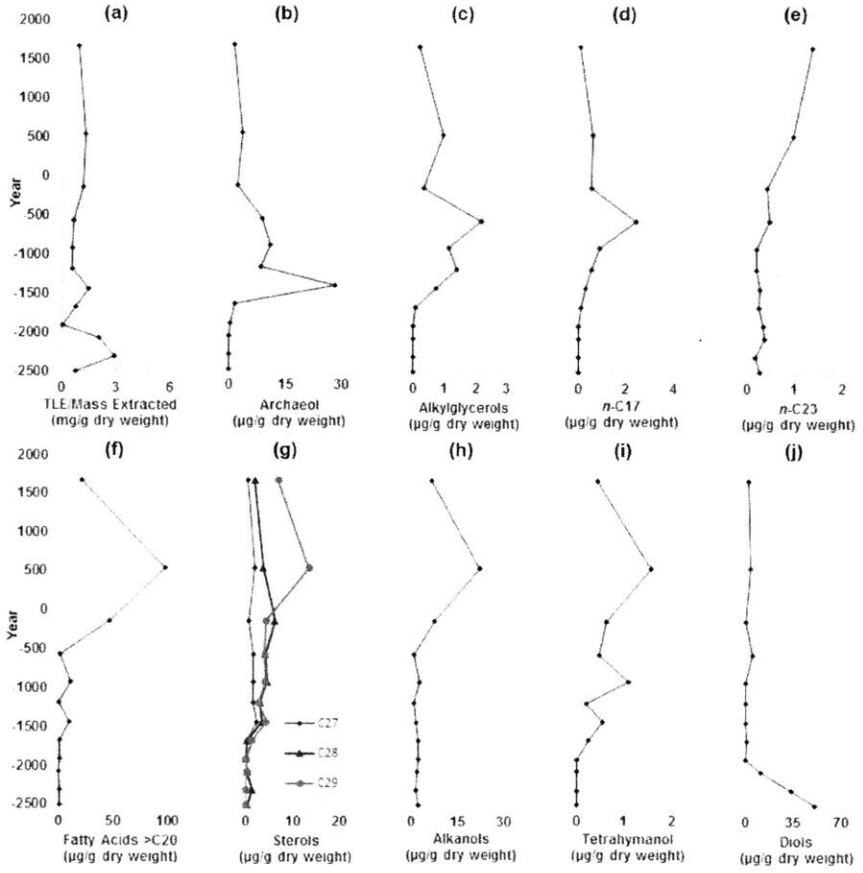

Figure 4.5: Laguna Miñiques records normalized to the amount of dried sediment extracted of (a) amount of extractable lipids, (b) archaeol, (c) alkylglycerols, (d) *n*-C_{17}, (e) *n*-C_{23}, (f) long chain fatty acids, (g) sterol groups, (h) total alkanols, (i) tetrahymanol and (j) total diols. Shading marks different time periods discussed in the text.

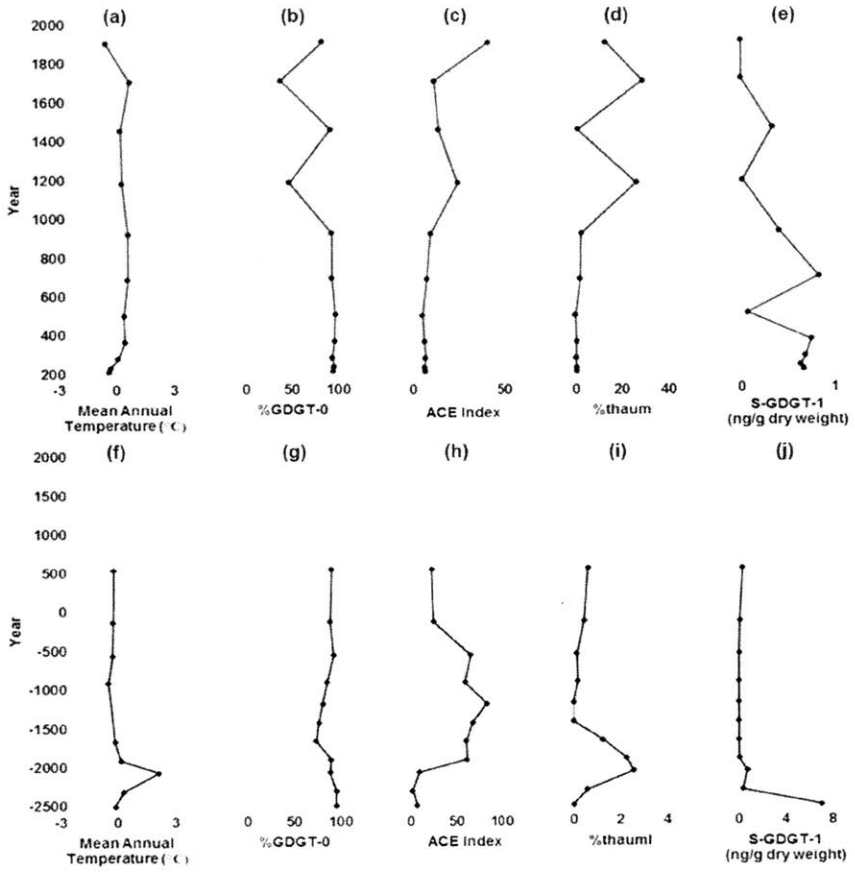

Figure 4.6: GDGT based records for (a-e) Laguna Miscanti and (f-j) Laguna Miñiques. Records include (a+f) Mean annual temperature estimates based on the MBT/CBT proxy, (b+g) percentage of GDGT-0 compared to total isoprenoidal GDGTs, (c+h) the ACE index salinity proxy, (d+i) the %thaum lake level proxy and (e+j) the concentration of S-GDGT-1 normalized to the dry weight of extracted sediment. Shading marks different time periods discussed in the text.

Table 4.1: Concentrations of various aliphatic and polar compounds

Sample Depth (cm)	Date	TLE/Mass Extracted (mg/g)	*n*-C_{23} (µg/g dry weight)	*n*-C_{17} (µg/g dry weight)	alkanols (µg/g dry weight)	long chain fatty acids (µg/g dry weight)	diols (µg/g dry weight)
L. Miscanti							
11	1905	16.1		0.6	7.9	470.4	0.0
21	1708	3.8	18.8	0.0	16.7	179.4	2.3
31	1454	6.5	3.9	0.8	7.0	286.9	7.2
41	1182	0.9	0.8	0.3	7.8	151.0	0.0
51	920	4.5	9.0	0.1	40.9	851.5	10.8
61	688	8.2	15.5	0.1	10.8	542.3	19.3
71	501	1.8	4.9	0.1	10.2	248.8	5.7
81	365	12.6	18.4	0.7	16.1	774.0	20.9
91	279	2.5	5.6	0.1	19.2	172.4	3.6
101	233	2.8	1.3	0.7	12.1	171.5	5.6
111	212	2.0	0.8	0.1	12.1	213.6	1.1
L. Miñiques							
16	1670	0.9	1.4	0.1	3.0	20.3	2.0
31	536	1.3	1.0	0.6	6.8	97.3	3.6
46	-139	1.2	0.4	0.6	16.7	46.9	0.5
60	-567	0.6	0.5	2.5	6.4	1.0	5.1
75	-915	0.6	0.2	0.9	1.6	10.5	0.0
90	-1189	0.6	0.2	0.5	4.4	0.0	0.1
105	-1432	1.5	0.3	0.3	1.3	10.0	0.6
120	-1671	0.8	0.3	0.1	1.0	0.4	1.0
135	-1910	0.1	0.4	0.0	22.2	0.3	0.2
145	-2070	2.1	0.4	0.0	0.9	0.1	11.7
160	-2309	3.0	0.2	0.0	0.5	0.6	33.6
175	-2500	0.8	0.3	0.0	2.9	0.5	51.5

Table 4.1 continued: Concentrations of various aliphatic and polar compounds

Sample Depth (cm)	Date	archaeol (µg/g dry weight)	alkoxyglycerols (µg/g dry weight)	tetrahymanol (µg/g dry weight)	C_{27} sterols (µg/g dry weight)	C_{28} sterols (µg/g dry weight)	C_{29} sterols (µg/g dry weight)
L. Miscanti							
11	1905	0.0	0.0	4.9	0.0	26.4	104.7
21	1708	0.0	0.0	3.2	0.0	6.6	109.1
31	1454	0.0	0.0	2.1	0.0	6.1	127.6
41	1182	0.0	0.0	0.3	0.0	0.0	36.0
51	920	3.0	0.0	2.0	0.0	15.3	248.1
61	688	0.0	0.0	1.4	0.0	9.5	117.4
71	501	0.0	0.0	0.0	0.0	3.0	38.2
81	365	5.6	0.0	2.0	0.0	9.6	137.2
91	279	0.0	0.0	0.0	0.0	4.5	54.0
101	233	26.1	1.7	1.4	0.0	9.4	51.8
111	212	0.0	0.0	0.6	0.0	0.0	12.3
L. Miñiques							
16	1670	1.4	0.2	0.4	0.5	1.7	6.8
31	536	3.3	1.0	1.6	1.8	3.7	13.5
46	-139	2.3	0.3	0.6	0.7	6.2	4.3
60	-567	8.8	2.2	0.5	1.6	4.2	4.1
75	-915	11.1	1.1	1.1	1.6	4.6	4.2
90	-1189	8.6	1.4	0.2	1.5	3.0	2.8
105	-1432	28.5	0.7	0.6	2.3	3.5	4.4
120	-1671	1.5	0.1	0.3	0.3	0.5	1.4
135	-1910	0.2	0.0	0.0	0.0	0.0	0.1
145	-2070	0.0	0.0	0.0	0.0	0.3	0.3
160	-2309	0.0	0.0	0.0	0.0	1.4	0.0
175	-2500	0.0	0.0	0.0	0.0	0.4	0.0

Table 4.2: GDGT based indices, proxies, and select concentrations.

Sample Depth (cm)	Date (CE)	BIT Index	ACE Index	%thaum	MAT (°C)	%GDGT-0 (vs. isoGDGTs)	S-GDGT-1 (ng/g dry weight)
L. Miscanti							
11	1905	0.99	41.0	13.2	-0.5	82.9	0.00
21	1708	0.86	11.9	29.0	0.7	38.2	0.00
31	1454	0.99	14.0	1.1	0.2	92.0	0.34
41	1182	0.85	24.5	26.3	0.3	47.6	0.02
51	920	0.99	9.7	2.5	0.6	93.4	0.41
61	688	1.00	7.4	1.9	0.6	93.1	0.83
71	501	1.00	5.2	0.0	0.4	97.1	0.07
81	365	1.00	6.2	0.5	0.5	96.1	0.75
91	279	1.00	6.9	0.3	0.1	93.9	0.68
101	233	1.00	6.3	0.4	-0.3	95.8	0.64
111	212	1.00	7.0	0.6	-0.4	94.8	0.67
L. Miñiques							
31	536	0.97	23.5	0.6	0.2	91.0	0.34
46	-139	0.99	25.5	0.5	0.4	89.5	0.12
60	-567	0.98	65.8	0.2	-0.2	93.2	0.04
75	-915	0.98	59.2	0.2	-0.2	86.1	0.00
90	-1189	0.99	83.3	0.0	-0.3	81.2	0.00
105	-1432	0.99	67.8	0.0	-0.5	77.0	0.00
120	-1671	0.97	60.6	1.3	-0.1	74.3	0.00
135	-1910	0.99	61.7	2.3	0.2	90.4	0.06
145	-2070	0.98	9.3	2.6	2.1	89.0	0.73
160	-2309	0.99	2.1	0.6	0.3	95.9	0.34
175	-2500	0.97	7.2	0.0	-0.1	95.8	7.06

Chapter 5

Conclusions and Future Directions

This thesis has applied organic geochemistry to reconstruct paleoenvironmental conditions across multiple timescales and extremes. It has demonstrated the broad range of tools, from the most traditional approaches using *n*-alkane distributions to recent proxies still being established. Further, isotopic investigations have revealed the larger scale information about the carbon cycle and hydrologic conditions in some cases.

In Chapter 2 core material from Western India was studied to reveal the potential for hyperthermal investigation in that region. Through integrated biostratigraphy, palynology and stable isotope geochemistry it was demonstrated that at significant depth the Early Cenozoic hyperthermal events are likely present. Further, in conducting the isotopic investigation the application of pyrolysis-GC-IRMS to the examination of kerogens was developed. This application was then utilized to show that the individual components of kerogen as released during pyrolysis have carbon isotopic compositions that accurately reflect the changes that are seen in extractable hydrocarbons.

Further examination of the core palynology has the potential to refine the age determination of the samples. This could allow for more firm conclusions to be drawn about the stratigraphic locations of hyperthermal events. Additionally the

quantification of the palynological data would allow for the biomarker distributions to be compared directly to changes in floral composition.

This study has indicated above all else that the Cambay Basin holds great potential for detailed examination of hyperthermal events. This is immensely important as it would provide climate records from the paleoequator which are currently lacking and would be of great benefit to climate modelling of the time. If study in this region improves our understanding of the global variability of responses to rapid intense warming due to carbon input to the ocean-atmosphere system it would then be applicable to refining future predictions of the effects of anthropogenic climate change. However, the region is also complex and would call for an interdisciplinary team including geologists with a knowledge of regional stratigraphic variations and biostratigraphers and geochronologists to confidently date any core material. Finally, scientific drilling would be very beneficial as opposed to taking samples from industrial cores. This would allow for the control of contamination, the archiving of samples, and more detailed lithology to be established.

The final contribution of this project was the use of pyrolysis-GC-IRMS for the study of kerogens. Establishing that kerogens record the same isotopic information as extractable hydrocarbons lends weight to this process being applied to kerogens from other scenarios as well. For instance, ancient rocks that lack extractable hydrocarbons often still retain kerogens. This method would allow for

detailed investigation of the isotopic makeup of the kerogens and possibly reveal information as to its possible biogenicity.

Another possible application of this method is to organic rich rocks that may contain isotopic excursions. For instance, in the Cambay Basin there are areas with massive lignite seams that were potentially forming during hyperthermal events. By applying pyrolysis-GC-IRMS directly to raw sample powder it would be possible to generate compound-specific isotope curves rapidly and without any need for extraction. By locating excursions this way time and resources can be saved by targeting areas of interest for more detailed study.

Chapter 3 examined the same time period but at the opposite extreme than India in the Canadian High Arctic. There paleosols and a shale unit were examined for biomarker distribution and isotopic content. A number of interesting conclusions can be drawn from this work. First, the isotopic composition of *n*-alkanes preserved in paleosols is comparable to that preserved in shale units from the same time and area. The hydrogen isotopic composition in particular shows a very different value than modern meteoric water and implies that the region was ice free during this time period. Further, proxy data confirms the highly elevated temperature of the region during the Early Cenozoic. Biomarker distributions demonstrate angiosperm contributions that may be overlooked in this area based on fossil evidence. Also, a clear shift from marine to near coastal deposition from the Paleocene to the Eocene is shown for the Strathcona Fiord area. Sampling resolution at Strathcona Fiord was limited but the established lithology combined with the confirmation of high

biomarker preservation indicates that Strathcona Fiord is a desirable target for future investigations, particularly those that can take advantage of the high amount of carbonate deposition.

The final study has demonstrated the centennial scale variability within the high altitude Lagunas Miscanti and Miñiques in the Chilean Altiplano. Situated at a very different extreme, the high elevation combined with the location near the Atacama Desert makes the lakes a very cold dry environment. These lakes have been shown to contain sedimentation dating back tens of thousands of years yet no biomarker record of their history exists. Here, shorter coring has established that even within the last several millennia the lakes have undergone periods of significant variability both in biotic community structure and physical/chemical alterations. The application of newly introduced proxies based on GDGTs has revealed a story of lake history in which they all provide complementary explanations. In the future the sedimentology and geochemistry of the cores will be established and provide new insights that will paint an even more detailed picture of these lakes.

In the end three different regions have been thoroughly examined using multiple approaches of organic geochemical investigation. These investigations have revealed paleoenvironmental information ranging from the global scale to within a single lake and from tens of millions of years to just a few millennia. What all these studies have in common though is they have revealed the relatively untapped potential of these sites as suppliers of important climatic and ecological information.